Titre: Title:	Millimeter-Wave Substrate Integrated Waveguide Antenna and Front-End Techniques for Gigabyte Point-to-Point Wireless Services
Auteur: Author:	Nasser Ghassemi
Date:	2013
Type:	Mémoire ou thèse / Dissertation or Thesis
Référence: Citation:	Ghassemi, N. (2013). Millimeter-Wave Substrate Integrated Waveguide Antenna and Front-End Techniques for Gigabyte Point-to-Point Wireless Services [Thèse de doctorat, École Polytechnique de Montréal]. PolyPublie. https://publications.polymtl.ca/1320/

UNIVERSITÉ DE MONTRÉAL

MILLIMETER-WAVE SUBSTRATE INTEGRATED WAVEGUIDE ANTENNA AND FRONT-END TECHNIQUES FOR GIGABYTE POINT-TO-POINT WIRELESS SERVICES

NASSER GHASSEMI

DÉPARTEMENT DE GÉNIE ÉLECTRIQUE

ÉCOLE POLYTECHNIQUE DE MONTRÉAL

THÈSE PRÉSENTÉE EN VUE DE L'OBTENTION

DU DIPLÔME DE PHILOSOPHIAE DOCTOR

(GÉNIE ÉLECTRIQUE)

DÉCEMBRE 2013

UNIVERSITÉ DE MONTRÉAL

ÉCOLE POLYTECHNIQUE DE MONTRÉAL

Cette thèse intitulée:

MILLIMETER-WAVE SUBSTRATE INTEGRATED WAVEGUIDE ANTENNA AND FRONT-END TECHNIQUES FOR GIGABYTE POINT-TO-POINT WIRELESS SERVICES

présentée par : GHASSEMI Nasser
en vue de l'obtention du diplôme de : Philosophiæ Doctor
a été dûment acceptée par le jury d'examen constitué de :

M. LAURIN Jean-Jacques, Ph.D., président
M. WU Ke, Ph.D., membre et directeur de recherche
M. CALOZ Christophe, Ph.D., membre
M. SEBAK Abdel Razik, Ph.D., membre

To my parents,

To my love Zeynab

ACKNOWLEDGMENT

First of all, I would like to express my gratitude to my PhD advisor Prof. Ke Wu, who offered me support whenever I needed it. His passion for research, his persistence, and his innovative ideas gave me the drive and the motivation to explore new frontiers and to accomplish this thesis.

I would also like to thank all the personnel at the Poly-Grames Research Center when I studied in Canada, in particular Mr. Jules Gauthier, Mr. Traian Antonescu, Mr. Maxime Thibault, and Mr. Steve Dubé, whose technical assistance was essential for the realization of the prototypes. A special thank is extended to Mrs. Ginette Desparois and Mrs. Nathalie Lévesque for guiding me through the administration and to Mr. Jean-Sébastien Décarie for assistance with computer trouble.

I am also indebted to my student colleagues and friends for all the professional and personal advice, and to everybody who contributed directly or indirectly to this thesis especially. I would like to thank Simon Couture for his help to translate the abstract to French.

I would also like to thank all my teachers and professors at y master, bachelor and high school. A special thank is extended to Prof. Rashed Mohassel, Prof. Moradi, Prof. Sh. Mohanna, Prof. F. Mohanna, Prof. Arzaghi, Prof. Zarifkar, and Prof. Samiei.

A special thank goes to the members of the examination jury, who took their time to read the thesis and provided very valuable comments.

Lastly, and most importantly, I would like to thank my parents. They bore me, raised me, supported me, taught me, and loved me. I would like to express my deepest gratitude to my wife for her love, encouragement and support on short and long distance. To them I dedicate this thesis.

RÉSUMÉ

La relativement faible absorption atmosphérique dans les bandes de fréquences E et W a permis le développement de nombreuses applications sans-fil. Les bandes de fréquences de 71-76 GHz, 81-86 GHz et 94.1-97 GHz sont toutes assignées au spectre de communication sans-fil gigabyte par la Federal Communication Commission (FCC) des États-Unis. Lorsque la fréquence augmente vers la région des ondes millimétriques, l'efficacité et la qualité des lignes micro-ruban sont affectées par de sérieuses pertes de transmission et par l'interférence inter-signaux. D'un autre côté, la technologie des guides d'ondes classique est demeurée populaire pour la conception de systèmes haute perfomance dans la bande E/W. Cependant, cette technologie n'est pas appropriée pour une production à grande échelle et à faible coût à cause de sa structure encombrante et coûteuse. De plus, la structure non-planaire des guide d'ondes rend difficile la connection à des composantes planaires actives ainsi qu'à d'autres lignes planaires telles que les lignes micro-ruban et les guides d'ondes coplanaires (CPW). Afin de remédier à ce problème, les circuits intégrés aux substrats (SIC) ont été proposés comme une solution à faible coût, à efficacité élevée, planaire et intégrée au substrat pour des applications à hautes-fréquences. Les guides d'ondes intégrés aux substrats (SIW), faisant partie de la famille des SIC, possède non seulement les avantages des guides d'ondes rectangulaires mais aussi d'autres bénéfices comme un faible coût, une petite taille, un poids léger et la facilité de fabrication par les techniques de fabrication des PCB ou d'autres techniques. Dans cette thèse, nous élargissons la recherche sur les SIW en proposant et développant une variété d'antennes innovatrices, de réseaux d'antennes et de composantes passives millimétriques qui sont appliqués à la conception et à la démonstration de réseaux d'antennes intégrés et d'étages d'entrée de systèmes de communication en bande E/W.

Les contributions scientifiques principales du présent travail peuvent être résumées comme suit:

- Un réseau d'antenne 4x4 utilisant la technologie des guides d'ondes intégrés au substrat (SIW) pour la conception de son réseau d'alimentation est proposé et démontré. Des fentes longitudinales gravées sur la surface métallique du dessus du SIW sont utilisées pour alimenter les éléments du réseau d'antennes. Des cubes composés d'un matériau diélectrique à faible permittivité sont placés au-dessus de chaque réseau d'antenne 1x4 afin d'augmenter le gain des antennes patch. La largeur de bande de deux réseaux

d'antennes 4x4 est d'environ 7.5 GHz (94.2-101.8 GHz) avec un gain de 19 dBi.

- La conception d'une antenne planaire basée sur une tige diélectrique est proposée et étudiée. L'antenne est alimentée par un guide d'ondes diélectrique non rayonnant intégré au substrat (SINRD). Cette antenne présente plusieurs caractéristiques intéressantes telles qu'une grande largeur de bande (94-104 GHz), un gain relativement élevé et stable, l'utilisation d'un substrat à permittivité élevée et un rayonnement parallèle au substrat guidé par celui-ci.
- Une antenne à guide d'onde co-planaire (CPW) en forme de spirale, compacte, uni planaire, à polarisation circulaire est étudiée théoriquement et expérimentalement pour des applications à large bande. L'antenne est alimentée directement par un CPW de 50 Ω par le côté extérieur de la spirale de sorte qu'un balun d'adaptation n'est pas requis. Cette alimentation permet la capacité d'obtenir un réseau planaire d'antennes spirales. Cette antenne spirale est avantageuse à cause de sa structure uni planaire facile à fabriquer aux fréquences d'ondes millimétriques.
- Un antenne cornet pyramidale dans la bande W composée de circuits imprimés (PCB) multi-couches à faible coût est développée et démontre une grande largeur de bande couvrant 71-76 GHz, 81-86 GHz et 94.1-97 GHz. L'antenne cornet proposée a aussi l'avantage d'avoir un rayonnement dans la direction perpendiculaire au substrat et d'utiliser le SIW pour son alimentation. Des fentes transversales sur la surface métallique du dessus à la fin du SIW sont déployées afin d'alimenter l'antenne cornet. Des vias métallisés sont utilisés pour réaliser les murs du cornet.
- Une antenne à fentes de type antipode, à rétrécissement linéaire et chargée par un matériau diélectrique (ALTSA) est étudiée. Utilisant le concept du cornet alimenté par un SIW, cette antenne planaire chargée par un matériau diélectrique est caractérisée par un faible coût, un gain élevé et une efficacité élevée et est conçue pour des services sans-fil gigabytes à ultra large bande dans la bande E/W (71-97 GHz). Le gain mesuré d'un élément de cette antenne est 14±0.5 dBi tandis qu'une efficacité de rayonnement mesurée de 84.23% est obtenue à 80 GHz. Le gain mesuré d'un réseau 1x4 de cette antenne est 19±1 dBi.
- Une transition SIW large bande conçue sur un substrat diélectrique dont la permittivité

décroît dont la bande passante couvre toute la bande E/W. Cette transition est composée d'une couche unique d'un substrat ayant une constante diélectrique élevée et dont la largeur est progressivement rétrécie qui fait la connection entre deux SIW. Grâce à sa structure basée sur un guide d'ondes, cette transition est isolée électromagnétiquement de l'extérieur et le bruit dû aux interférences est minimal.

- Un nouveau résean d'antennes patch à haute efficacité et ayant un gain élevé est réalisé pour les services sans-fil gigabyte point-à-point dans la bande E (81-86 GHz). La largeur de bande simulée et mesurée du réseau d'antenne sont de 7.2% ce qui permet de couvrir la bande de fréquence désirée de 81-86 GHz. Le gain mesuré du réseau d'antenne est 18.5 dBi et est presque constant sur la bande de fréquences d'intérêt. Une efficacité de rayonnement de 90.3 % est obtenue.
- Un système de réception intégré au substrat opérant sur la bande de fréquences de 81-86 GHz avec une grande largeur de bande qui atteint 5.5 GHz est présenté pour la première fois. L'étage d'entrée proposée intègre des composantes actives et passives dans un assemblage unique. Un substrat à faible constante diélectrique est utilisé pour fabriquer l'antenne afin d'augmenter sa largeur de bande et son gain tandis que des circuits actifs incluant un LNA, un multiplicateur et des multiplicateurs de fréquence sont montés en surface par MHMIC.

Les réseaux d'antennes sont une composante critique des systèmes sans-fil point-à-point dans la bande E/W car les antennes doivent satisfaire plusieurs critères. Les nouvelles antennes proposées ont un faible coût, une efficacité élevée, une grande largeur de bande ainsi qu'un gain élevé et stable ce qui les rend appropriées pour cette application. Différentes structures d'antennes qui rayonnent parallèlement ou perpendiculairement au substrat sont proposées et démontrées.

Les résultats de cette thèse ont déjà été acceptés et publiés dans 4 articles du journal IEEE Transactions on Antennas and Propagation, 2 lettres dans le IEEE Antennas and Wireless Propagation Letters, un article du journal IEEE Transactions on Components, Packaging and Manufacturing Technology, ainsi que d'autres articles de journaux et de conférences qui sont mentionnés à la fin de cette thèse.

ABSTRACT

The relatively low atmospheric absorption over E-band and W-band (frequency window) has been spurred many wireless applications. Frequency bands of 71-76 GHz, 81-86 GHz, and 94.1-97 GHz are all allocated by the US Federal Communication Commission (FCC) as parts of gigabyte wireless spectrum. As frequency increases to millimeter wave region, the efficiency and quality of microstrip lines suffer from serious transmission losses and signal interferences. On the other hand, classical waveguide technology has been popular in the design of high-performance millimeter-wave systems at E/W-band. However, this technology is not suitable for low-cost and mass production because of its expensive and bulky structure. In addition, the non-planar structure of waveguide makes it difficult to get connected to planar active components and other planar lines such as microstrip line and coplanar waveguide (CPW). To overcome this bottleneck problem, substrate integrated circuits (SICs) have been proposed as low-cost and high-efficient integrated planar structures for high-frequency applications. Substrate integrated waveguide (SIW), which is part of the SICs family, has manifested not only the advantages of rectangular waveguide but also other benefits such as low cost, compact size, light weight, and easy fabrication using PCB or other processing techniques. In this Ph.D. thesis, we extend the research of SIW to the proposal and development of various innovative antennas, antenna arrays and millimetre-wave passive components, which are applied to the design and demonstration of integrated antenna arrays and E/W-band front-end sub-systems.

The principal scientific contributions of this thesis work can be summarized in the following:

- A 4×4 antenna array is proposed and demonstrated using substrate-integrated waveguide (SIW) technology for the design of its feed network. Longitudinal slots etched on the SIW top metallic surface are used to drive the array antenna elements. Dielectric cubes made of low-permittivity material are placed on top of each 1×4 antenna array to increase the gain of circular patch antenna elements. Measured impedance bandwidths of two 4×4 antenna arrays are about 7.5 GHz (94.2–101.8 GHz) with 19 dBi gain.
- Design of planar dielectric rod antenna is proposed and studied, which is fed by Substrate Integrated Non-Radiative Dielectric (SINRD) waveguide. This antenna presents numerous interesting features such as broad bandwidth (94-104 GHz), relatively high and stable gain, use of high dielectric constant substrate, and substrate-oriented end-fire radiation.

- A compact, uniplanar, circularly polarized coplanar waveguide (CPW) spiral antenna is investigated theoretically and experimentally for wideband applications. The antenna is directly fed by a 50 Ω CPW from the outside edge of the spiral, thus a matching balun is not required. This feeding provides a capability of having an entire uniplanar array of spirals. This spiral antenna is desirable due to its uniplanar structure that offers easy fabrication at millimeter-wave frequency.
- W-band integrated pyramidal horn antenna made of low cost multilayer printed circuit board (PCB) process is developed and it shows a broad bandwidth covering 71-76 GHz, 81-86 GHz, and 94.1-97 GHz. The proposed horn antenna also has the advantages of radiation along the broadside to the substrate and it makes use of SIW as its feeder. Transverse slot on the top metallic surface at the end of SIW is deployed to drive the horn antenna. Metalized via holes are used to synthesize the horn walls.
- A dielectric loaded antipodal linearly tapered slot antenna (ALTSA) is studied with which the concept of SIW-fed horn is used to design a low-cost, high-gain and efficient planar dielectric-loaded antenna for ultra-wideband gigabyte wireless services at E/W-band (71-97 GHz). Measured gain of single element antenna is 14±0.5 dBi while measured radiation efficiency of 84.23% is obtained at 80 GHz. Measured gain of 1×4 array antenna is 19±1 dBi,
- Broadband transition of SIW designed on high-to-low dielectric constant substrate whose bandwidth covers the entire E/W-band. The transition has a single layer structure that consists of a tapered high dielectric constant substrate connecting two SIWs. Thanks to the waveguide-based structure of the transition, it has a self-shielded configuration, and its noise interference is minimum.
- A novel high-efficient and high-gain patch antenna array is realized for E-Band gigabyte point-to-point wireless services (81-86 GHz). Simulated and measured bandwidths of the antenna array are 7.2% that covers the desired frequency range of 81 - 86 GHz. Measured gain of the 4×4 antenna array is 18.5 dBi that is almost constant within the antenna bandwidth of interest. Measured radiation efficiency of 90.3% is obtained.
- A substrate integrated receiver system operating over the band of 81-86 GHz with a broadband up to 5.5 GHz is presented for the first time. The proposed front-end sub-

system integrates active and passive components within a single package. A substrate with low dielectric constant is used to fabricate the antenna for increasing its bandwidth and gain While actives circuits including LNA, mixer and frequency multipliers are surface-mounted using MHMIC.

Antenna array is a critical part of the E/W-band point to point wireless system demonstrations, because antenna should have several specifications to be suitable for point to point wireless system. The proposed novel antennas are low cost, high efficient, broad band, and also they have high and stable gain, which make them appropriate for this application. Different antenna structures which radiate end fire, or broadside to the substrate are proposed and demonstrated.

The results of this PHD dissertation are already accepted and published as four journal papers in IEEE Transactions on Antennas and Propagation, two letters in IEEE Antennas and Wireless Propagation Letters, one journal paper in IEEE Transactions on Components, Packaging and Manufacturing Technology, and some other journal and conference paper which are mentioned in detail at the end of this thesis.

TABLE OF CONTENTS

LIST OF FIGURES

LIST OF TABLES

LIST OF ACRONYMS AND ABBREVIATIONS

2-D	Two-Dimensional
3-D	Three-Dimensional
ADS	Advanced Design System
AIA	Active Integrated Antenna
ALSTA	Antipodal Linearly Tapered Slot Antenna
AM	Amplitude Modulation
CAD	Computer Aided Design
CBCPW	Conductor-Backed Co-Planar Waveguide.
CPW	Coplanar Waveguide
CST-MWS	Microwave Studio® (Computer Simulation Technology)
DC	Direct Current
EBG	Electromagnetic Band Gap
EIRP	Equivalent Isotropic Radiated Power
FET	Field-Effect Transistor
FHMSIW	Folded Half Mode Substrate Integrated Waveguide
FOM	Figure of Merit
FSIW	Folded Substrate Integrated Waveguide
HB	Harmonic Balance
HFSS	High Frequency Structure Simulator
HMSIW	Half Mode Substrate Integrated Waveguide
IF	Intermediate Frequency
IM3	Third-order Intermodulation
IP3	*Third-order Intercept Point*

LNA	Low Noise Amplifier
LO	Local Oscillator
MEMS	Micro Electro Mechanical systems
MICs	Microwave Integrated Circuits
MMICs	Microwave Monolithic Integrated Circuits
MPT	Microwave Power Transmission
MW	Magnetic Wall
PA	Power Amplifier
PAE	Power Added Efficiency
PCB	Printed Circuits Board
RF	Radio Frequency
SIC	Substrate Integrated Circuits
SINRD	Substrate Integrated Non-Radiative Dielectric Guide
SIIG	Substrate Integrated Image Guide
SIW	Substrate Integrated Waveguide
TE	Transverse Electric
TEM	Transverse Electric Magnetic
TM	Transverse Magnetic
TSA	Tapered Slot Antenna
TTL	Transistor–Transistor Logic
VCO	Voltage Controlled Oscillator
VNA	Vector Network Analyzer

CHAPTER 1 INTRODUCTION

1.1 Background and Motivation

Operating frequencies of wireless communication systems have increased in order to assign radio access to a less crowded part of the electromagnetic spectrum and also provide a wider bandwidth for data transmission. The relatively low atmospheric absorption rate at E/W-band, 140 GHz, 220 GHz, 340 GHz, and 410 GHz (Figure 1.1) as transmission windows has spurred many applications and innovations at millimeter-wave frequencies and beyond [1]. A wide range of applications have attracted much attention from industry and academia to the exploitation of E/W-band (71-97 GHz) [3]-[4]. The E/W-band spectral window offers possibility great potential of gigabyte data wireless transmission over several kilometers in normal weather conditions [5]. Frequency bands of 71-76 GHz, 81-86 GHz (usually referred as E-band), and 94.1-97 GHz (part of W-band) are all allocated by the US Federal Communication Commission (FCC) as gigabyte wireless spectrum [3]-[4]. Over those frequency windows, the atmospheric absorption drops to less than 1dB/Km and spells out the capability of long-range gigabyte point-to-point wireless services [5]. Obviously, wide bandwidth and low atmospheric loss allow for the E/W-band implementation of high resolution and long-range radars [6], detectors, and sensors [7], which may be used in helicopter, aircraft/automobile collision avoidance radar, passive millimeter wave imaging, and radar sensors [8]-[10].

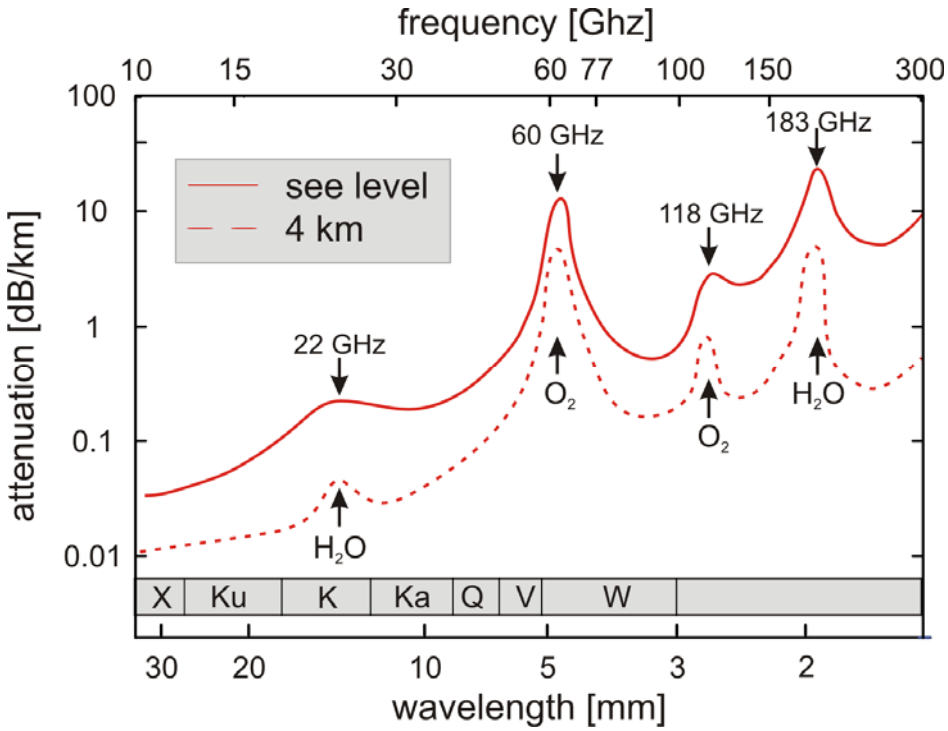

Figure 1.1. Average atmospheric attenuation versus frequency [1]-[2].

The application range over E/W-band is extensive and evolving quickly. Figure 1.2 (a) shows one of the main applications of E/W-Band frequencies is related to on-campus LAN connectivity that provides users with a flexible, fast and safe way to establish the network with fiber optic backbone access. E/W-band is also used for Wireless Backhaul services (Figure 1.2 (b)) to provide users with high speed, low cost and scalable means of increasing data and voice traffics to and from hard-to-reach cell towers or where the deployment of terrestrial fiber is not economically viable [11]. We can summarize the potential applications of E/W-band as follows [3]:

- Fiber backbone POP access
- Enterprise campus connectivity
- Local area network (LAN) extension
- Local area loop
- Metropolitan area network (MAN)
- Wide area network (WAN) access

- Central office bypass
- Wireless backhaul
- High definition video
- Storage access

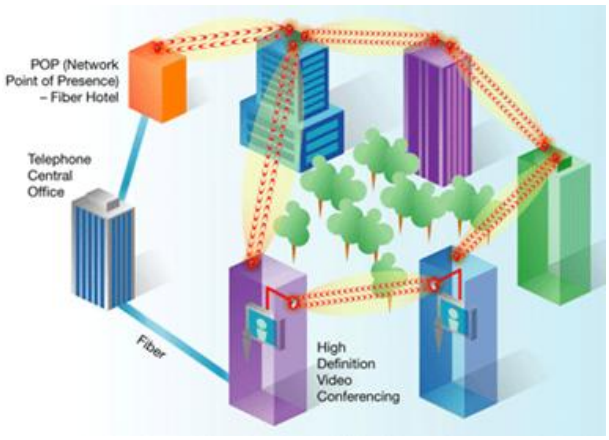

(a)

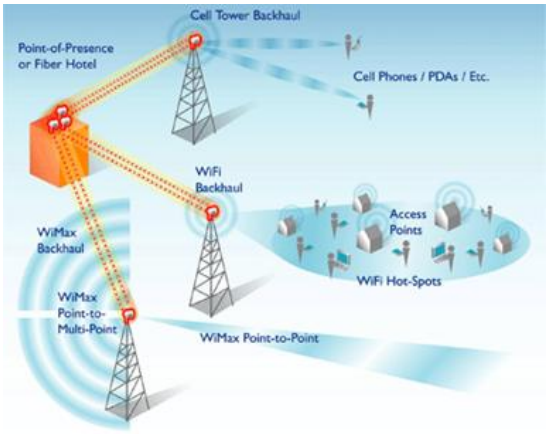

(b)

Figure 1.2. Applications of E/W-band gigabyte point-to-point communication (a) campus LAN, (b) wireless backhaul [11].

Front-end technologies have been known as the critical enabling mover for the development of millimeter-wave systems and applications. In this connection, transmission line techniques have been playing the instrumental role in the development of such front-end platforms. Microstrip

lines have been used since decades for microwave applications due to their low-cost planar structures for a full scale of integration. As frequency increases to millimeter wave region, the efficiency and quality of microstrip lines suffer from serious transmission losses and signal interferences. On the other hand, classical waveguide technology has been popular in the design and development of high-performance millimeter-wave circuits and systems. However, the waveguide technology is not suitable for low-cost and mass production because of its expensive and bulky structure. In addition, the non-planar nature of waveguide without the possibility of integration makes it difficult to get connected to planar active components. To overcome this bottleneck problem, substrate integrated circuits (SICs) have been proposed as low-cost and high-efficient integrated planar structures for a wide range of high-frequency applications. Substrate integrated waveguide (SIW) that is part of SICs, presents not only the inherent advantages of rectangular waveguide but also offers other desirable benefits such as low cost, compact size, light weight, and easy fabrication using PCB or other processing techniques. Generally speaking, SIW consists of arrays of metallic via holes or slot trenches created in a planar substrate. Furthermore, SIWs can easily be connected to or integrated with microstrip and coplanar waveguides utilizing a wideband transition on the same substrate [12]-[16].

Thanks to the low-loss transmission characteristics of the non-radiative dielectric (NRD) waveguide, it has been demonstrated as a promising candidate for millimeter-wave applications. However, the fabrication and integration of NRD waveguides are generally not easy because of their mechanical tolerance and bulky geometry especially at millimeter-wave frequency. Substrate integrated non-radiative dielectric (SINRD) waveguide has been demonstrated successfully to overcome such fabrication and integration hurdles of the original NRD waveguide. SINRD guide presents a planar topology and can easily be connected to any other planar lines and active components. In the design and development of an SINRD guide, drilling an array of air holes reduces the effective permittivity of the bilateral surrounding areas of the central guiding strip, thus creating a dielectric channel of waveguide in planar substrate. The effective dielectric constant can be controlled by choosing an appropriate set of geometrical parameters of the array holes [17]-[20]. Other SICs structures are Substrate Integrated Image Guide (SIIG) [21], half-mode SIW (HMSIW) [22]-[28], folded HMSIW (FHMSIW) [29], and folded SIW (FSIW) [30]-[31], ridge SIW [32] etc. Generally, any non-planar structure can be synthesized into its planar counterpart through the concept of SICs such as substrate integrated

coaxial lines. This research work is primarily focused on novel antenna and front-end sub-system based on SIW technology for gigabyte point to point wireless communication at E/W-band.

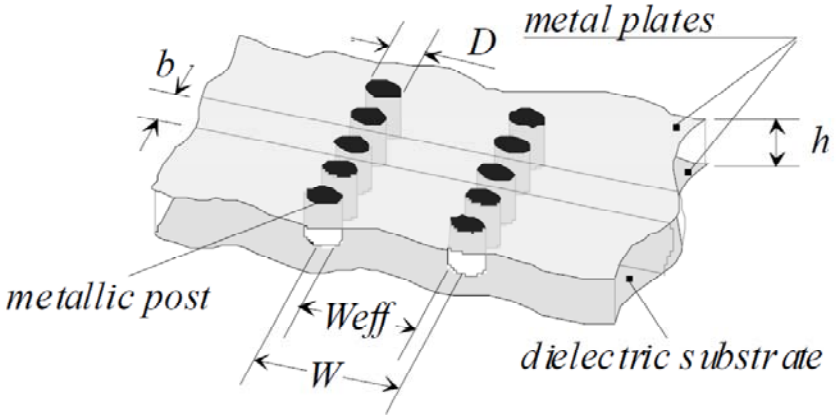

Figure 1.3. Topology of an SIW guide realized on a dielectric substrate [12].

As Figure 1.3 suggests, placing two rows of metalized hole in substrate is used to synthesize the rectangular waveguide inside the substrate. Spacing *b* between the holes, diameter *D* of the holes, and spacing *W* between the two rows of metallic vias are basic physical parameters that are necessary in the design of an SIW. To reduce potential leakage loss between adjacent vias, period *b* must be kept small. Because the diameter of via and the period length are interrelated to each other, ratio *D/b* is considered to be more critical than the period length in the design. The SIW can no longer be regarded as a normal homogeneous waveguide, and it is in fact an artificial periodic waveguide [33]. The diameter of via may significantly affect the return loss of the waveguide section in view of its input port. Two basic design rules have been deducted of different SIW geometries [12]:

$$\begin{aligned} D &< \lambda_g / 5 \\ b &\le 2D \end{aligned} \tag{1}$$

Propagation properties of TE_{10}-like mode in SIW are very similar to the TE_{10} mode ofrectangular waveguide. Experiments and simulations show that TE_{10} mode dispersion characteristics of the

SIW are the same as its equivalent rectangular waveguide. Subsequently, the width of SIW can be approximated by using the following equations [34]-[37]:

$$W_{eff} = W - \frac{D^2}{0.95b} \tag{2}$$

Equation (1) is valid for $b < \lambda_0 \times \sqrt{\varepsilon_r}/2$ and $b < 4D$, where D is the diameter of the metallic holes.

For the fabrication and design of SIW structures at E/W-band, appropriate fabrication tolerance and material selection should be considered. First of all, because of small dimensions of the SIW at E/W-band, mechanical fabrication tolerance could have a significant impact on the performance of SIW circuits. Cut-off frequency of TE_{10} mode along SIW can be calculated from:

$$f_{c10} = \frac{1}{2W_{eff}\sqrt{\varepsilon\mu}} \tag{3}$$

Then, a simple calculation shows that 1 mil (25 μm) tolerance can change the cut-off frequency of an SIW on Alumina substrate ($\varepsilon_r = 9.8$) by about ± 2 GHz at 63 GHz, and on Rogers/duroid 6002 substrate ($\varepsilon_r = 2.98$) by ± 1 GHz. This can visibly change the operating frequency of SIW based-circuits especially filters and cavities. Cutting with laser beam, drilling and punching are three main techniques for making vias on substrates. Material characterization such as mechanical and thermal stability, rigidness, flexibility, and thickness of substrate usually determines which technique is appropriate for different substrate. The dimension of via and the width of SIW should always be measured accurately after fabrication. For the laser beam cutting, even the diameter of beam can be critically important. As an example, a laser beam with 2 mils diameter will reduce the width of SIW by 2 mils, which, according to equation (3) can change the cut-off frequency of SIW on Alumina substrate ($\varepsilon_r = 9.8$) by ± 4 GHz at 63 GHz, and SIW on Rogers/duroid 6002 substrate ($\varepsilon_r = 2.98$) by ± 2 GHz.

The characteristics of substrate are the other important aspect that should be accounted for in the design of SIW circuits at E/W-band. As frequency increases, dielectric constant and dielectric loss tangent of the material will generally change even though dielectric constant exhibits in a very stable manner. The first step of designing E/W-band circuits and components is measuring the dielectric constant and loss tangent of the substrate. As an example, according to equation (3),

changing the dielectric constant of the substrate from 2.98 to 2.8 can change the cut-off frequency of SIW by 2 GHz at 66 GHz. This can be critical in designing resonant structures such as antenna, filter and cavities.

As it is mentioned in [38]-[39], the characteristics of SIW components may change by changing the operating temperature of substrate, which should be considered in the related design process.

Figure 1.4 illustrates the effect of dielectric and metallic losses on insertion loss of one centimeter SIW on 4 mils and 20 mils thickness substrate. It is clear that, as the thickness of the substrate decreases metallic losses will increase and dielectric losses remains constant. Decreasing the thickness of the substrate also increases the effect of the roughness of the metal.

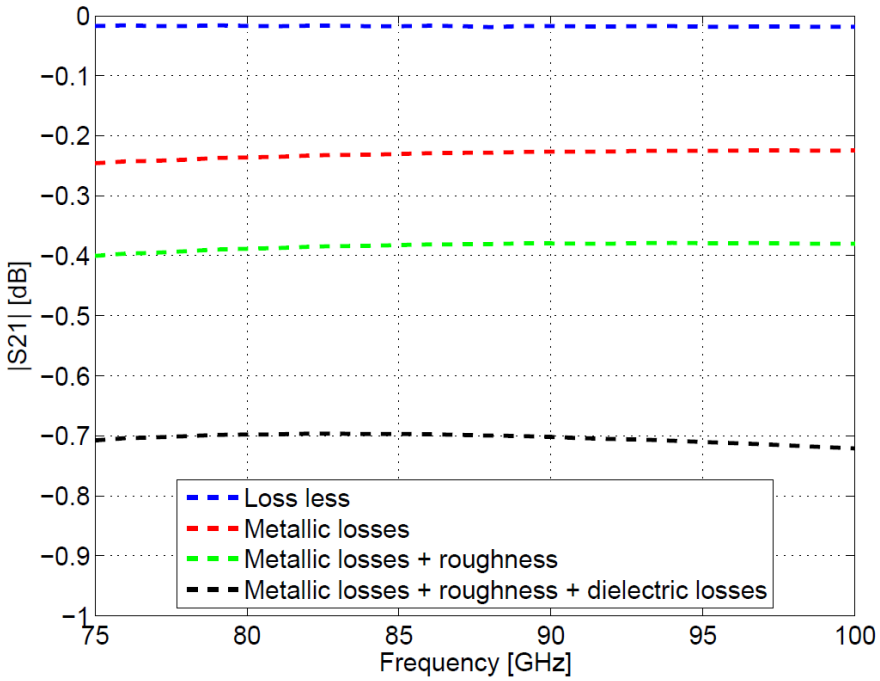

(a)

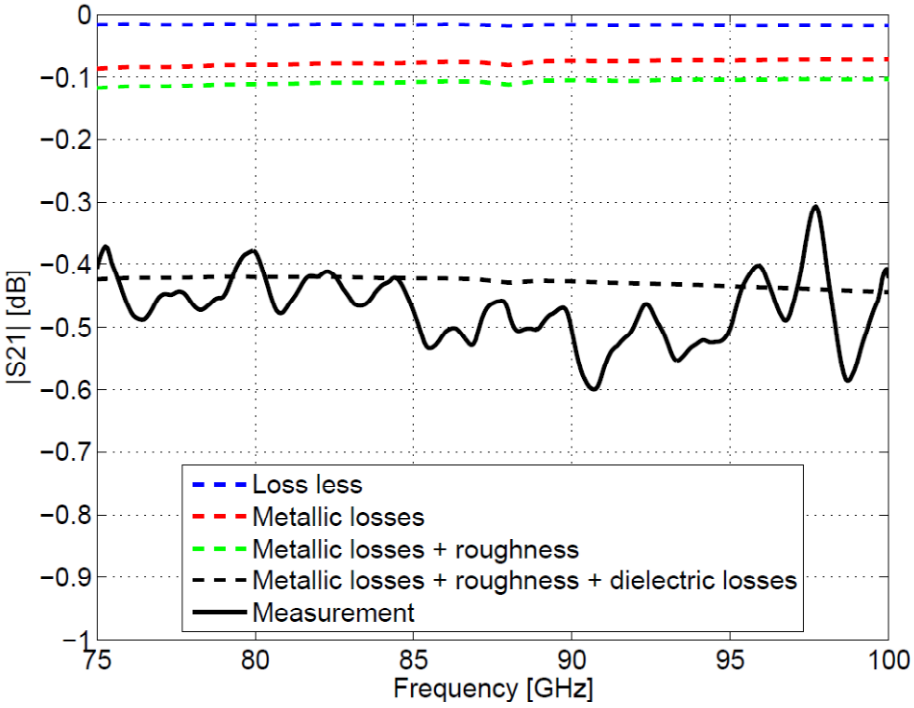

(b)

Figure 1.4.Effect of dielectric and metallic losses on insertion loss of one centimeter SIW on (a) 4 mils, and (b) 20 mils thickness substrate

1.2 Outline of thesis

This thesis research is concerned with the design and development of original and innovative antennas, antenna arrays, and front-end sub-systems based on SICs technology for E/W-band wireless applications such as back-haul interconnectivity. Although several SICs-based antennas, antenna arrays and beam forming networks have been recently proposed and developed, most of them have been designed and demonstrated for applications with operating frequencies lower than 40 GHz. This thesis demonstrates a number of millimeter-wave examples at E/W-bands by deploying the low-cost PCB techniques. In fact, it pushes the limiting performances and features of SIW with such techniques. The first goal of this research work is to investigate, design and demonstrate a class of novel low-cost antennas and front-end configurations for gigabyte data wireless transmission at E/W-band. The proposed antennas exhibit wide bandwidth, high gain, high efficiency and stable radiation pattern and gain within the frequency band of interest. This thesis structure is organised as follows. Chapter 2 presents a wideband CPW fed, circular

polarized spiral antenna that can be easily fabricated at high frequency. Chapter 3 presents a set of novel SIW antennas for 94-97 GHz applications. The first antenna radiates along the broadside to the substrate while the second antenna presents substrate-oriented end-fire radiation. Chapter 4 focuses on applying SIW technology to design two novel wideband antennas whose bandwidth covers the entire E/W-band of interest (71-97 GHz). In this part of the work, one antenna radiates along the broadside to the substrate, while other antenna radiates substrate-oriented end-fire. Subsequently, Chapter 5 presents a novel broadband transition of SIW on high-to-low dielectric constant substrates. Chapter 6 presents a wideband 81-86 GHz receiver front-end that is integrated into package. Finally, the last chapter concludes the thesis work by highlighting and summarizing the key concepts and contributions developed in this work as well as the future work in connection with this research project.

CHAPTER 2 COMPACT COPLANAR WAVEGUIDE SPIRAL ANTENNA WITH CIRCULAR POLARIZATION FOR WIDEBAND APPLICATIONS

This chapter presents a compact, uni-planar, circularly polarized, coplanar waveguide (CPW) spiral antenna for wideband applications. The antenna is directly fed by a 50 Ω CPW from the outside edge of the spiral, thus a balun for matching is not required. This feed provides the capability to have an entire uniplanar array of spirals. It is found that a thick substrate of high dielectric constant absorbs most of the radiated power and results in a unidirectional radiation pattern, which is desirable in many applications. Therefore, this antenna structure is fabricated on a substrate of high dielectric constant, resulting in miniaturization and capability for integrated system applications. The proposed topology is desirable due to its uni-planar structure which offers easy fabrication at millimeter-wave frequencies. Due to the fabrication limitation at our lab, the antenna structure is re-designed and fabricated at Ku band to prove the concept. It is experimentally verified that the proposed spiral antenna has stable radiation pattern, and its axial ratio is less than 3 dB over the frequency range of 11.4-17.5 GHz.

2.1 Background and introduction

In fact, most of the materials used for fabricating integrated circuits present relatively high dielectric constants, which provide the capability of designing antennas for integrated system applications. Spiral antennas [40] have numerous applications due to their wide bandwidth and circular polarization. Unfortunately, unless integrated with differential circuits, they generally suffer from two main disadvantages. First of all, their input impedance is not 50 Ω, and thus a wideband balun for impedance matching is required. Secondly, the central feeding leads to a thickness that incurs high fabrication cost, especially at high frequencies. Also, the central feeding makes planar array design more of a challenge.

Although different microstrip spiral antennas were studied, as frequency increases, microstrip-based configuration suffers from serious losses especially in millimeter-wave bands [14]. Coplanar waveguide is desirable due to its high efficiency at millimeter wave frequencies, and also its unbalanced and uniplanar structure. Therefore, different structures of CPW-fed spiral

antennas with external feed have been reported [41]-[43]. Although these structures provide a wide impedance bandwidth, they present circular polarization over a relatively narrow bandwidth. An externally fed three-arm spiral antenna was proposed in [44]. This antenna has a circular polarization over the frequency range of 2.3 to 3.7 GHz. Increasing the dielectric constant of the substrate decreases the dimension of the antenna but, unfortunately, also increases the axial ratio. For a substrate with dielectric constant of 6.15, the axial ratio is more than 3 dB for circular polarization. To obtain a unidirectional radiation pattern, that spiral antenna must be mounted a quarter-wave length above the ground plane, thus introducing frequency dependence [44].

Therefore, this chapter presents a compact externally fed CPW spiral antenna which is designed on an Alumina substrate of dielectric constant of 9.8. MHMIC technology is used to fabricate the spiral antenna with good processing precision. The effect of radiation absorption of thick substrates with high dielectric constant [45], [46] is used to obtain a unidirectional radiation pattern. (Note that in [45], the high dielectric constant is foremost a consequence of integration with the CMOS fabrication process.) This simple method results in a thinner antenna compared to the technique that consists of mounting the circuit a quarter-wave length above the ground plane. The proposed method also provides a stable radiation pattern for wideband applications because it is no longer dependent on wavelength. A CPW feed is desirable due to its uniplanar structure, and it does not require a balun for impedance matching; moreover, it has a high efficiency at millimeter wave frequencies. Feeding from the outside edge of the antenna provides the design capability of a uniplanar antenna array and reduces the cost of fabrication, especially at millimeter wave frequencies. Experimental results show that the antenna is circularly polarized and has a stable radiation pattern over a wide portion of the Ku-band for various radar and communications applications.

2.2 Antenna design

The proposed antenna structure consists of a CPW line which curls up three times. This 50 Ω CPW line is tapered linearly to its 100 Ω counterpart at the center of the antenna, and is terminated by connecting a 100 Ω resistor. Top and 3D views of the spiral antenna are shown in Figure 2.1.

The maximum radiation occurs when currents in neighboring CPW lines are in phase. To achieve the in-phase condition with respect to neighboring lines, the length of one turn must be equal to one wavelength. This means that as frequency increases, the proposed antenna will become more intensively radiating at the part more contiguous to the center. If the length of one turn is equal to one wavelength, circularly polarized radiation will also take place because the radiated electric field from points A (Ey) and B (Ex), see Figure 2.1. , will be 90 degree out of phase. This can easily be expressed mathematically by using the following equation:

$$\lambda = \frac{c_0}{f\sqrt{\varepsilon_{eff}}} = \pi(R_1 + R_2) \qquad (2.1)$$

where R_1 and R_2 are, respectively, the small and large radius of the curved line, then radius of one turn is approximately the average of R_1 and R_2. And ε_{eff} is the effective dielectric constant. This expression suggests that the size of the antenna has an inverse relationship with $\sqrt{\varepsilon_{eff}}$.

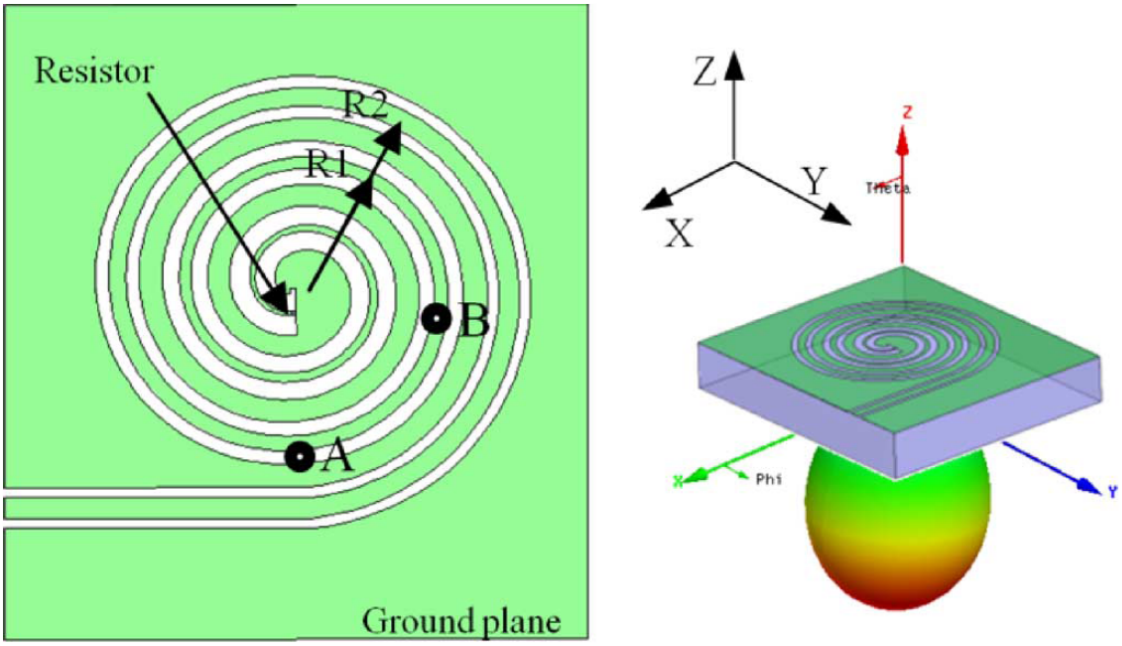

Figure 2.1. Geometry and 3-D view (including radiation pattern) of the CPW fed spiral antenna

The radiation mechanism of the antenna is based on phase difference in two gaps, beside of the signal line of the curved CPW line, which creates common mode propagation. To increase the

radiation efficiency and decrease the power level reaching the center of the antenna, the impedance of the CPW line is increased from 50 Ω at the outside of the spiral to 100 Ω at its center. Increasing the line impedance decreases the ground plane width and puts two CPW lines closer together. This would potentially generate higher-order modes. However, our simulation results suggest that their effects are in fact negligible. These simulation results are beyond the scope of this work and thus are not shown here.

Figure 2.2. illustrates the effect of the high dielectric constant (9.8) substrate thickness (T) on the front to back radiation ratio of the Ku-band CPW spiral antenna, as analyzed by Ansoft HFSS software. Figure 2.2. suggests that by increasing the thickness of the substrate to 1.75 mm, most of the radiated energy is concentrated inside the dielectric, and a unidirectional radiation pattern is thus obtained. The effect of radiation absorption of thick substrates with high dielectric constants is illustrated in detail in [45]. Alumina is of interest for this antenna design due to its high dielectric constant (9.8) and low dielectric losses (tan δ=0.0001).

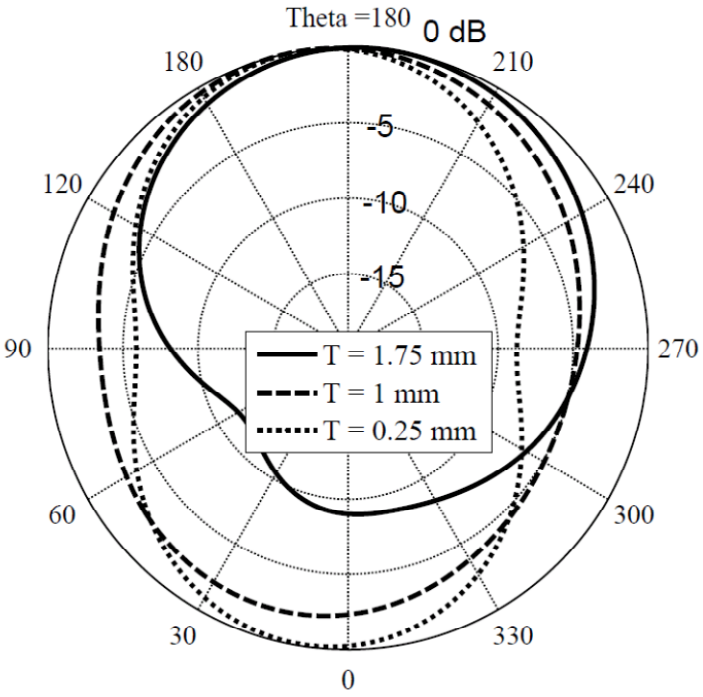

Figure 2.2. Impact of the high dielectric constant (9.8) substrate thickness (T) on the front to back radiation ratio of the compact CPW spiral antenna at 14.5 GHz.

Figure 2.3. illustrates how the axial ratio of the antenna is dependent on the thickness of the substrate and loading at the end of the CPW line. We consider four cases: with and without resistor at T=1.75 mm, and with resistor at T=1mm and 0.25 mm. As shown in Figure 2.3. , the thickness of the substrate with high dielectric constant has significant effect on the axial ratio of the spiral antenna. The best axial ratio of the antenna (1 dB at 12 GHz) is obtained by utilizing the 1.75 mm thick substrate.

Consequently, using a thick substrate with high dielectric constant decreases the axial ratio and the dimensions of the antenna; it also provides a unidirectional radiation pattern which is suitable for many applications.

Figure 2.3. also shows the effect of loading the end of the CPW line with a 100Ω resistor. Without this termination, the reflected waves increase axial ratio, because they radiate in the opposite circular polarization. The 100 Ω termination limits the reflection of waves at the end of the CPW. Terminating the CPW line has a significant effect on reducing the axial ratio although it also decreases the radiation efficiency of the antenna. The effect of loading on the radiation efficiency at different frequencies is dependent on the portion of the wave that reaches the end of the CPW line. Figure 2.4. illustrates this effect. The simulated efficiency of the loaded spiral antenna is more than 72% within the operating frequency of the antenna. Note that all dielectric, metallic, and mismatch losses have been considered in the simulations.

When designing antennas on high dielectric constant substrates, the excitation of surface waves might decrease the efficiency of the antenna and also cause side lobes. However, a comparison of radiation efficiency of the proposed compact spiral antenna in Figure 2.4. with the efficiencies of similar spiral antennas on low dielectric constant substrate, shows that the efficiencies are similar and that side lobes are absent in the simulated radiation patterns.

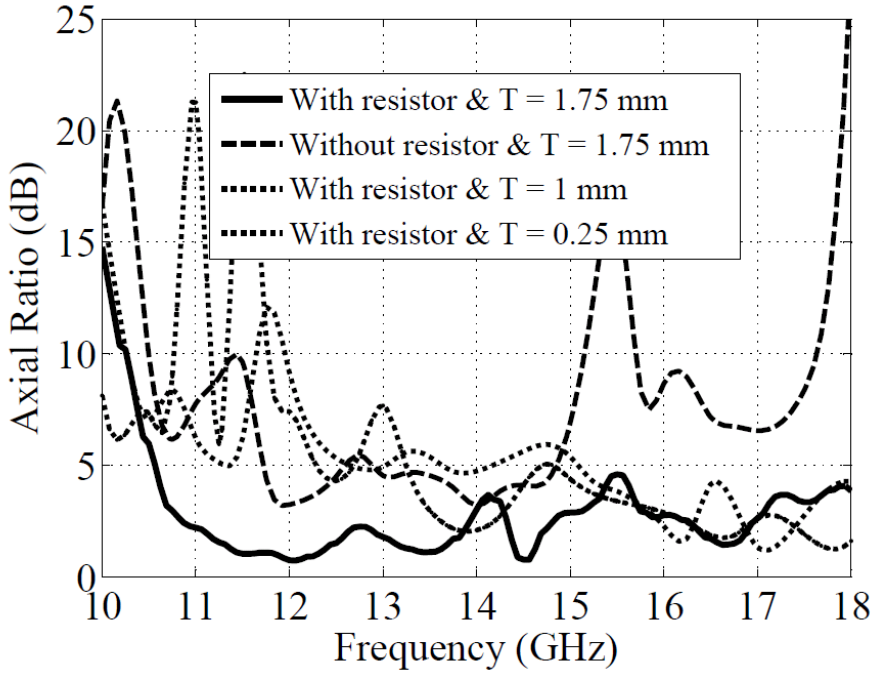

Figure 2.3. Effect of CPW line termination and thickness of the substrate (T) on the axial ratio of the compact CPW spiral antenna.

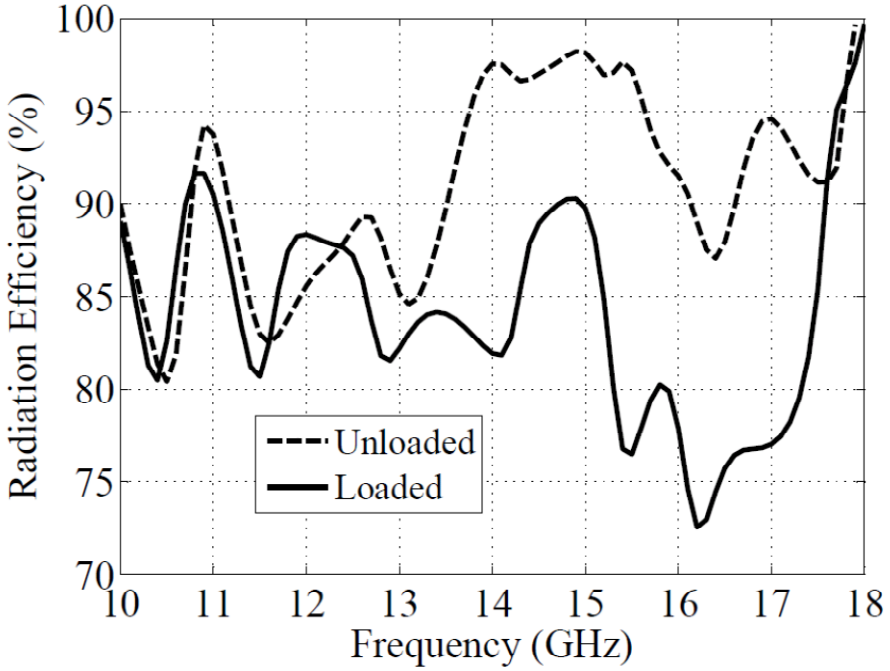

Figure 2.4. Effect of CPW line termination on the radiation efficiency of the compact CPW spiral antenna.

The width of the CPW signal line at the outside edge of the antenna is 0.3 mm which is tapered linearly to a 0.05 mm width at the center of the antenna in order to increase the impedance of the CPW line from 50 Ω to 100 Ω. The results show that the proposed structure can be used as a circularly polarized compact spiral antenna for wideband application in millimeter-wave frequency bands. To verify the antenna structure, a Ku-band spiral antenna was designed, simulated and measured, as shown in the next section.

2.3 Fabrication and Measurement Results

MHMIC technology, a promising technology for small scale production, is used to fabricate the proposed spiral antenna on 20 mil (0.508 mm) thick Alumina substrate. The dielectric loss tangent of this Alumina substrate is 0.0001 (at 10 GHz). A 9 mm ×7.5 mm rectangular Rogers/duroid 6010 substrate of 50 mil (1.270 mm) thickness with a dielectric constant of 10.2 is attached to the 20 mil Alumina substrate to increase the thickness of the substrate to 70 mil (1.8 mm). Note that the effect of adhesive between the layers is included in the simulation results. The spiral antenna is fabricated from a 1 μm thick gold film on the ceramic substrate (Figure 2.5.).

The 100 Ω resistor is fabricated from a thin film of Ti. Its location is shown in the inset of Figure 2.5. a. The dimensions of the resistor are 150 μm × 150μm and 20 nm in thickness. A micro-photograph of the top view of the fabricated spiral antenna, the surface resistor and a 3-D view are shown in Figure 2.5. Measured and simulated return losses of the compact spiral antenna are plotted in Figure 2.6. over the 10-20 GHz frequency range. The return loss was measured using an Anritsu 3739C vector network analyzer. The discrepancy between the simulated and measured results is attributed to the proximity of the test fixture (Anritsu 36801K right angle) to the antenna, although the test fixture was covered with a thin absorber (see Figure 2.5. b).

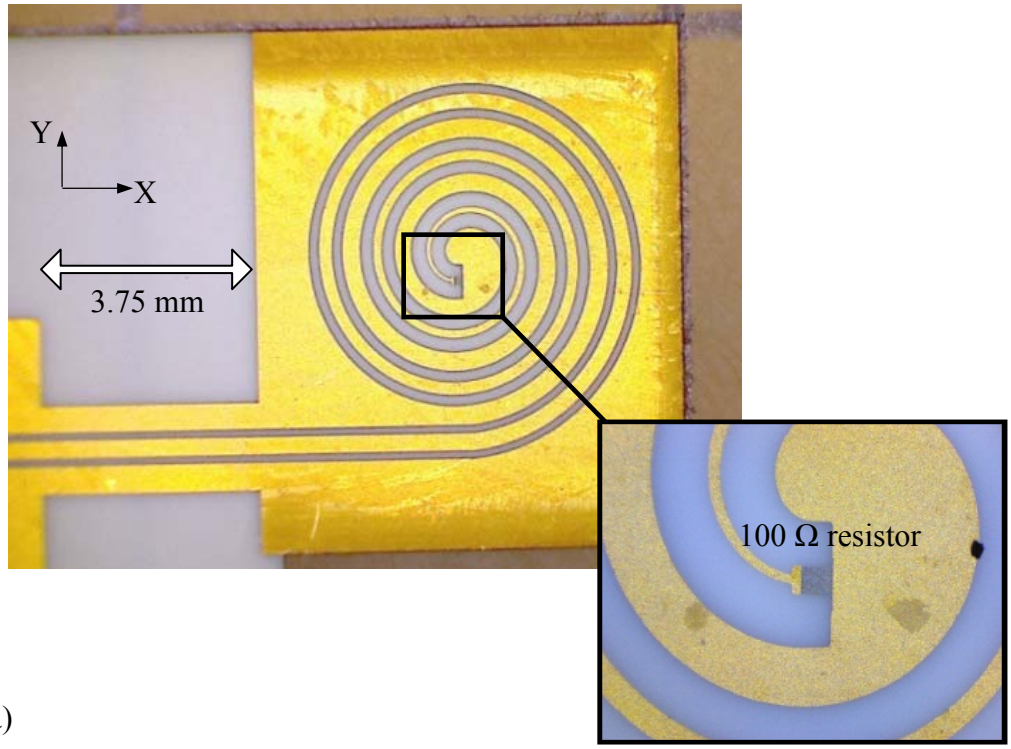

(a)

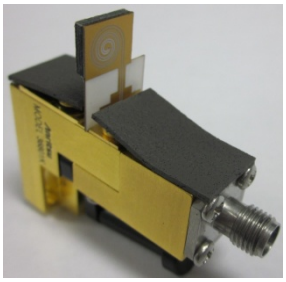

(b)

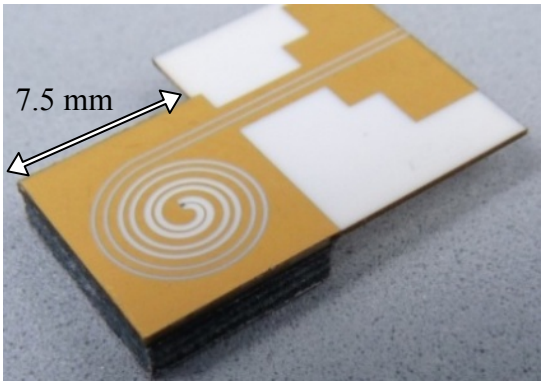

(c)

Figure 2.5. Micro-photograph of the fabricated compact spiral antenna using MHMIC technology; (a) top view, (b) 3-D view with test fixture, (c) 3-D view.

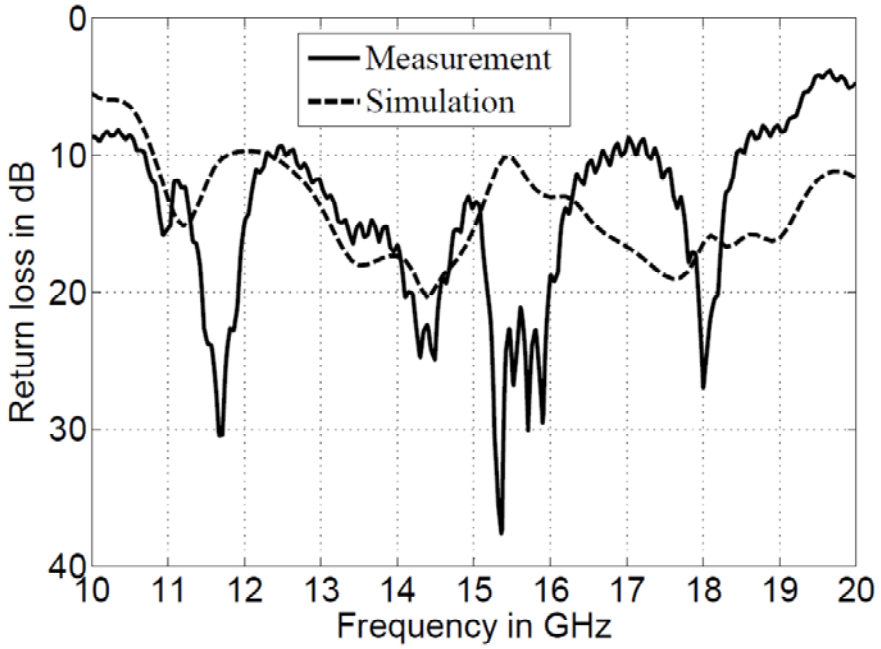

Figure 2.6. Measured and simulated return losses of the compact spiral antenna.

Figure 2.7. shows simulated and measured gains of the compact spiral antenna over the frequency range of 11-18 GHz. In the gain measurement setup, the frequency step is 0.2 GHz. The reference plane is the YZ plane (c.f. Figure 2.1.) for both simulations and measurements. Note that dielectric and metallic losses are included in the simulated gain of the antenna. The measured gain is determined at an elevation angle of $\theta = 180°$. As the gain measurements suggest, the use of a high dielectric constant thick substrate allows a relatively constant gain within a wide bandwidth from 11.5-17.5 GHz. This frequency range is used for numerous applications in radars and communications.

Figure 2.8. compares the measured and simulated axial ratios of the compact spiral antenna. The magnitude at two orthogonal states is used to calculate the axial ratio of the antenna. The measured axial ratio of the antenna is less than 3.3 dB over the frequency range of 11.4-18 GHz. The discrepancy between the simulation and measurement is attributed to the effect of the test fixture that has been used to feed the antenna in our anechoic chamber.

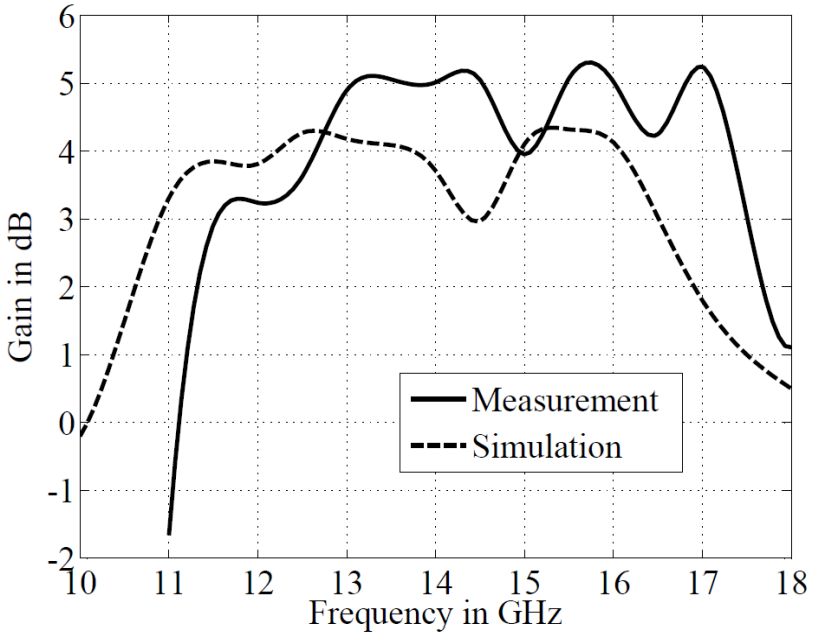

Figure 2.7. Measured and simulated gains of the compact spiral antenna.

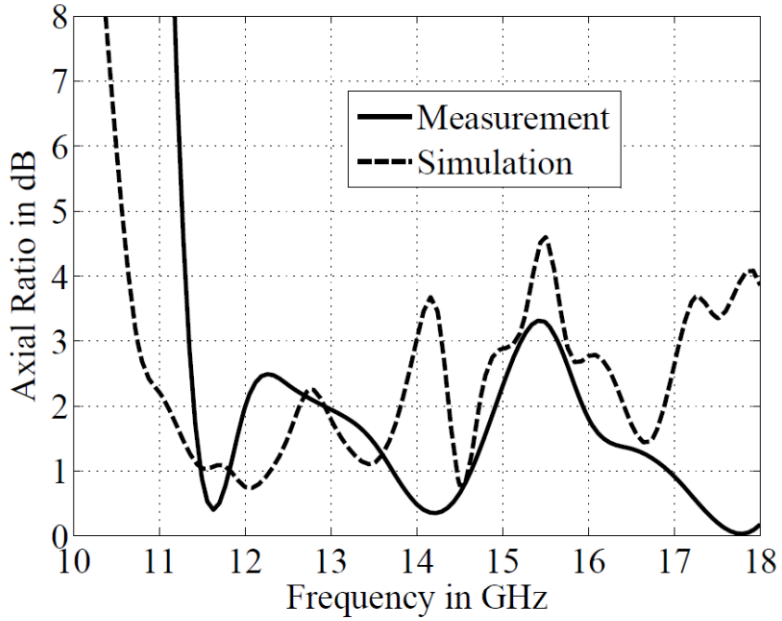

Figure 2.8. Measured and simulated axial ratios of the compact spiral antenna.

Measured (in YZ plane) and simulated (in both YZ and XZ planes) radiation patterns of the compact spiral antenna are shown in Figure 2.9. The measured radiation pattern of the antenna has around 10 dB front to back ratio. This suggests that most of the power is concentrated within the substrate due to the high dielectric constant, and a stable unidirectional radiation pattern is obtained over a wide bandwidth. The test fixture that has been used to feed the antenna in the

anechoic chamber has an effect on the radiation pattern, especially at θ = 100° and θ = 255°. This is because the size of the antenna is small and the antenna is too close to the test fixture, which inevitably has effects on the radiation.

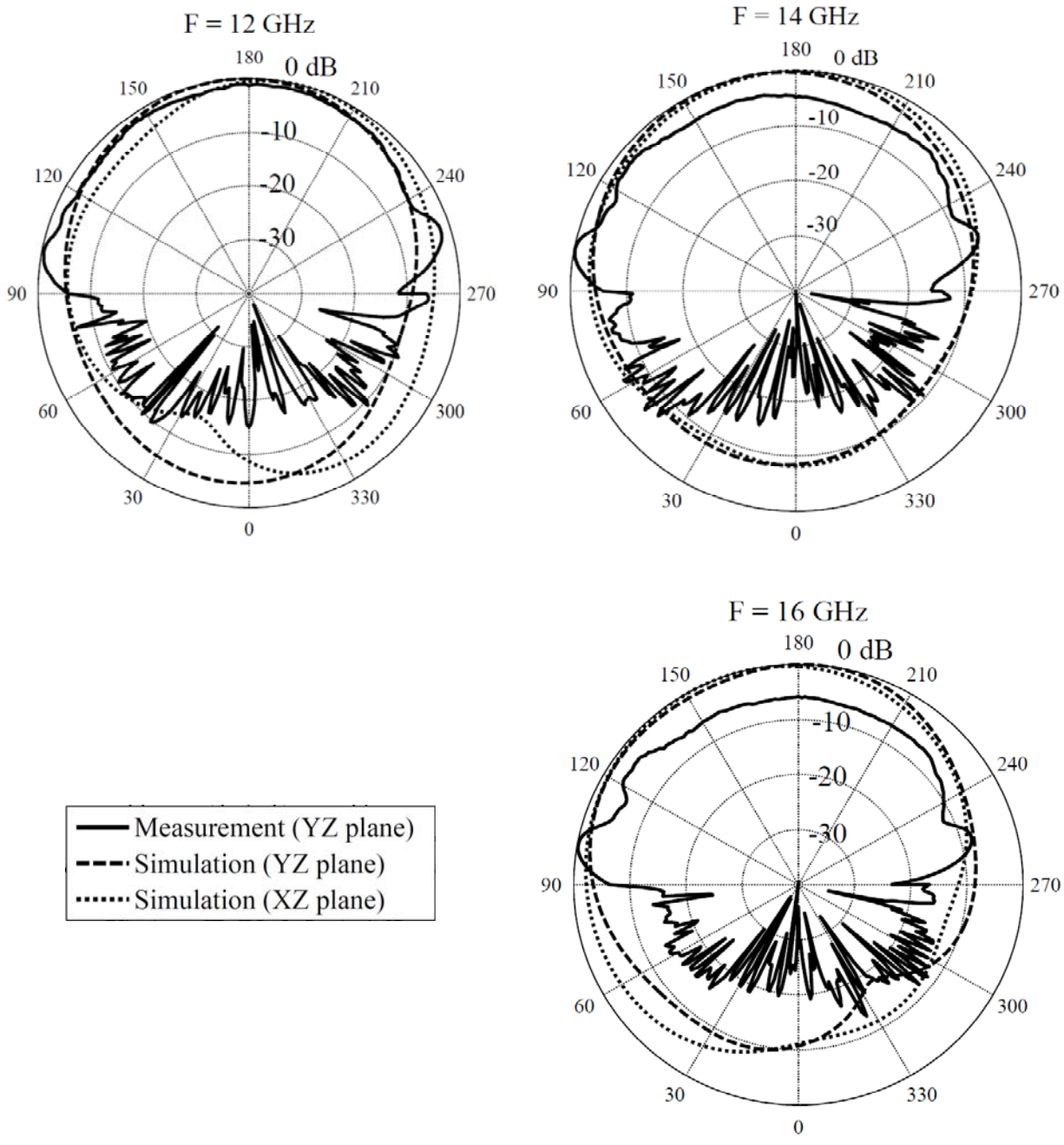

Figure 2.9. Measured CP radiation pattern of the compact spiral antenna at frequencies of 12, 14 and 16 GHz.

2.4 Conclusion

A new compact spiral antenna is designed and validated both theoretically and experimentally. A CPW feed from the external edge of the antenna has been used to excite the antenna. The proposed topology is desirable due to its uniplanar structure which offers easy fabrication at millimeter-wave frequencies. The second advantage of using CPW is low radiation losses at high frequency compared to microstrip lines. This spiral antenna does not require a balun due to the unbalanced CPW feed. The use of a substrate with high dielectric constant has effectively reduced the antenna size. It is found that a thick substrate of high dielectric constant absorbs most of the radiated power and results in a unidirectional radiation pattern, which is desirable in many applications. This antenna structure is fabricated on a substrate of high dielectric constant, resulting in miniaturization and capability for integrated system applications. It is experimentally verified that the proposed spiral antenna has stable radiation pattern, and its axial ratio is less than 3 dB over the frequency range of 11.4–17.5 GHz. It is shown that using a thick substrate and terminating the CPW at the center of the spiral antenna decrease the axial ratio. Nearly constant unidirectional radiation patterns over a wide bandwidth are obtained with a thick substrate of high dielectric constant.

Next chapters will present antennas with higher gain and efficiency which are more appropriate for E band gigabyte point to point wireless communication. The goal of the following chapters is presenting some antennas with novel structures to be able to fabricate them at E band with low cost PCB fabrication process.

CHAPTER 3 LOW-COST AND HIGH-EFFICIENT ANTENNA FOR W-BAND APPLICATIONS

This chapter presents two novel low cost, high gain and high efficient antennas for applications over W-band, e.g. 94-97 GHz in our case. The first antenna is a 4×4 antenna array that is designed on a low dielectric constant substrate and it radiates along the broadside to the substrate. The second antenna is a dielectric rod antenna designed on a high dielectric constant substrate and it features a substrate-oriented end-fire radiation.

3.1 Low-Cost and High-Efficient E-Band SIW Antenna Array Made of Printed Circuit Board Process

A novel class of low-cost, small-footprint and high-gain antenna arrays is presented in this section for applications over the E-band and beyond. A 4×4 antenna array is proposed and demonstrated using SIW technology for the design of its feed network and longitudinal slots on the SIW top metallic surface to drive the array antenna elements. Rectangular cubes of low-permittivity material are placed on top of each 1×4 antenna array to increase the gain of the circular patch antenna elements. This new design is compared to a second 4x4 antenna array which, instead of dielectric cubes, uses vertically stacked Yagi-like parasitic director elements to increase the gain. Measured impedance bandwidths of the two 4×4 antenna arrays are about 7.5 GHz (94.2-101.8 GHz) at 19 dBi gain level, with radiation patterns and gains of the two arrays remaining nearly constant over this bandwidth. While the fabrication effort of the new array involving dielectric cubes is significantly reduced, its measured radiation efficiency of 81 percent is slightly lower compared to 90 percent of the Yagi-like design.

3.1.1 Overview and introduction

Due to its directive radiation pattern, the Yagi antenna has been widely applied in the design of communication systems. However, it requires a boom to structurally support individual antenna elements [47]. To avoid the use of a boom, printed Yagi antennas were demonstrated in X band [48]-[49], with radiation in a plane parallel to the substrate. However, such antennas have a very large footprint. In many applications, an antenna is desired to have a broad radiation pattern in the plane perpendicular to the substrate. Therefore, an interesting approach is to use stacked director elements in a Yagi-like arrangement to increase the gain of printed antennas [50]. Later, this technique has been used in a multilayer Yagi-like microstrip antenna at 31 GHz [51], a dipole stacked Yagi antenna at 5.8 GHz [52], a dual polarized circular patch Yagi antenna at 5.8 GHz [52] and a stacked Yagi antenna at 60 GHz [53] with a very small footprint.

In this section, we present a different design technique of low-cost and high-efficiency 4×4 antenna array for E/W-band applications over the range of 94.1-97 GHz. SIW technology is used to feed the antenna elements through longitudinal slots etched on the top metallization of the SIW. The main difference compared to a similar Yagi-like array [53], which has been redesigned and is also presented for comparison, is that the original multi-layered Yagi arrangement is replaced by a dielectric block, thus significantly simplifying the fabrication process while the characteristics of the antenna array remain almost the same. Compared with previously reported millimeter-wave SIW slot antennas [54]-[56], the antenna structures proposed and developed in this section can result in higher gain, larger bandwidth and higher radiation efficiency with a more stable (less dispersive) gain within the operational bandwidth.

3.1.2 Design of 4×4 antenna arrays

The proposed 4×4 W-band antenna array consists of four 1×4 antenna arrays as shown in Figure 3.1. Each 1×4 element has three basic layers. The bottom layer is the SIW feed network of the antenna, which is designed using a 20 mil Rogers/Duroid 6002 substrate. It is shown in Figure 3.2 for the entire 4×4 array including the one-to-four power divider. The four circular antenna elements in Figure 3.1 are fed in phase by four longitudinal, linearly polarized slots on the top metallization of the SIW. Their centers are half a wavelength apart, which amounts to

1.375 mm at the center frequency of 97 GHz. All the dimensions of the antenna are illustrated in Table 3.1. The SIWs are terminated by short circuits that are three quarter wavelengths away from the center of the last slot in order to align the slots at the peaks of the standing wave in the SIW. The design procedure is similar to the work presented in [55], and the reader is referred to [55] for further details.

The middle layer consists of circular patches of diameter D1 that are placed over slots on an Ultralam 3850 substrate of thickness S1 and dielectric constant of 2.9. The resonant frequency of the patches depends on the patch diameters and the dielectric constant of their top and bottom layers [57]. To reach the maximum gain and bandwidth, the dimension of the circular patches, the slots, and the thickness of Ultralam 3850 substrate are optimized with Ansoft HFSS.

The top layer of the 1×4 array is a rectangular dielectric cube with relative permittivity of 2.2, which is placed on top of the patches to increase the gain of the antenna. It is found that width W and thickness S2 (c.f. Figure 3.1) of this dielectric cube have a strong effect on the radiation pattern and gain of the antenna. Figure 3.3 shows the simulated gain versus width W of the dielectric rectangular cube at different thicknesses S2 of the array. It is shown that the maximum gain of 14 dBi is obtained using the dielectric rectangular cube with dimensions S2 = 2 mm and W = 1.24 mm, instead of 11 dBi without the dielectric cube. Therefore, a 3 dB gain increase is obtained through the addition of a dielectric rectangular cube. The effect of the dimension of the dielectric on the bandwidth of the antenna is negligible. Note that the mentioned simulated gain is based on IEEE gain.

Figure 3.4 shows the normalized radiation pattern of the antenna with and without the dielectric rectangular cube (W = 1.24 mm). It is observed that the antenna's directivity is increased by adding the rectangular dielectric cube.

Simulated |S21| and |S11| of the Y- and T-shaped junctions are shown in Figure 3.5. It is noted that the T junction leads to a higher reflection coefficient than the Y junction due to the existence of 90 degree bends in this structure. In order to decrease the mutual coupling between the four 1×4 arrays, they are separated by a distance equal to 0.95λ. Due to the high directivity of the 1×4 arrays, the level of grating lobes, which results from an increase in separation between 1×4 arrays from 0.5λ to 0.95λ will be less than the side lobe level.

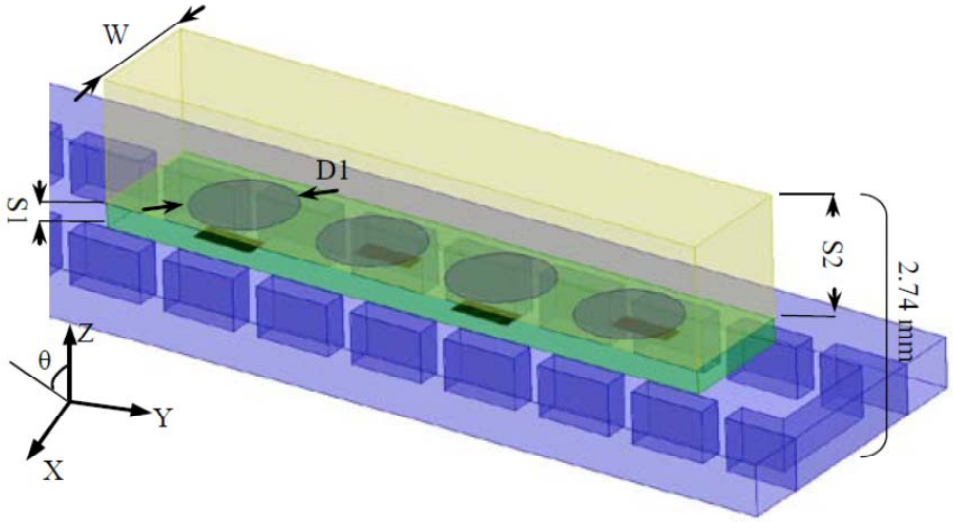

Figure 3.1. Layout of a 1×4 antenna array (S1 = 0.1 mm, S2 = 2 mm, and D1=0.75 mm)

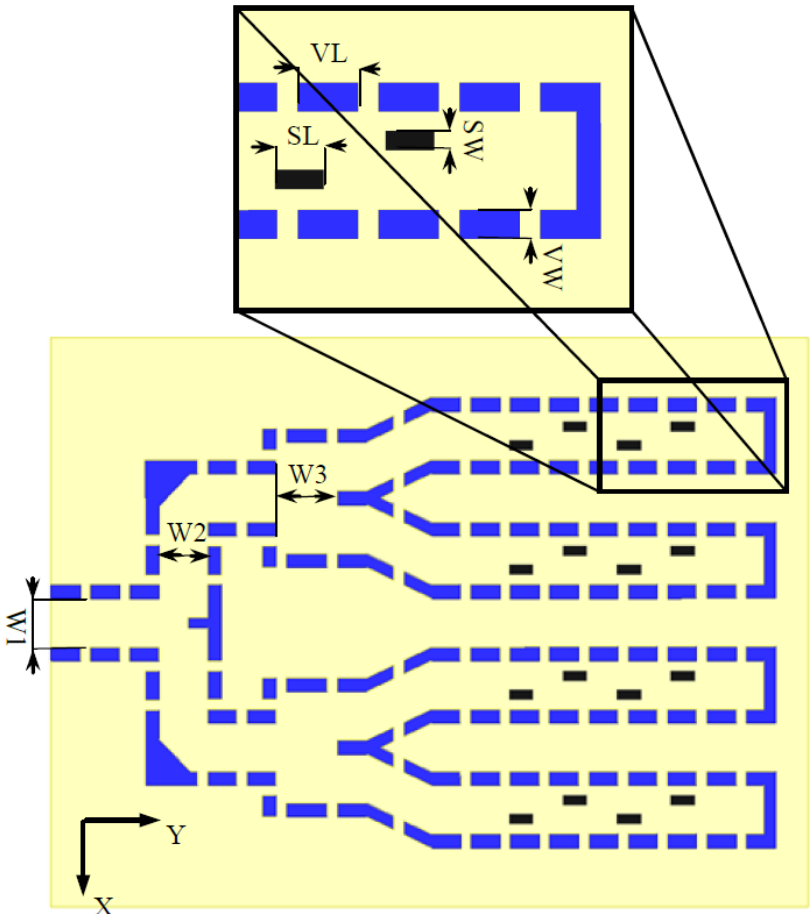

Figure 3.2. Layout of the 4×4 power divider and dimensions of the slots.

Table 3.1: Dimensions of the 4 ×4 antenna array

Symbol	Value (mm)	Symbol	Value (mm)
G1	0.1	VL	0.75
G2	0.25	W	1.24
D1	0.75	W1	1.24
SW	0.24	W2	1.24
SL	0.6	W3	1.55
VW	0.254		

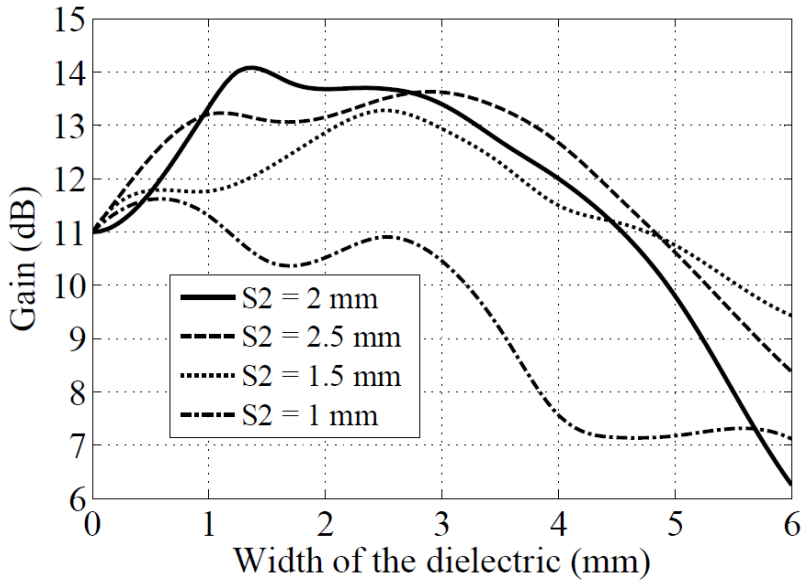

Figure 3.3. Gain at 97 GHz versus width W of the rectangular dielectric cube at thicknesses (S2) of 1, 1.5, 2, and 2.5 mm for a 1×4 array antenna. Note that dielectric or metallic losses are not considered in this simulation.

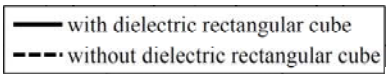

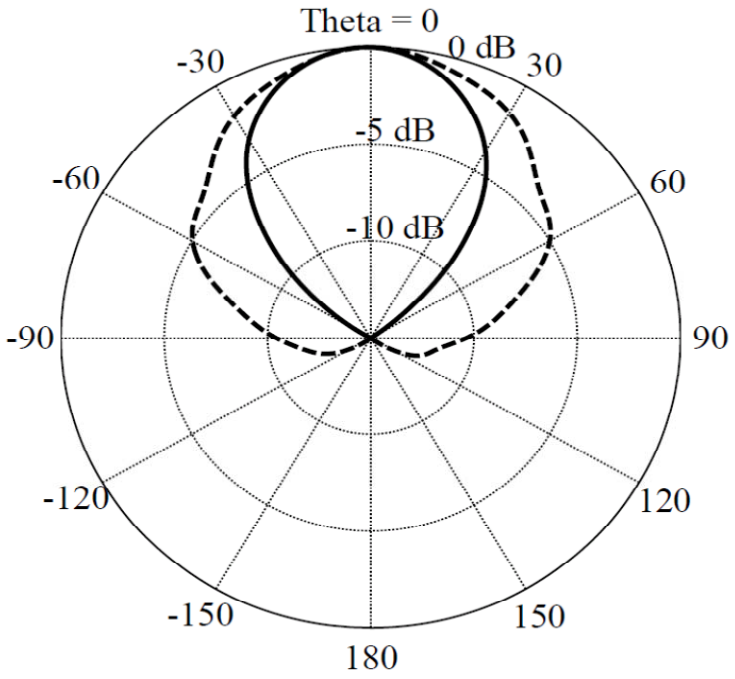

(a)

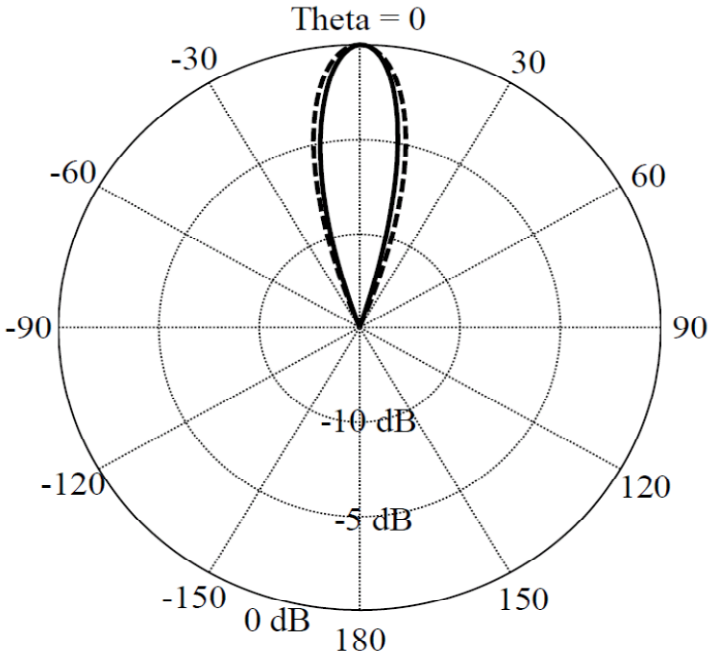

(b)

Figure 3.4. Radiation pattern in (a) XZ plane, (E plane), (b) YZ plane (H plane), (c.f. Figure 3.1) of the 1×4 antenna array considering the effect of the rectangular dielectric cube. Solid: with dielectric rectangular cube, and dashed: without dielectric rectangular cube.

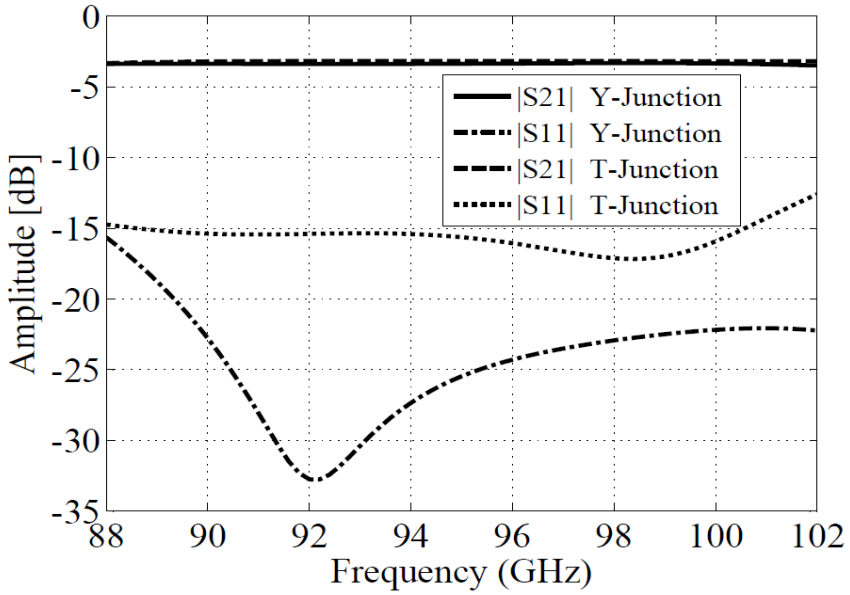

Figure 3.5. Simulated |S11| and |S21| of the T-shaped and Y-shaped junctions.

Figure 3.6 illustrates the effect of the circular patches and dielectric rectangular cube on gain (Figure 3.6a) and |S11| (Figure 3.6b) of the 4×4 antenna array. It is shown in Figure 3.6b that the bare slot array (structure of Figure 3.1 without the rectangular dielectric cube and circular patches) has one resonant frequency with 3% impedance bandwidth. By adding the circular patches on the top of the slots (structure of Figure 3.1 without the rectangular dielectric cube), the bandwidth of the structure is increased. Although adding the circular patches does not have a significant effect on the gain of the antenna, it increases the bandwidth to 7.2% (7 GHz). Figure 3.6a also shows that adding the dielectric rectangular cube on top of the patches increases the gain of the antenna array by 3.5 dB. Figure 3.6b shows that the dielectric rectangular cube does not have a significant effect on bandwidth of the antenna. For the above investigation of the effect of patches and rectangular dielectric cubes, the dimensions of the patches and slots are changed to be compatible with the structure because the resonant frequency of the circular patch depends on the dielectric constant of the top and bottom layers.

Note that for the slot array and the structure without the dielectric rectangular cube, metallic and dielectric losses are considered in the simulation. Simulated results show that including metallic loss decreases the gain of the antenna array by 0.14 dB while including dielectric loss decreases the gain by 1.18 dB; both losses do not reduce the bandwidth. To estimate the dielectric loss tangent of the substrate at 94 GHz, two different lengths of SIW are used; one to calibrate the vector analyzer, and the other to estimate the total loss. Then, HFSS

(a)

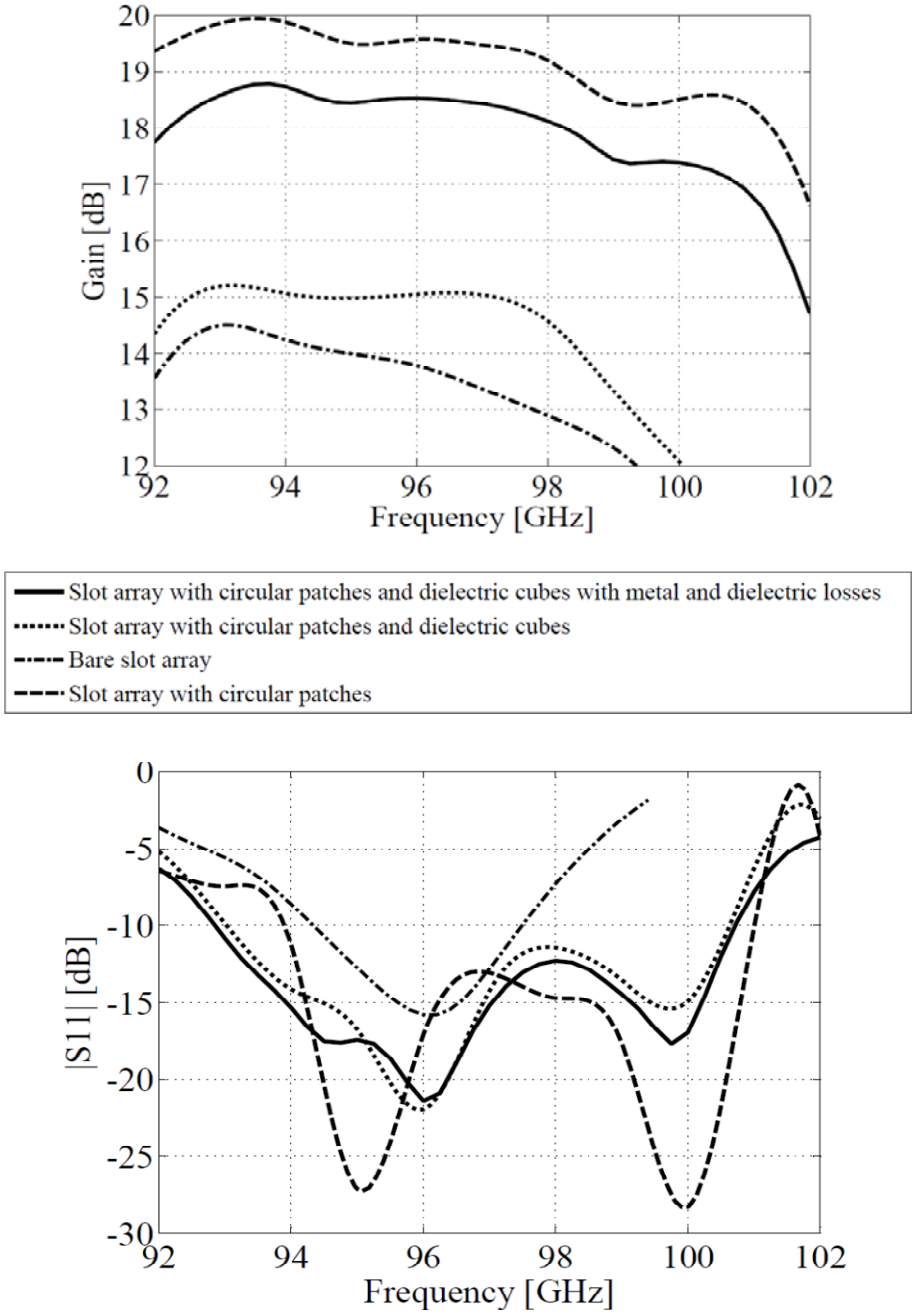

(b)

Figure 3.6. Simulated gain (a) and |S11|, (b) of the 4x4 antenna array considering the effect of the dielectric and metallic losses.

software is used to compare the simulated |S21| with the measured results. This method was used in [26] to estimate the dielectric loss tangent at 60 GHz. It is concluded that the metallic and dielectric losses do not have a significant effect on the bandwidth of the antenna array. However,

it is found that the radiation efficiency is decreased from 97% to 85% due to the dielectric and metallic losses.

In order to compare the 4×4 W-band array with an antenna using a different top layer, another array based on a vertically stacked Yagi-like antenna has been designed and demonstrated in this work. The design procedure is similar to [53] with the exception that instead of circular disks, circular rings are employed as directors [53]. The layout of a 1×4 W-band array is shown in Figure 3.7.

The bottom and second layers are identical to those previously presented in this section. The ring-shaped director elements are vertically stacked over the circular patch. The director elements are used to increase the gain of the circular patch and provide a nearly constant radiation pattern across the bandwidth of the antenna. The radius of the directors and spacing between the directors are optimized using Ansoft HFSS. Detailed design procedures are similar to those presented in [50]-[53]. The director elements are etched on low-cost Rogers/Duroid 5880 substrate with thickness of $o.12\lambda_d$ (G2=10 mil) and dielectric constant of 2.2. All the dimensions of the antenna are illustrated in Table 3.2.

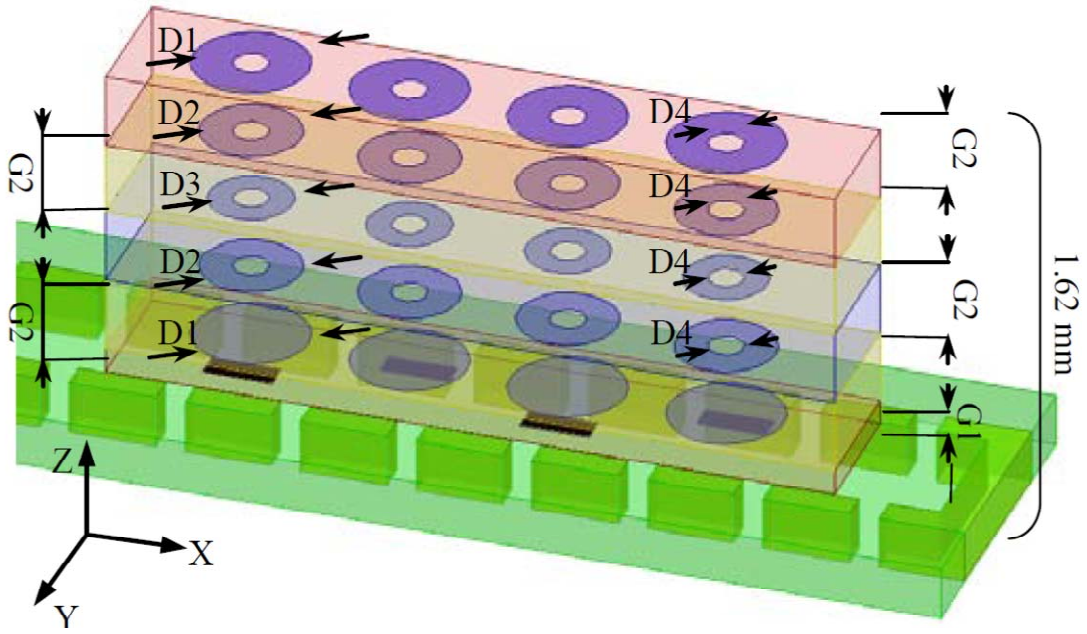

Figure 3.7. Layout of the 1×4 vertically stacked Yagi-like antenna array.

Table 3.2: Dimensions of the 4 ×4 Yagi-like antenna array (unit: mm)

Symbol	Value (mm)
G1	0.1
G2	0.25
D1	0.75
D2	0.65
D3	0.64
D4	0.3

3.1.3 Fabrication and measurement of 4×4 antenna arrays

A low-cost standard PCB process is used to fabricate the proposed 4×4 antenna array with dielectric blocks. Figure 3.8 shows the top view (Figure 3.8a), the bottom view (Figure 3.8b) as well as the array under test including the WR10-to-SIW transition (Figure 3.8c). The SIW feed network is fabricated on a rectangular (30 mm × 20 mm) Rogers/Duroid 6002 substrate. The simulated and measured SIW losses are 0.52 dB per cm at 94 GHz. The rectangular dielectric cubes are made up of two layers of low-cost Rogers/Duroid 5880 substrates, one 20 mil thick and the other 60 mil thick. The two layers are glued together to achieve the desired thickness of 80 mil. The adhesive is an epoxy with dielectric constant of 3.5 and its thickness is less than 5 μm. Note that the effect of the adhesive is considered in the simulation results of this work. To avoid the excitation of surface waves, linear arrays of metallic via holes are placed around the dielectric rectangular cubes.

The |S11| of the prototype antenna is measured by using an Anritsu 3739C vector network analyzer. A wideband transition between rectangular waveguide (WR10) and SIW (e.g. [60], [61]) is used to measure the antenna parameters. Figure 3.9 shows the measured |S11| performance. The measured bandwidth is 7.6 GHz (94.2-101.8 GHz) which is similar to the simulation results.

This value of 7.7% bandwidth represents a considerable improvement to what was previously reported, e.g. 2.7 percent [54], 4.1 percent [55], and 2 percent [56]. As shown in Figure 3.9, a frequency shift of about 1.4% towards higher frequencies occurs. It has been shown that the resonant frequencies of the slots in the SIW slot antennas are very sensitive to the positioning of the slots [56]. It has also been indicated that the measurement probes can cause frequency shifts at 60 GHz [59]. The observed discrepancy between the simulated and measured |S11| results can be attributed to the combined effect of inaccuracy of the patches and slot placement, the WR10 to SIW transition, and the inaccuracy of the dielectric constant. This frequency shift will be taken into account in plotting radiation patterns and gain; i.e., the measured radiation pattern is plotted at 97 GHz in comparison with the simulated radiation at 95.6 GHz.

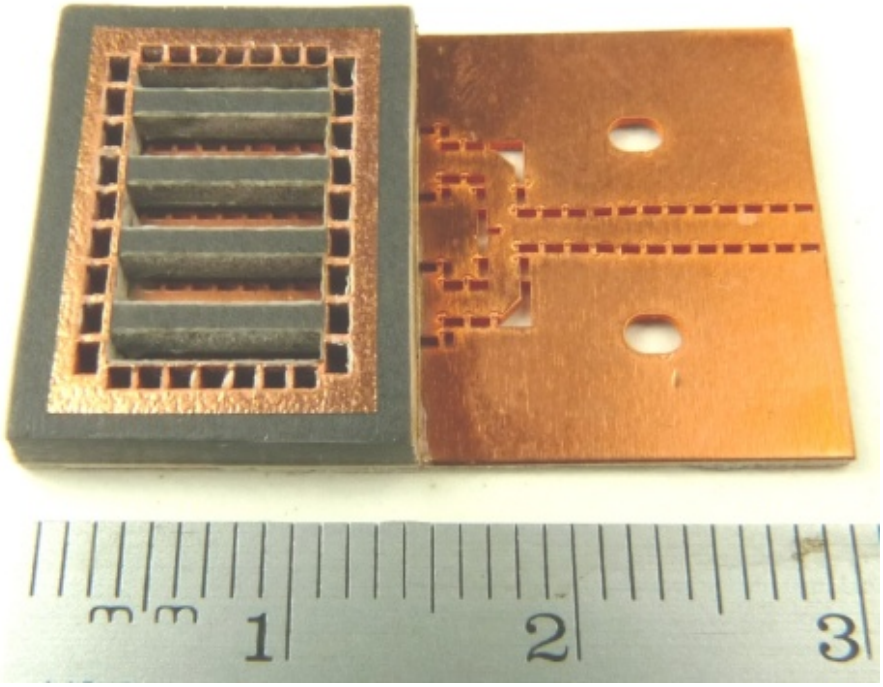

(a)

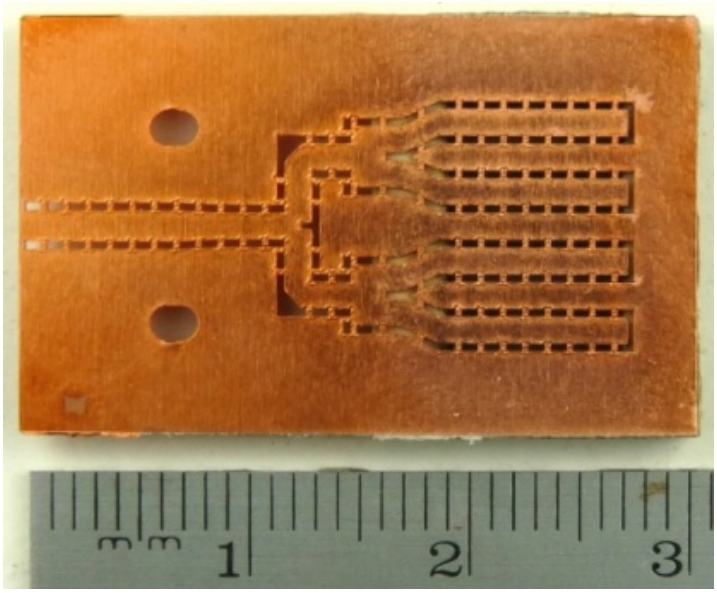

(b)

(c)

Figure 3.8. Photograph of the fabricated 4x4 antenna array with dielectric cubes; (a) top view, (b) bottom view, (c) antenna under test.

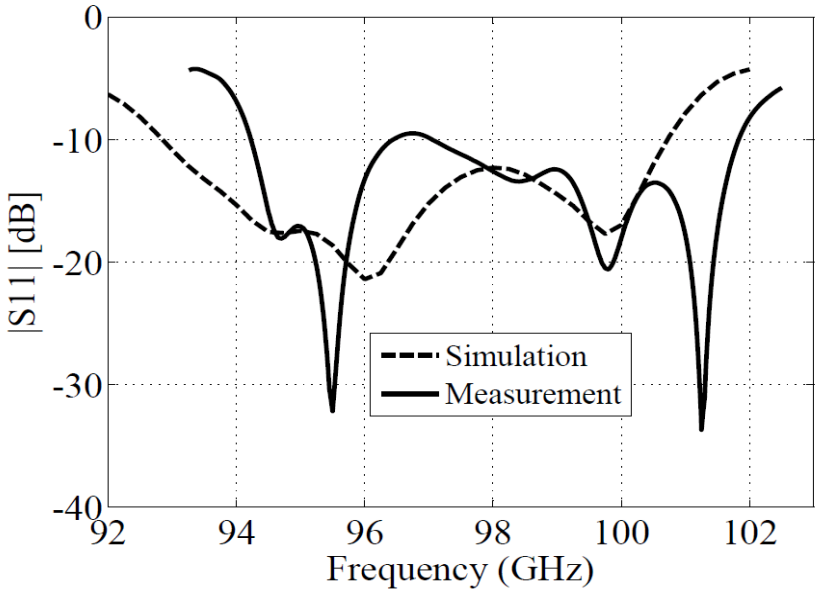

Figure 3.9. Measured and simulated reflection coefficients of the 4×4 antenna array with dielectric cubes.

Figure 3.10 shows the measured E- and H-plane radiation patterns at frequencies of 95.25, 97, 98.75 and 100.5 GHz, respectively. Good agreement can be observed between simulated and measured patterns. The side lobe level is less than 13 dB in both E- and H-planes.

As shown in Figure 3.10, there are discrepancies between the measured and simulated radiation patterns, especially in the H-plane. These discrepancies are caused by the combined effect of the fabrication inaccuracy and the waveguide to SIW transition (c.f. Figure 3.8c). One of the advantages of this antenna is that a constant gain of 18 ±0.75 dB is obtained over the ~7.5 GHz bandwidth. In addition, the measured cross polarization of less than 23 dB is obtained over the bandwidth of 7.5 GHz. The estimated radiation efficiency from the measured gain and directivity, e.g. [55], is 81% at 95.25 GHz, while the simulated radiation efficiency is 85%. Note that the dielectric, metallic, and mismatch losses have been considered in the simulation results.

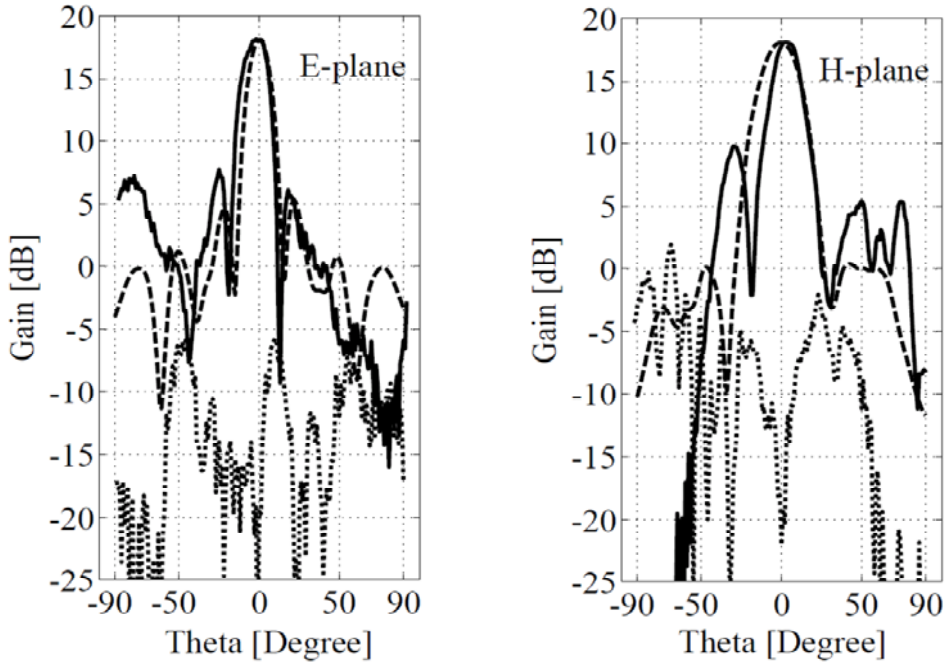
E-plane
H-plane
Gain [dB]
Theta [Degree]
20
15
10
5
0
-5
-10
-15
-20
-25
-90
-50
0
50
90

(a)

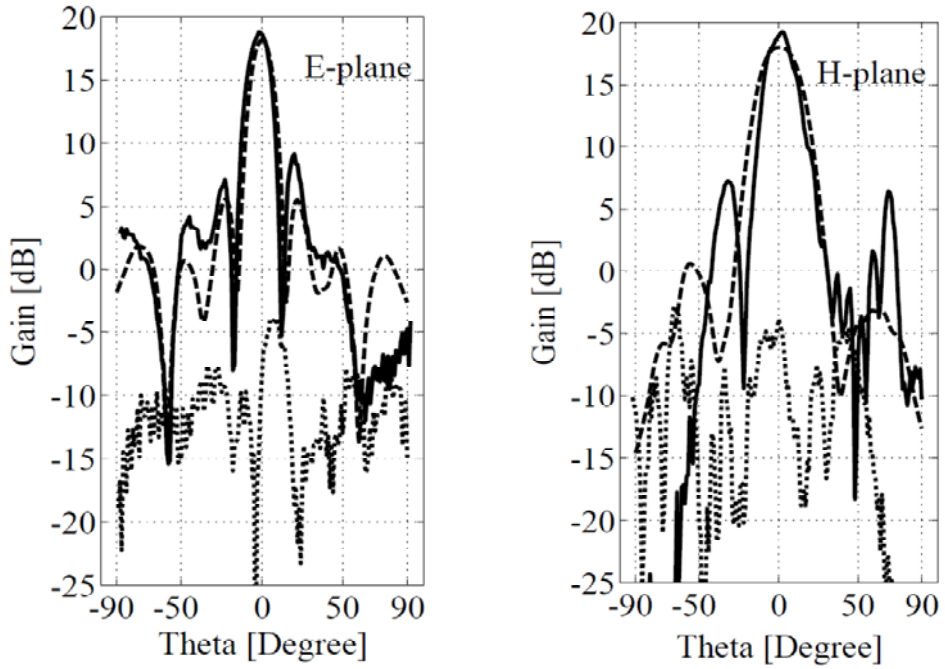
E-plane
H-plane
Gain [dB]
Theta [Degree]
20
15
10
5
0
-5
-10
-15
-20
-25
-90
-50
0
50
90

(b)

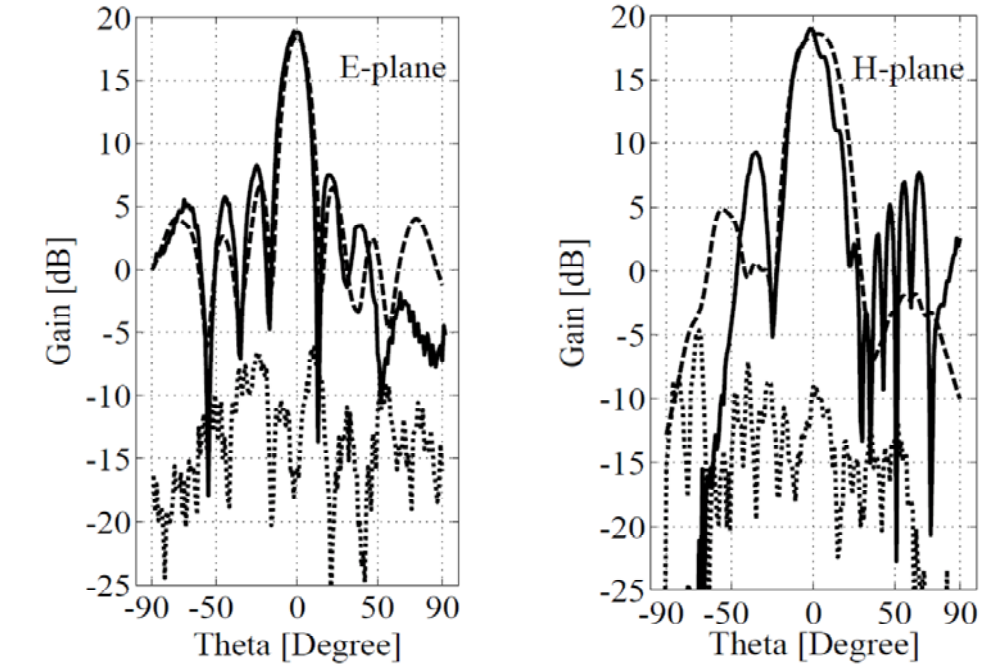

(c)

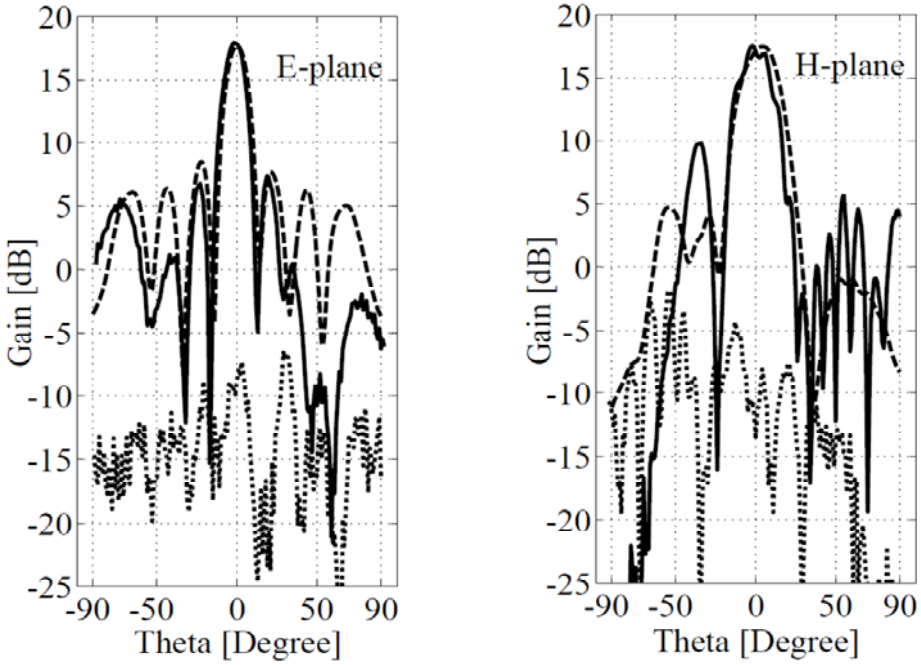

(d)

Figure 3.10. Simulated and measured co-polarization and measured cross-polarization patterns in the E- and H-planes at (a) 95.25 GHz, (b) 97 GHz, (c) 98.75 GHz, and (d) 100.5 GHz. Solid: measured, dashed: simulated, and dotted: measured cross-polarization.

Figure 3.11 shows a photograph of the vertically stacked Yagi-like 4×4 antenna array. To reduce the mutual coupling between the 1×4 arrays, the dielectric between them is removed. The measured reflection coefficient of the 4×4 vertically stacked Yagi-like antenna array is shown in Figure 3.12. The measured bandwidth of the antenna array is 7.5 GHz (about 7.6%) and is comparable to that obtained for the array using dielectric cubes. Again, we observe a 1.7% (1.65 GHz) shift in frequency which we attribute to the reasons discussed earlier in this section. Note that this frequency shift is taken into account when plotting radiation patterns; i.e. the measured radiation pattern is plotted in 97 GHz whereas the simulated one is plotted at 95.35 GHz.

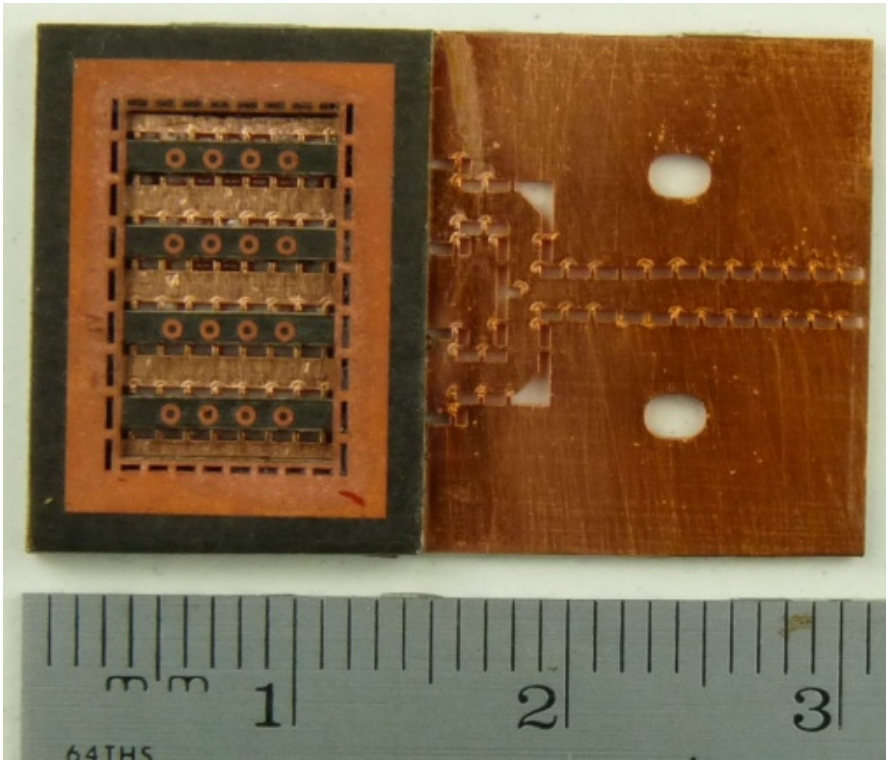

Figure 3.11. Photograph of the fabricated 4×4 vertically Yagi-like antenna array.

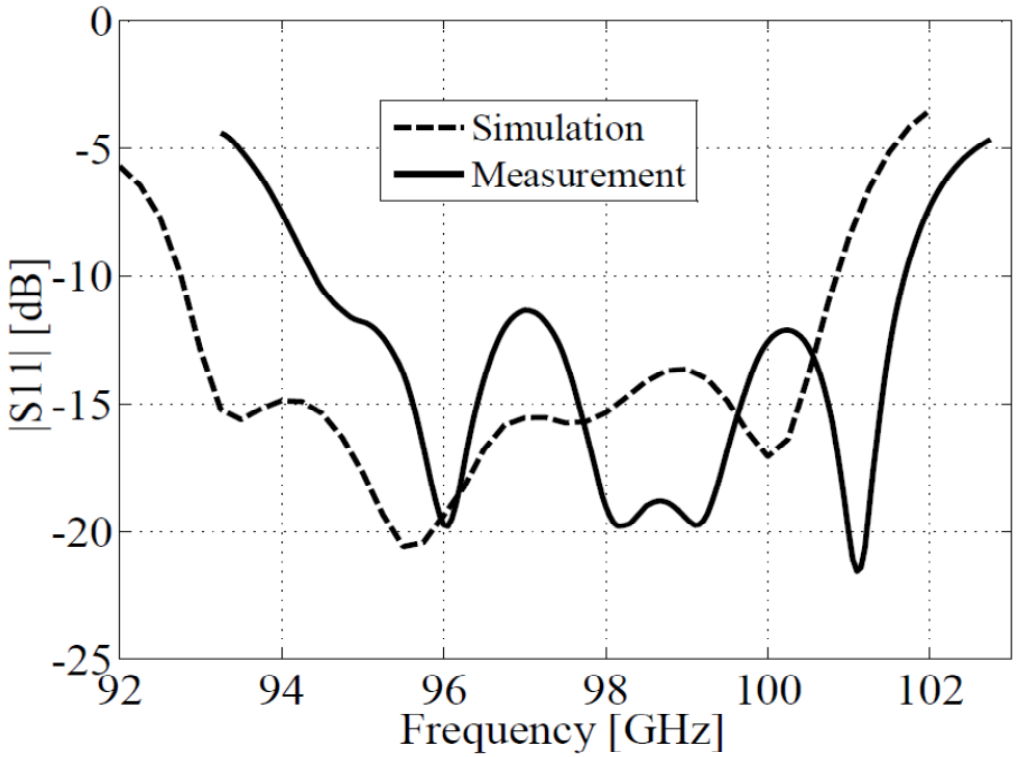

Figure 3.12. Measured and simulated |S11| of the 4×4 vertically Yagi-like antenna array.

The measured E- and H-plane radiation patterns of the vertically stacked Yagi-like antenna array are shown in Figure 3.13 at frequencies of 95.25, 97, 98.75 and 100.5 GHz. Good agreement is observed between the simulated and measured responses at the four frequencies. The antenna has a constant gain (18 dBi ± 0.75 dB) across the 7.5 GHz bandwidth. The measured side lobe level is 13.5 dB in the H-plane and is 10 dB in the E-plane. The discrepancies between simulated and measured side lobe levels are caused by the combined effect of the fabrication inaccuracy and the waveguide to SIW transition. The measured cross polarization of the antenna array is less than 17 dB over the 7.5 GHz bandwidth. The estimated radiation efficiency from the measured gain and directivity is 90% at 98.75 GHz. The dielectric, metallic, and mismatch losses have been considered in the simulation.

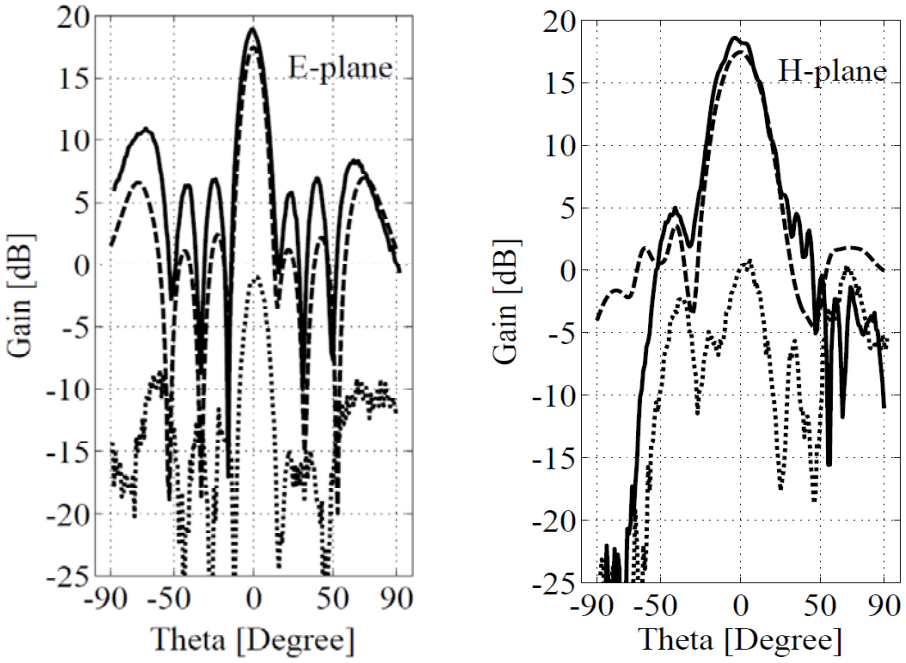
E-plane
H-plane
Gain [dB]
Theta [Degree]
20
15
10
5
0
-5
-10
-15
-20
-25
-90
-50
0
50
90

(a)

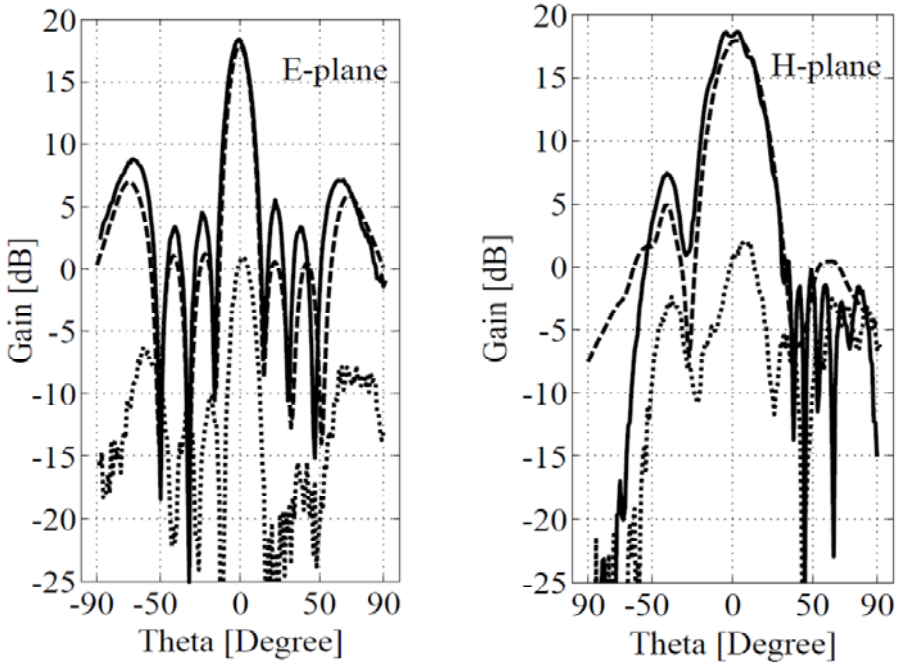
E-plane
H-plane
Gain [dB]
Theta [Degree]
20
15
10
5
0
-5
-10
-15
-20
-25
-90
-50
0
50
90

(b)

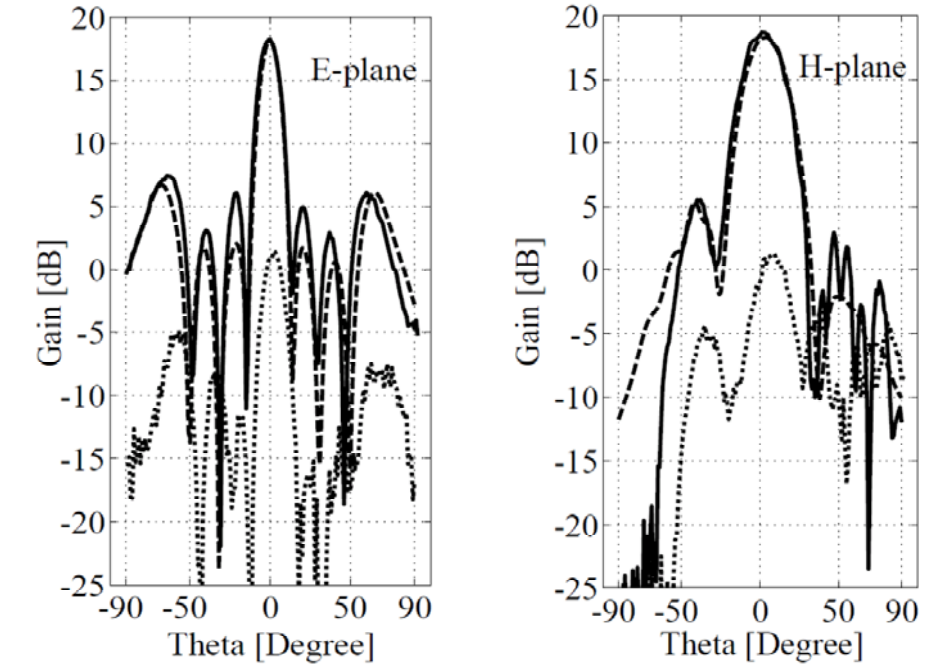

(c)

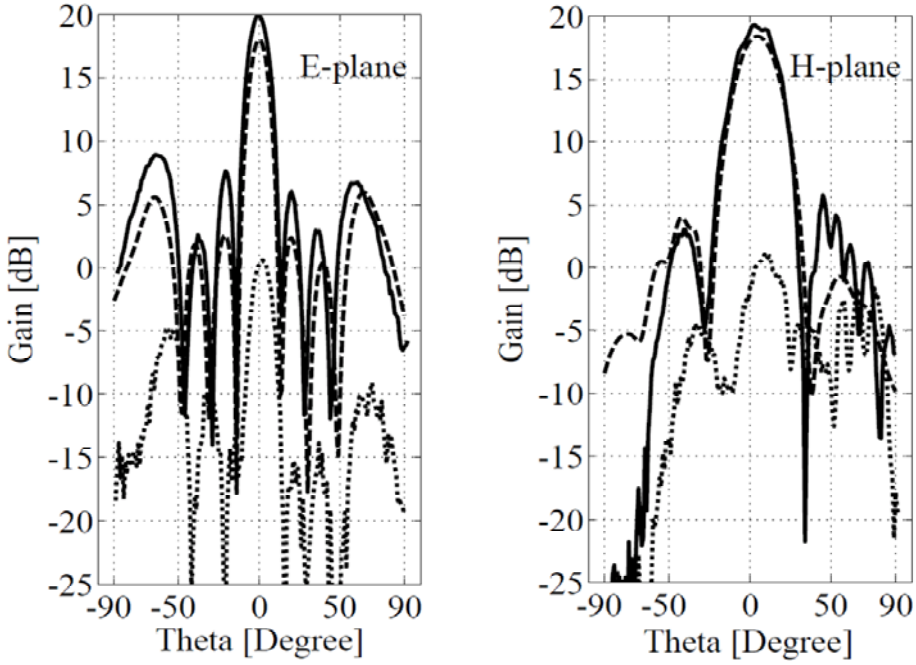

(d)

Figure 3.13. Simulated and measured co- and cross- polarization patterns in E- and H-planes at (a) 95.25 GHz, (b) 97 GHz, (c) 98.75 GHz, and (d) 100.5 GHz. Solid: measured, dashed: simulated and dotted: measured cross-polarization.

3.2 Planar dielectric rod antenna for gigabyte wireless communication at E band

A wideband planar dielectric rod antenna with substrate integrated non radiative dielectric (SINRD) waveguide feed is presented in this section for E-band and up-millimeter-wave applications. The antenna and its feeding structure are integrated into a single layer substrate, which decreases the fabrication cost and integration complexity. Simulated and measured results show that the antenna has a wide bandwidth. Due to the structure of the SINRD guide which is shielded on top and bottom of the substrate, the proposed antenna is suitable for multilayer structure techniques such as low temperature co fired ceramic (LTCC) or on-chip antenna. This antenna presents numerous features such as broad bandwidth, relatively high and stable gain, use of high dielectric constant substrate, and substrate-oriented end-fire radiation. The proposed antenna is suitable for gigabyte point to point wireless communications at E band. Measured bandwidth of the antenna is 10 GHz (93-103 GHz) while a relatively flat gain of 9.5i ± 1 dB is obtained over the bandwidth of interest.

3.2.1 Introduction of SINRD waveguide

Due to the low-loss transmission characteristics of the non-radiative dielectric (NRD) waveguide [62], it has been demonstrated as a promising candidate for millimeter-wave applications. However, the fabrication and integration of NRD waveguides are generally not easy because of their mechanical tolerance and bulky geometry especially at millimeter-wave frequency. SINRD waveguide [63]-[64] has been demonstrated successfully to overcome the fabrication and integration hurdles of the original NRD waveguide. SINRD guide presents a planar structure and can easily be connected to any planar lines and active components [63]. In the development of an SINRD guide, drilling an array of air holes reduces the effective permittivity of the bilateral surrounding areas of the central guiding strip, thus creating a waveguide dielectric channel in planar substrate. The effective dielectric constant can be controlled by choosing an appropriate set of geometrical parameters of the array holes [65]. A detailed discussion about the design procedure and underlying characteristics of SINRD waveguides was presented in [66].

Dielectric rod antennas, or Polyrod antennas, were investigated in [67] as a class of dielectric antennas, which has high radiation efficiency, wide bandwidth, and relatively high gain [68]-[70].

However, the feed of such antennas is usually a metallic horn or a direct metallic waveguide feed, which is non-planar, bulky, and expensive. Definitely, it is not easy to connect this structure to active components. A planar substrate integrated image guide (SIIG) fed dielectric rod antenna was presented in [71]. Because of the image guide based structure of the antenna, which is not shielded on top of the substrate, it is not suitable for multilayer configurations, and also the radiation pattern of the antenna is not substrate oriented end fire.

This section presents a low-cost E-band integrated dielectric rod antenna fed by SINRD waveguide. The structure of the antenna and its feed network are integrated in a single layer substrate which is suitable for low-cost and high-efficient millimeter-wave applications. Due to the attractive characteristics of the antenna such as broad bandwidth, being shielded on the top and bottom of the substrate, relatively high and stable gain, designed on a high dielectric constant substrate, and also substrate-oriented end-fire radiation, the proposed antenna is suitable for multilayer applications especially for gigabyte E band communication.

3.2.2 Design considerations of the antenna and the feed

A conventional dielectric rod antenna, fed by a horn, is shown in Figure 3.14 The length of the dielectric rod has the most influence on the gain and radiation pattern of the antenna [65]. The horn-shaped feed of the conventional dielectric rod antenna is non-planar and also is costly to fabricate it, especially over millimeter-wave frequency range. In this case, micromachining facilities are generally required to fabricate a horn-shaped feed. In order to integrate the dielectric rod antenna in a single layer substrate, SINRD waveguide [64] is used to feed the antenna (Figure 3.14 b). To develop an SINRD waveguide, an array of air holes should be drilled on a high dielectric constant substrate, to reduce the equivalent permittivity of the bilateral surrounding areas of the central strip. Then, a non-radiative dielectric (NRD) channel is created in a single layer substrate that supports the propagation of LSM10 and LSE10 modes. In this work, LSM10 is excited and used to feed the antenna because it is less lossy. The effective dielectric constant can be controlled by choosing geometrical properties of the array holes. As it was shown in [64], the static effective dielectric constant of one periodic cell is:

$$\varepsilon_{eff} = \frac{\varepsilon_r .(S_{cell} - S_{air}) + S_{air}}{S_{cell}} \tag{3.1}$$

where S_{air} is the area of the air holes in the unit cell, S_{cell} is the area of the unit cell [63], and ε_r is the dielectric constant of the substrate material. The design procedure of the SINRD waveguide was explained in detail in [63]-[66].

Figure 3.14 (b) shows the structure of the SINRD guide-fed planar dielectric rod antenna designed for 94 GHz applications. The antenna is designed on a low-loss Alumina substrate with dielectric constant of 9.6 and dielectric loss tangent of 0.0006 reported at 100 GHz [72]. Due to the complexity of the effect of tapers on total radiation pattern, there is no accurate synthesis available in the literature. If the rod is wide at the feeding point and smoothly tapered to the end, a low side lobe level can be achieved [73], although a slightly reduced gain is obtained compared to the maximum gain design [73]. The width of the rod at the input is equal to the width of the SINRD guide and is linearly tapered to the end to gradually make the guided wave matched to free space. Figure 3.15 shows the simulated electric field distribution of the SINRD guide-fed dielectric rod antenna. Ansoft HFSS v.13 is used in this work to simulate the characteristics of the antenna. Simulated electric field distribution, and radiation pattern of the antenna shows, radiation from the transition region between the SINRD waveguide and the rod antenna is negligible and it does not disturb the radiation pattern. The simulated radiation efficiency of the antenna is 95 percent over most of the bandwidth of the antenna.

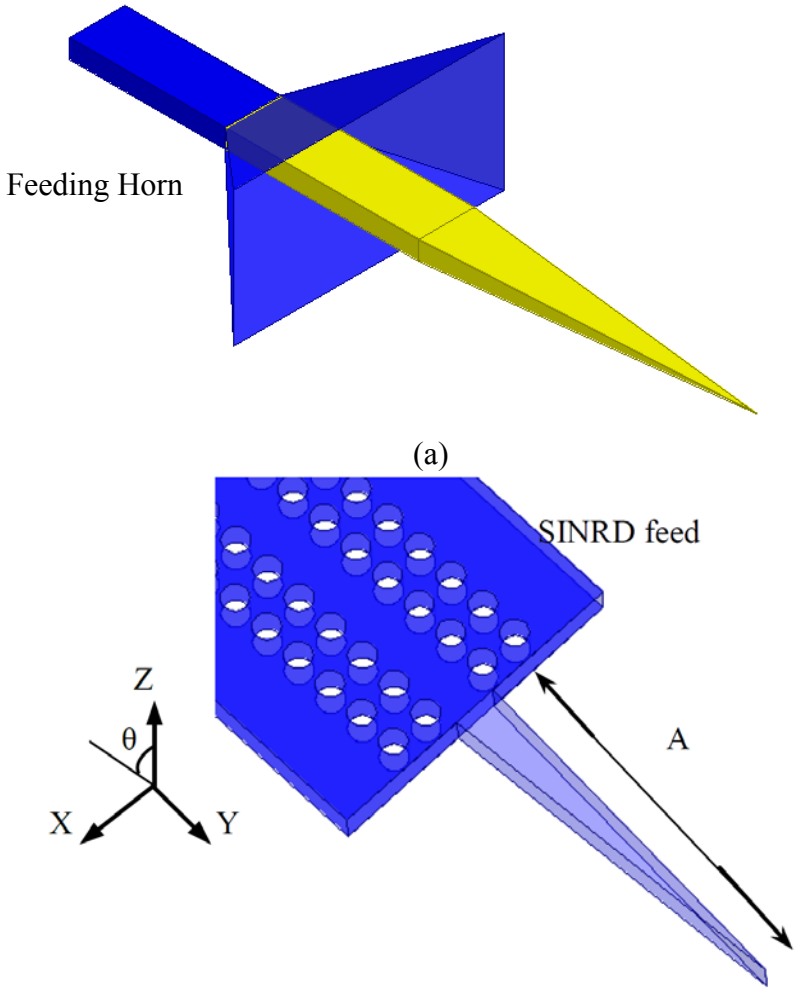

Figure 3.14. (a) Conventional horn fed dielectric rod antenna, (b) planar SINRD guide-fed integrated dielectric rod antenna.

The length of the dielectric rod has the most pronounced effect on the radiation pattern and gain of the antenna. Figure 3.16 shows the influence of the length of the dielectric rod on the gain of the antenna within the bandwidth of 90 – 102 GHz. Simulation results suggest that the length of the dielectric rod does not have a significant effect on the bandwidth and matching of the antenna. Although increasing the rod length (A) increases the gain of the antenna, the rod is fabricated with 7 mm length in this section to yield a good mechanical stability.

Compared to the SIIG fed dielectric rod antenna [71], the proposed planar SINRD fed rod antenna, has the advantage of being shielded on both of its top and bottom surfaces, then it is

made suitable for multilayer applications with a better mode control within the structure. This advantage is due to the structure of the SINRD guide which is shielded with the top and bottom metallic plates of the substrate, while SIIG is not shielded on top of the substrate, which is not suitable for the implementation in a multilayer configuration. Symmetrical and substrate oriented end-fire radiation pattern is the second advantage of the proposed SINRD fed rod antenna. These two advantages along the other characteristics of the antenna such as, the use of a high dielectric constant substrate, relatively high and stable gain, and broad bandwidth, make the proposed antenna suitable for on-chip system applications especially for gigabyte chip-to-chip communication. Note that in [71], as shown in Figure 3.17, one can see that non-identical holes have been used, near the dielectric rod, to improve the matching condition whereas in the present work the walls of the SINRD guide are made of all identical holes for fabrication simplicity and also the use of non-identical holes has negligible effect on the input matching in the SINRD fed dielectric rod antenna structure.

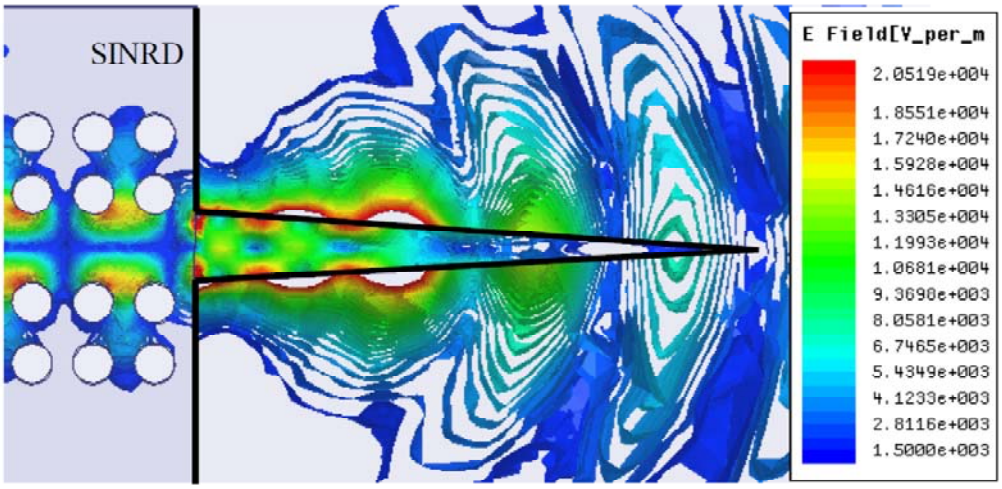

Figure 3.15. Top view of the simulated electric field distribution (Ansoft HFSS v.13) of the planar SINRD guide-fed dielectric rod antenna.

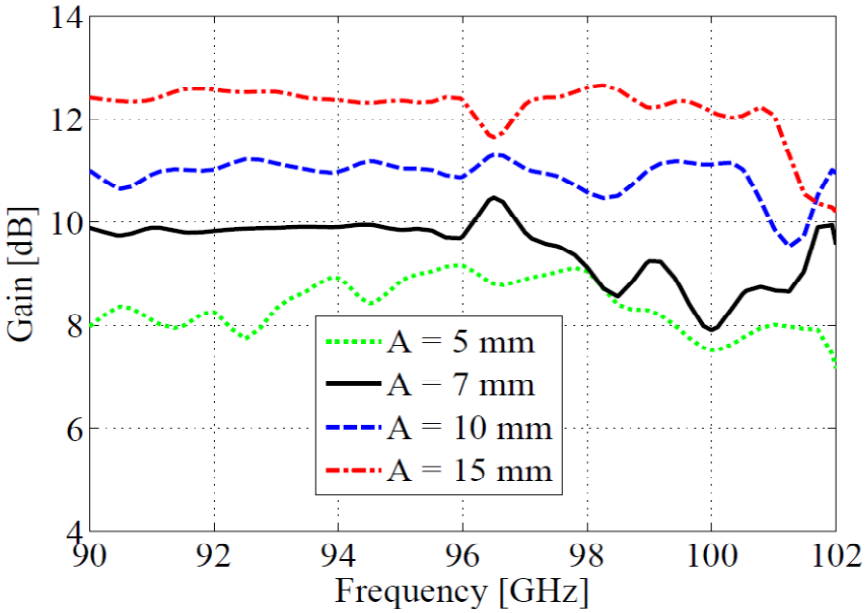

Figure 3.16. Influence of the length of the dielectric rod on the gain of the integrated SINRD guide-fed dielectric rod antenna.

SINRD guide can easily be connected to microstrip lines and active components [63]. To measure the characteristics of the antenna in our anechoic chamber, a WR10 waveguide-to-SINRD guide transition is required. Figure 3.17 illustrates the structure of this transition and the SINRD waveguide. To excite LSM10 mode, the SINRD guide is placed at the middle of the WR10 waveguide where the maximum E field takes place. To increase the bandwidth of the transition, the substrate is tapered inside the waveguide. Note that there is no metallic shield on the bottom and top of the tapered part of the substrate that is placed in the waveguide while, on the both sides of the substrate, on the SINRD guide part, there are metallic shields. The opening of the aperture of the WR10, on the bottom and top of the substrate, is covered by metal to decrease the transition loss. HFSS software is used to optimize L1, S3, and S4, to reach the maximum bandwidth. All the dimensions of the WR10-to-SINRD guide transition and also dimensions of the SINRD waveguide are shown in Table 3.3. Figure 3.18 shows the |S11| and |S12| of the back-to-back WR10 to SINRD guide transition when the length of the SINRD guide is 5.25mm.

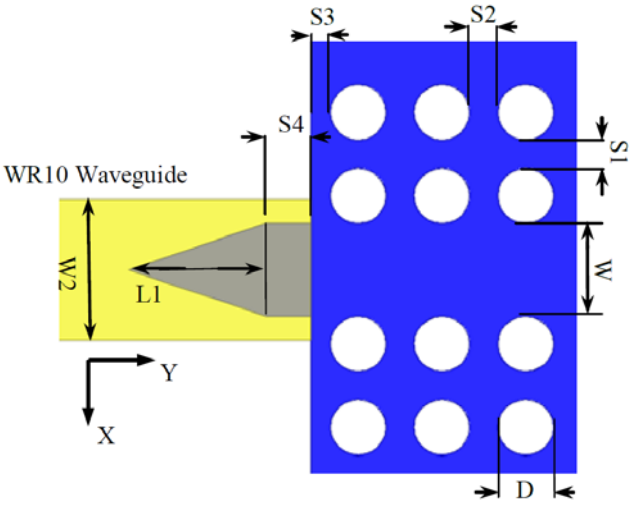

(a)

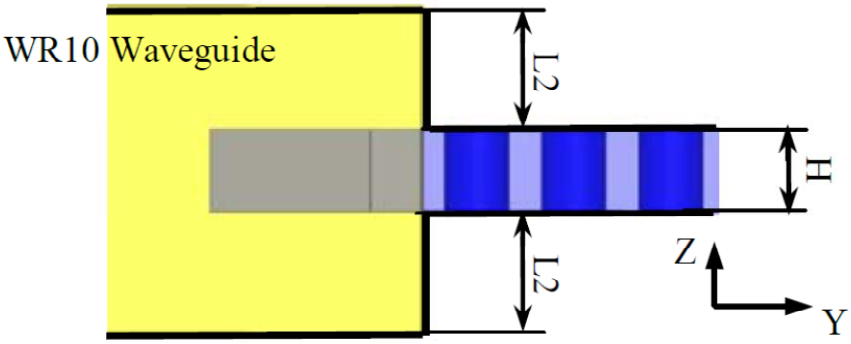

(b)

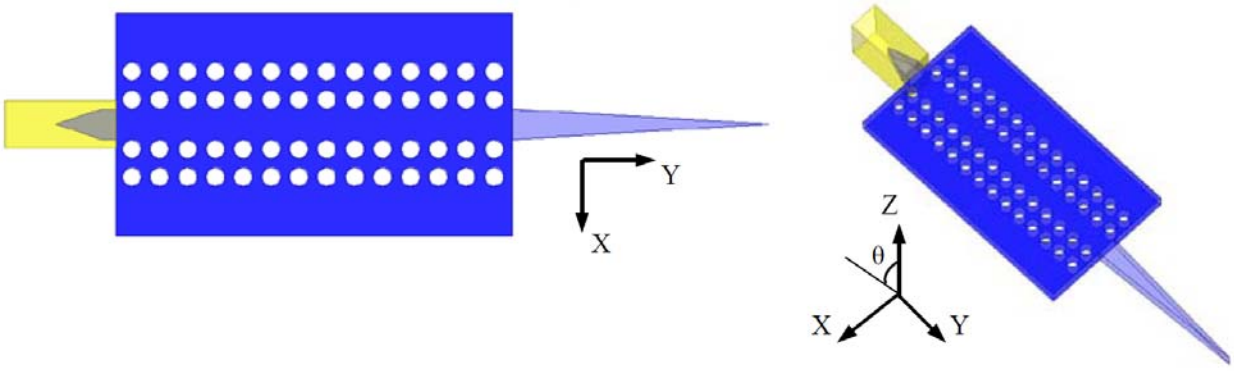

(c)

Figure 3.17. (a) Top view and, (b) side view, of the WR10-to-SINRD guide transition, (c) 3-D view and top view of the SINRD guide-fed dielectric rod antenna and the WR10 to SINRD guide transition.

Table 3.3: Dimensions of the Antenna and WR10-to-SINRD guide transition (unit: mm)

Symbol	Value (mm)	Symbol	Value (mm)
W	0.838	S4	0.4
H	0.635	L1	1.24
W2	1.27	A	7
S1	0.254	L2	0.94
S2	0.254	D	0.5
S3	0.177		

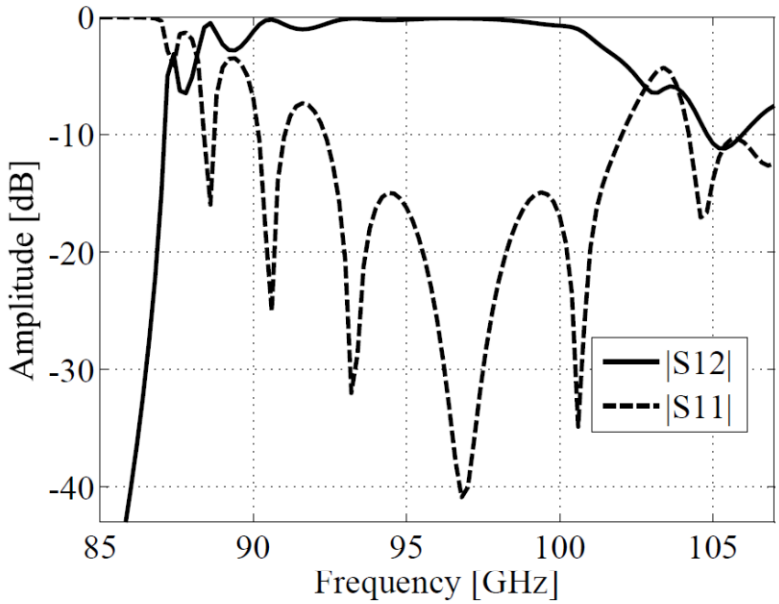

Figure 3.18. |S11| and |S12| of the back to back WR10 to SINRD guide transition.

3.2.3 Fabrication and Measurement of SINRD fed dielectric rod antenna

Miniature hybrid microwave integrated circuits (MHMICs) technology, which has been a promising technology for a small scale of production, is used to fabricate the proposed integrated SINRD guide-fed dielectric rod antenna on a 25 mil (0.635 mm) thick, low-loss Alumina substrate. MHMICs are an intermediate technology of micro-fabrication between microwave integrated circuits (MICs) and monolithic microwave integrated circuits (MMICs). In MHMICs, passive elements are produced during different stages of fabrication. Active devices are added or surface-mounted at the end of the process. The main advantage of MHMICs compared to MICs technologies is the direct utilization of metalized holes, air bridges, and dielectric layers in MHMICs [74]. Figure 3.19 shows the fabricated SINRD guide-fed dielectric rod antenna and the WR10-to-SINRD guide transition with an excellent precision. The impedance is measured using an Anritsu 3739C vector network analyzer. Measured and simulated return losses (|S11|) [dB]) of the integrated SINRD guide-fed dielectric rod antenna are plotted in Figure 3.20 over the 85-107 GHz frequency range. Good agreement is obtained between the simulated and measured |S11| of the antenna. Radiation pattern and gain of the antenna are measured in our anechoic chamber. Figure 3.21 compares the simulated and measured radiation patterns and gains of the antenna. Simulated and measured results show that the radiation pattern and gain of the antenna are almost unchanged within the bandwidth of 92 –102 GHz. The estimated radiation efficiency from the measured gain and directivity is 86.5 percent at 96GHz, and is 92.3 percent at 102 GHz.

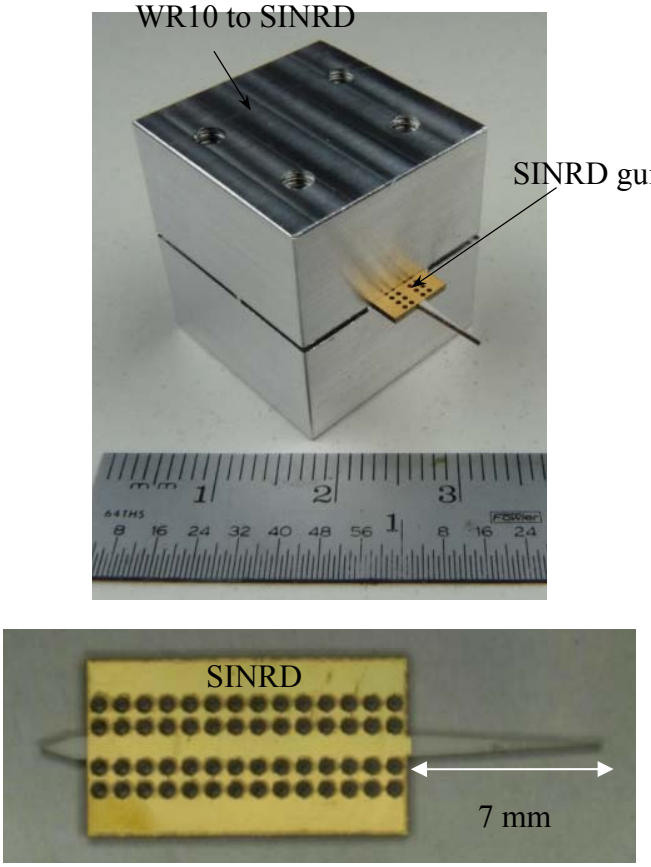

Figure 3.19. Photograph of the fabricated planar SINRD guide-fed dielectric rod antenna and the WR10 to SINRD guide transition.

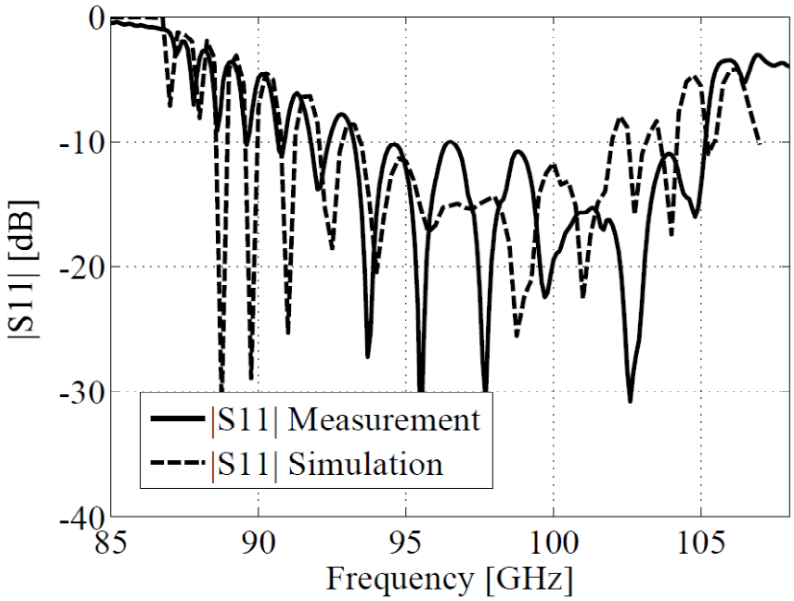

Figure 3.20. Measured and simulated return losses of the planar SINRD guide-fed dielectric rod antenna.

(a)

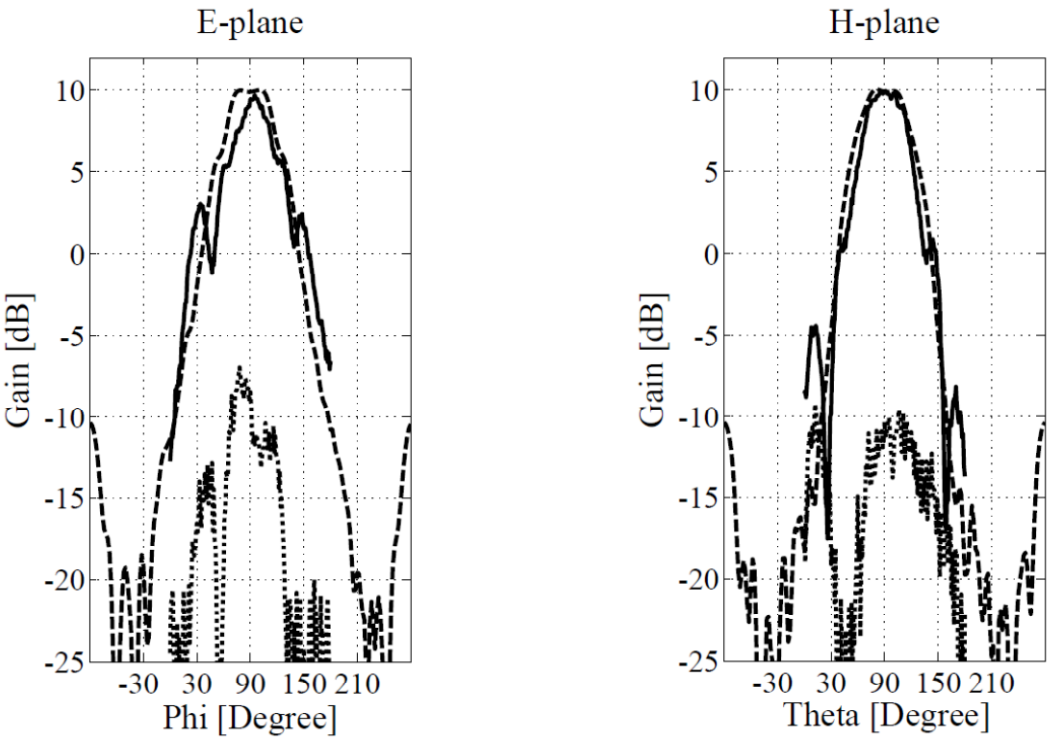
E-plane
H-plane
Gain [dB]
10
5
0
-5
-10
-15
-20
-25
-30 30 90 150 210
Phi [Degree]
Theta [Degree]

(b)

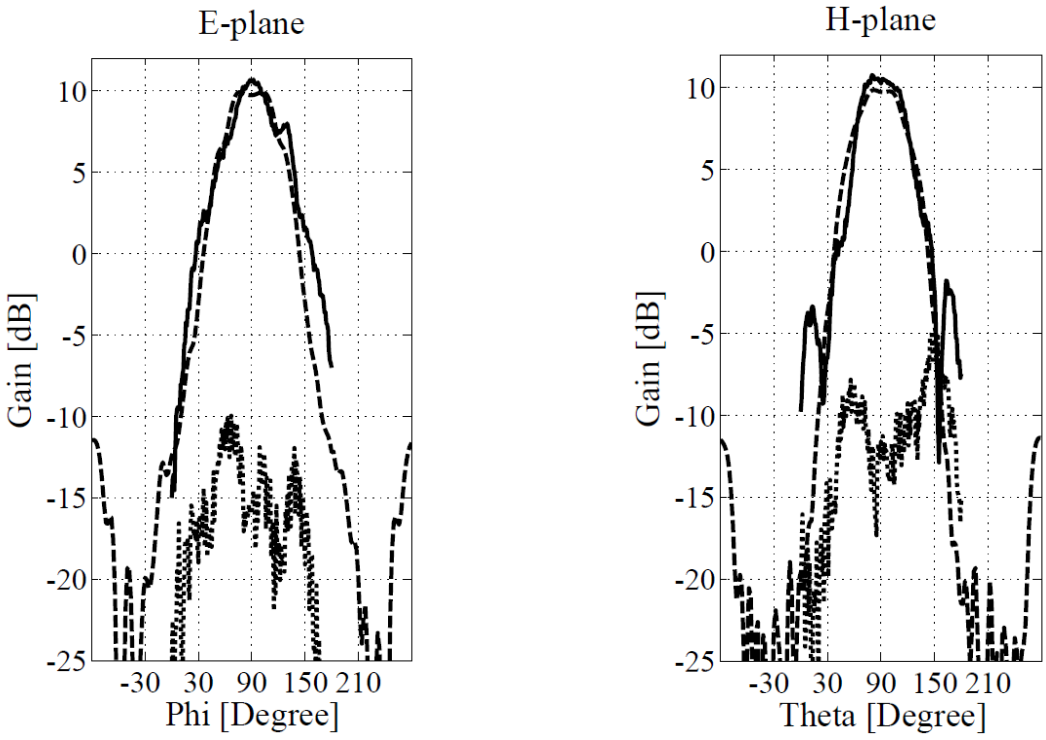
E-plane
H-plane
Gain [dB]
10
5
0
-5
-10
-15
-20
-25
-30 30 90 150 210
Phi [Degree]
Theta [Degree]

(c)

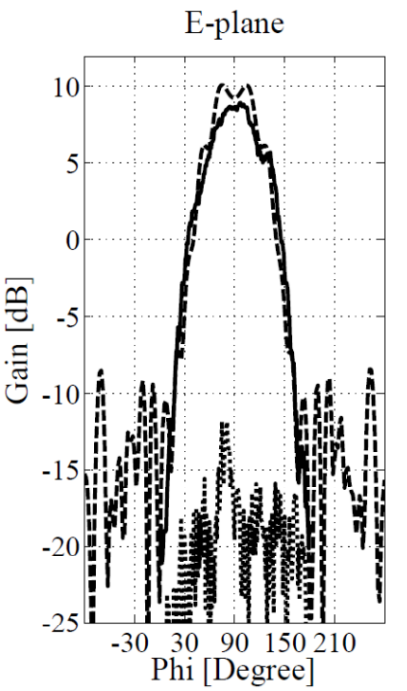

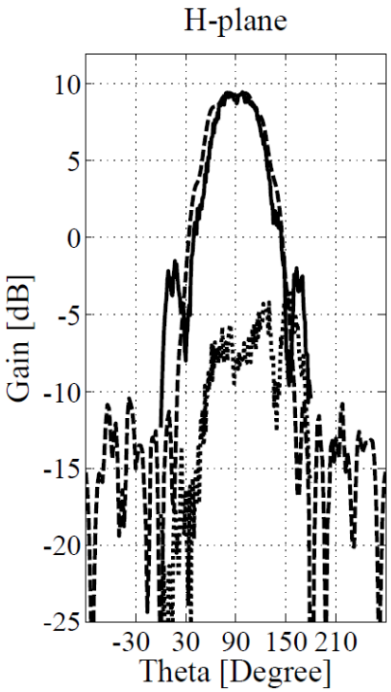

(d)

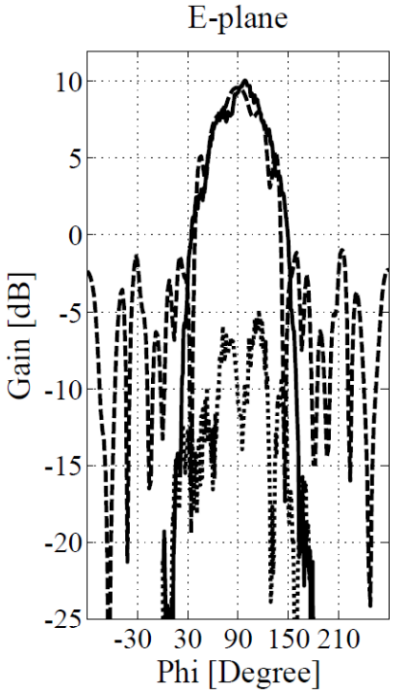

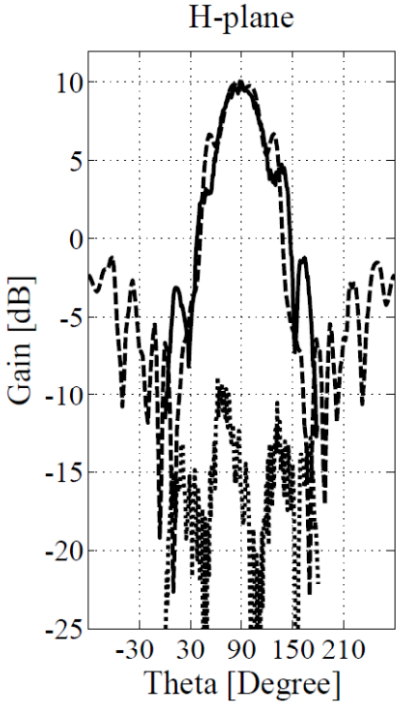

Figure 3.21. Simulated radiation patterns in YZ plane (H plane), and XY plane (E plane), (c.f. Figure 3.14) of the SINRD guide-fed integrated dielectric rod antenna at (a) 93 GHz, (b) 96 GHz, (c) 99 GHz, and (d) 102 GHz. Solid: measured, dashed: simulated and dotted: measured cross-polarizations.

3.3 Conclusion

In this chapter, two novel antennas employing the SICs concept are studied and developed for W-band applications over 94.1-97 GHz. The two antennas have different characteristics that can be used in different front-end structures. The first antenna radiates along the broadside to the substrate and it is fabricated on low dielectric constant substrate while the second antenna radiates at the substrate-oriented end-fire and fabricated on high dielectric constant substrate. Both antenna structures have the advantages of being low cost, high gain and high efficient.

The first antenna is a low-cost and high-efficiency antenna array for applications in the E/W-band which is proposed and demonstrated using a standard low-cost PCB processing. SIW technology is used to feed the antenna elements through the slots etched on the top metallic surface of the waveguide. One SIW T-junction and two Y-junctions are used to realize a four-way power divider to feed the 4×4 antenna arrays. The 4×4 antenna array prototypes are implemented using Rogers RT/Duroid substrate with low-cost multilayer PCB processing. It is found that the dielectric and metallic losses decrease the antenna gain by 1.3 dB, and also do not have significant effect on the bandwidth of the antenna. For the new 4x4 antenna array, a cube of dielectric is placed on the top of the 1×4 array of circular patches to increase the gain of the antenna. This dielectric cube is made of a low dielectric constant material and leads to an increased antenna gain by 3 dB. The measured gain of the 4×4 antenna array is 19 dBi over a 7.7% bandwidth centered at 98 GHz. The array with dielectric cubes consists of only three layers whereas the Yagi-like requires six layers. Thus, the fabrication processing cost of the antenna is almost half of that of the Yagi-like antenna. However, the Yagi-like antenna is 1.12 mm thinner. Compared with the regular SIW slot array antennas, the proposed antenna has higher gain and broader bandwidth. This work shows that it is possible to design high gain antenna arrays with high radiation efficiency in E/W-band by utilizing SIW techniques.

The second antenna is a substrate dielectric rod antenna that is integrated in a single layer substrate. Low-loss SINRD waveguide is used to feed the antenna structure. Antenna is designed for E/W-band applications, which can easily be extended to other millimeter-wave and terahertz bands. Radiation pattern and gain of the antenna remain almost unchanged within the wide bandwidth of the antenna. A wideband WR10 waveguide-to-SINRD guide transition is designed

to measure the characteristics of the antenna. This antenna presents numerous features such as broad bandwidth, relatively high and stable gain, use of high dielectric constant substrate, and substrate-oriented end-fire radiation. Measured bandwidth of the antenna is 10 GHz (93–103 GHz) while a relatively flat gain is obtained over the bandwidth of interest. Good agreement is obtained between the simulated and measured results.

CHAPTER 4 WIDE-BAND AND LOW-COST ANTENNA FOR E/W-BAND (71-97 GHZ) GIGABYTE POINT TO POINT WIRELESS SERVICES

This chapter presents two novel wide band, high gain, and low cost antennas to cover the whole bandwidth of the E/W-band (71-97 GHz). The first antenna is an integrated pyramidal horn antenna made of multilayer printed circuit board (PCB) process that radiates along the broadside to the substrate. The second antenna is a planar high gain dielectric loaded antipodal linearly tapered slot antenna (ALTSA), which radiates at the substrate-oriented end-fire. Both antennas are useful for different structures in support of gigabyte point-to-point wireless services at E/W-band.

4.1 Integrated pyramidal horn antenna made of multilayer printed circuit board (PCB) process

Due to the low atmospheric absorption over E/W-band, numerous applications are expected such as gigabyte point to point wireless services, which should be developed at low cost. Short wavelength makes the dimension of antennas in this frequency range small, which usually requires sophisticated and expensive fabrication process. This section presents a class of integrated wideband pyramidal horn antennas that can be made of low-cost multilayered printed circuit board (PCB) process. The proposed horn antenna radiates along the broadside to the substrate and uses SIW as its feeder. Transverse slot on the top metallic surface at the end of SIW is deployed to drive the horn antenna. Metalized via holes are used to synthesize the horn walls. The opening of the horn antenna is discretely flared from the bottom layer to the top layer. Measured bandwidth of the antenna is 35 GHz (70-105 GHz) while a relatively constant gain of 10 ± 1 dBi is obtained over most of the bandwidth.

4.1.1 Introduction

With reference to other antenna techniques, horn structure has found a large number of applications thanks to its simplicity, wide bandwidth, and high gain. The fundamental problem of this structure lies in its integration problem and cost issue. Several horn antennas over millimeter-wave and sub-millimeter-wave frequency range were presented [75]. As frequency increases, the dimension of the antenna becomes smaller due to shorter wavelength. Usually, it may need a micromachining fabrication process which then increases the cost of the antenna [10]. Especially, fabricating a corrugated or stepped horn antenna [76]-[79] is expensive and difficult at such high frequencies. At high millimeter-wave frequencies, connecting the horn antenna to active microwave components is also very difficult. Certainly, it would increase the cost of the antenna and its related system development. SIW-based H-plane horn antennas were presented in [80]-[83], which provide an alternative planar solution to classical horn techniques. Although these structures are low-cost and can easily be interfaced with CPW or microstrip lines, their bandwidth is relatively narrow and they radiates in parallel to the substrate which is not desirable for many practical applications.

This section describes a class of novel wideband integrated SIW-fed horn antennas in synthesized planar form that radiate along the broadside to the substrate. The proposed antenna is easy to integrate with CPW or other planar lines. A low-cost multilayer PCB process is used to fabricate the antenna on the basis of Rogers substrates. Measured bandwidth of the antenna is 40% (70-105 GHz) and measured gain of the antenna is about 9.5 dBi over the most of the antenna bandwidth. Compared to the other SIW-fed integrated horn antennas [80]-[83], the proposed structure presents a much wider bandwidth and it has a broadside-to- substrate radiation pattern, which is stable within the bandwidth of interest. Note that the antenna thickness in connection with the number of layer is increased.

4.1.2 Structure and design of integrated pyramidal horn antenna

Figure 4.1 shows the configuration of a waveguide-based horn antenna and its waveguide feed. The goal of this work is integrating this waveguide-based horn antenna made in a low cost

multilayer structure. The antenna should radiate along the broadside to the substrate. The waveguide feed is integrated by the use of an SIW technique, which can easily get connected to CPW line and active components. The SIW design procedure and dimension selection have been explained in detail in [84].

A schematic of the proposed multilayer integrated horn antenna is shown in Figure 4.2, which may be regarded as a discrete version of the original structure of Figure 4.1. The bottom layer is used to construct the SIW feed of the horn antenna while the structure of the horn antenna is designed on the upper layers. At the end of the SIW geometry on the top metallic surface, a transverse slot is etched to feed the horn antenna. The transverse slot plays the functional role of the required 90 degree bend, which is described in Figure 4.1. As such, the dimension of the transverse slot should be identical to that of the SIW cross section, i.e. width of the slot (SW) is equal to the thickness of the first layer (T), and length of the slot (SL) is equal to width of the SIW (W).

The concept of the stepped or discretized horn antenna [76]-[78] is used to create the originally non-planar antenna in a stacked planar form. The horn walls are made of metallic via holes with which the opening of the horn is flared from the second layer to the upper layers in steps. Within each layer, the width and length of the aperture are increased by G. Due to the mechanism of fabrication, the rectangular via holes (which are the walls of the horn antenna) are not continuous at the corners of the horn. Small dielectric cubes connect the dielectric outside the horn to the

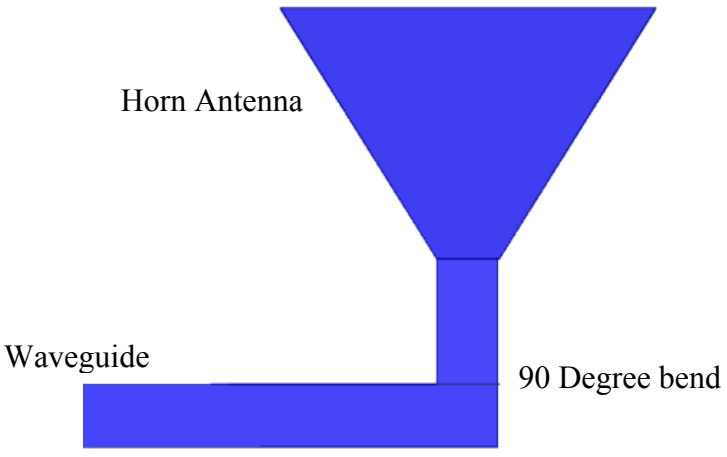

Figure 4.1. Configuration of basic waveguide-based horn antenna and its waveguide feed.

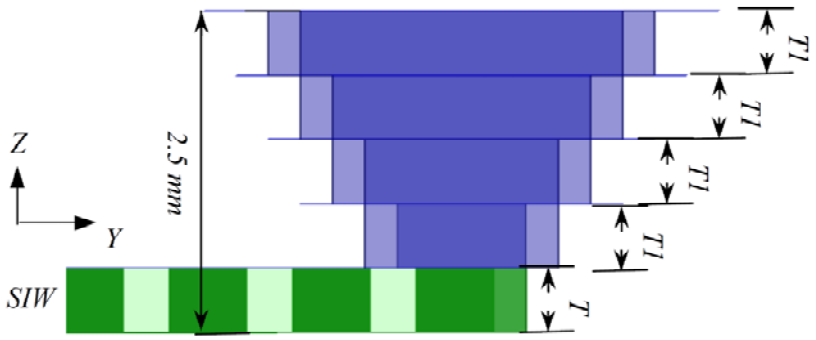

(a)

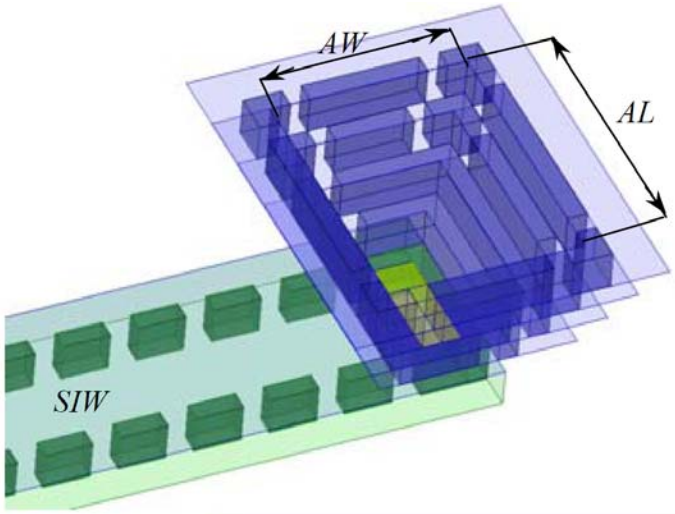

(b)

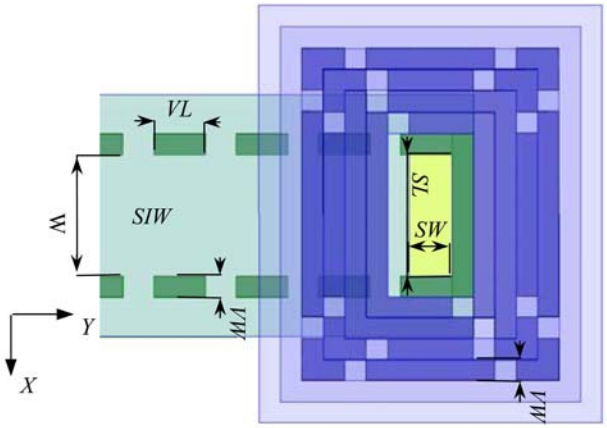

(c)

Figure 4.2. Configuration of multilayer integrated horn antenna (a) Side view, (b) 3D view, and (c) Top view

dielectric inside the horn, to avoid the separation of the dielectrics. An appropriate connection point (corners of the horn in this case at which weak current exists, is chosen such that the effect of these connections on gain and radiation patterns of the antenna becomes negligible. Note that it is preferred to have the minimum width for the connecting dielectrics even though 0.254 mm is chosen because of the limitation of our fabrication process. The SIW feed is designed on a substrate with dielectric constant of 2.94, while the upper layers are designed on other substrates with dielectric constant of 2.2. All the dimensions of the antenna are illustrated in Table 4.1.

Table 4.1: Dimensions of the integrated pyramidal horn antenna

Symbol	Value (mm)	Symbol	Value (mm)
T	0.5	VW	0.254
T1	0.5	VL	0.6
AW	3	SW	0.5
Al	3.5	SL	1.424
W	1.424		

Figure 4.3 illustrates the impact of the aperture size, i.e. AW and AL, on directivity of the antenna at 94 GHz. Ansoft HFSS V.13 is used to simulate the characteristics of the antenna. Figure 4.3 shows that increasing the length (AL) and width (AW) of the aperture enhances the directivity of the antenna in H and E planes, respectively. Due to the metallic shield over the back of the antenna, i.e. the bottom metallic surface of the SIW feed on the bottom layer, a good front-to-back ratio is obtained. Figure 4.3 shows that 20 dB front-to-back ratio can be obtained. Note that, for the applications that require higher front to back ratio, it is necessary to increase the dimension of the bottom layer.

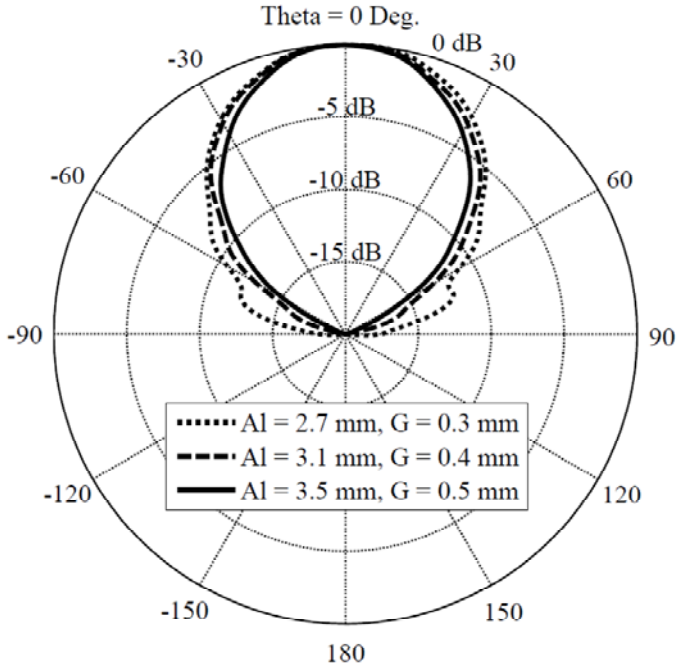

(a)

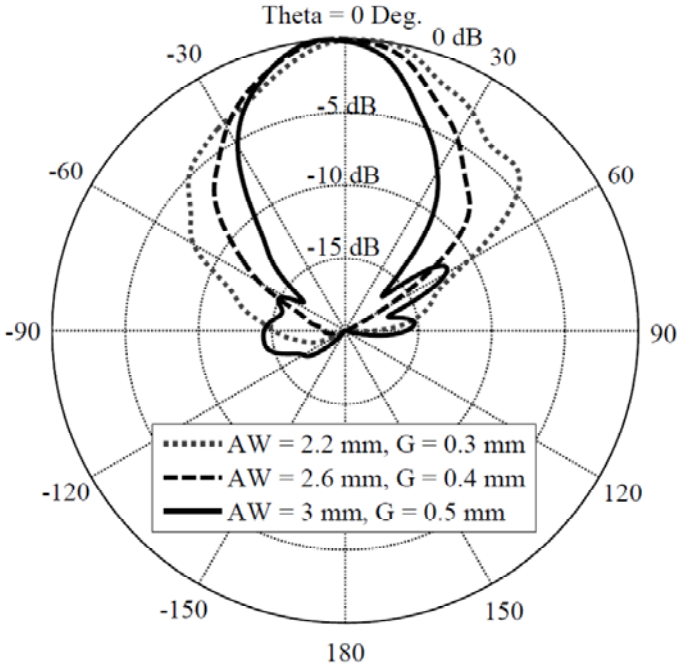

(b)

Figure 4.3. Impact of the aperture of the antenna on (a) H plane, (b) E plane at 94 GHz.

The antenna structure, as shown in Figure 4.2, contains 5 layers. Figure 4.4 illustrates the effect of each layer on gain and matching characteristics of the antenna. As Figure 4.2 suggests, increasing the aperture of the antenna (by increasing the number of layer), would increase the gain. For applications like beam forming array antennas that require lower gain, and also structures with smaller footprint, it is possible to decrease the aperture size. This can be obtained by decreasing the number of layer to one or two layers, for example. Note that the resonant frequencies as shown in Figure 4.4 are caused by the combined effects of the number of the flaring steps, and integration of the 90 degree bend. This is because in this integration process, it is not possible to use a corner or smooth bending to improve the performance of the 90 degree bend. Simulation results suggest that increasing the steps of flaring can improve the impedance matching condition of the integrated multilayer horn antenna. Of course, increasing the steps would then increase the number of layer and also the fabrication cost. In this work, the integrated horn antenna is designed in five layers to prove the concept, which is easy to fabricate by utilizing a low-cost printed circuit board (PCB) process.

Figure 4.5 shows simulated radiation efficiency of the antenna versus frequency. The radiation efficiency of the antenna is more than 81% within the bandwidth of the antenna. Note that in the simulated results, the effect of dielectric and metallic losses and also the effect of adhesive between layers are all considered. To estimate the dielectric loss tangent of the substrate in the W-band frequency range, two different lengths of SIW are used; one to calibrate the vector network analyzer, and the other to measure |S21|. Then, HFSS software is used to compare the simulated |S21| with the measured results so to estimate the dielectric loss tangent. This method was used in [19] to estimate the dielectric loss tangent at 60 GHz.

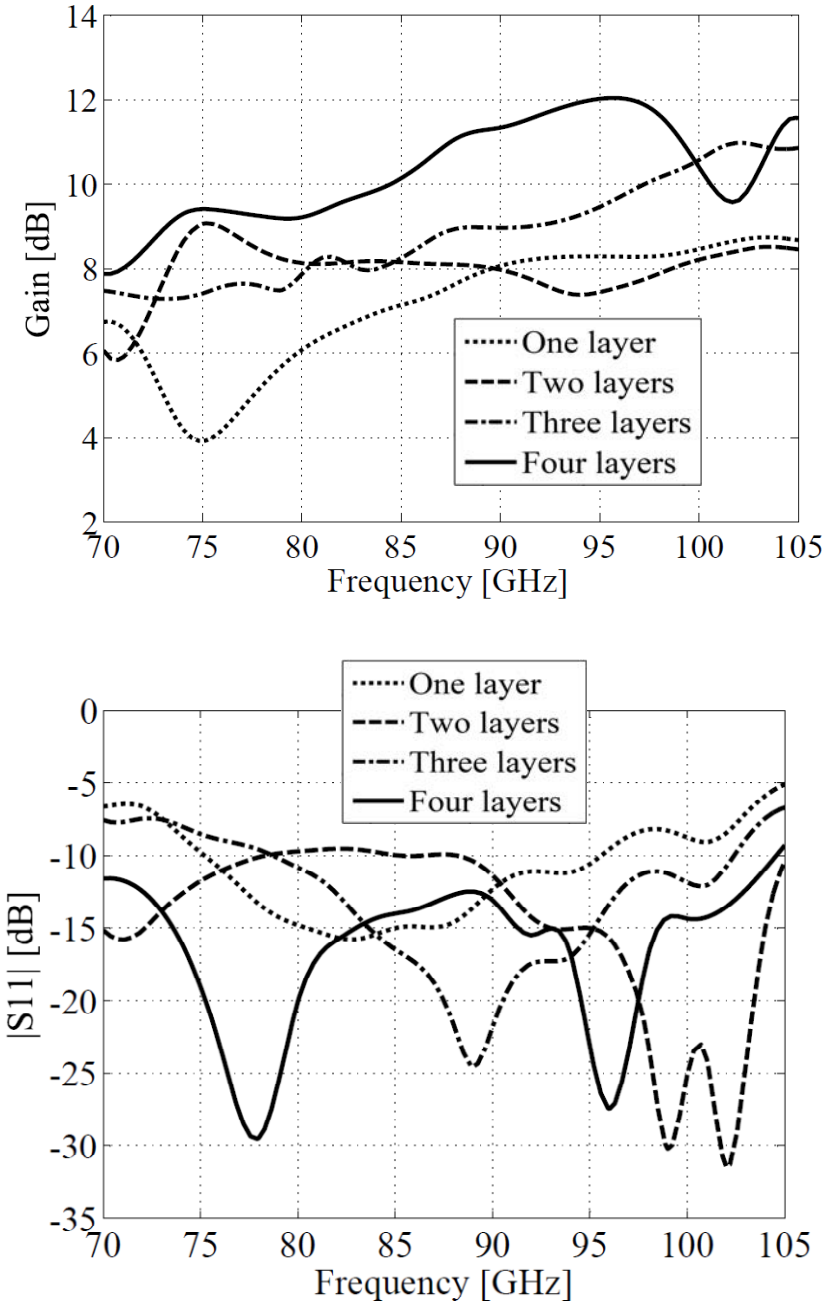

Figure 4.4. Effect of adding the layers on gain and bandwidth of the multilayer integrated horn antenna.

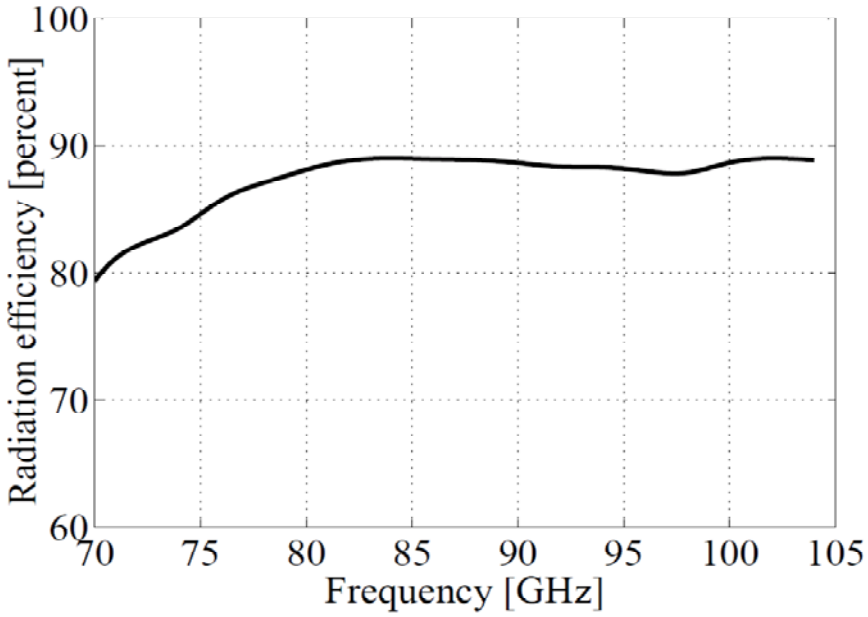

Figure 4.5. Simulated radiation efficiency of the integrated horn antenna

4.1.3 Fabrication and measurement of the integrated pyramidal horn antenna

A low-cost multilayer standard PCB process is utilized to fabricate the proposed multilayer integrated horn antenna on standard Rogers substrate. The first layer is fabricated on a 20 mils Rogers/duroid 6002 substrate with dielectric constant of 2.94, while the upper layers are made of 20 mils Rogers/duroid 5880 substrates with dielectric constant of 2.2. Photograph of the developed antenna is shown in Figure 4.6.

A wideband rectangular waveguide (WR10) to SIW transition [60]-[61] is used to measure the antenna parameters. Measured |S11| of the multilayer integrated horn antenna is shown in Figure 4.7. The measured bandwidth of the antenna is 35 GHz (40%), which is suitable for many applications over the E/W-band frequency range. The observed discrepancy between the simulated and measured |S11| of the antenna is attributed to tolerances of the fabrication process.

Radiation pattern and antenna gain measurement were conducted in our anechoic chamber. Figure 4.8 compares the simulated and measured gains of the antenna. One of the advantages of the proposed antenna is its relatively stable gain within the wide bandwidth of interest. Figure 4.9 shows measured H- and E-plane radiation patterns of the proposed horn antenna at three different frequencies. The discrepancy between the measured and simulated radiation patterns may be caused by the combined effects of the inaccuracy (tolerances) of the fabrication and also the

roughness of the horn walls which are made of metalized via holes. The use of other metallization processes that are common in other fabrication processes may reduce this effect although it will increase the fabrication cost. Simulated cross polarization of the antenna is less than 21 dB in the H plane and less than 36 dB in the E plane.

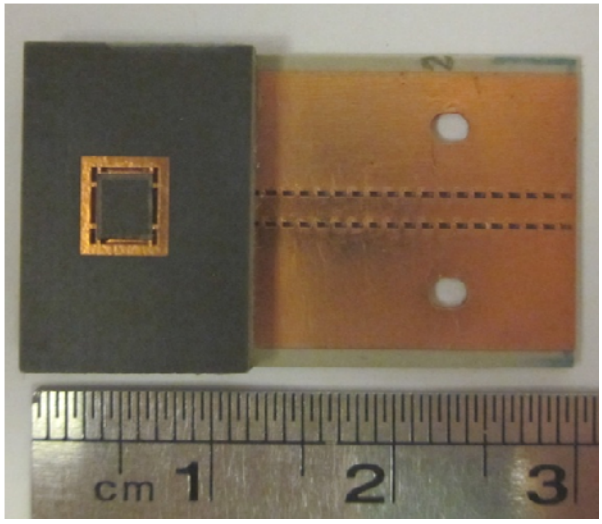

(b)

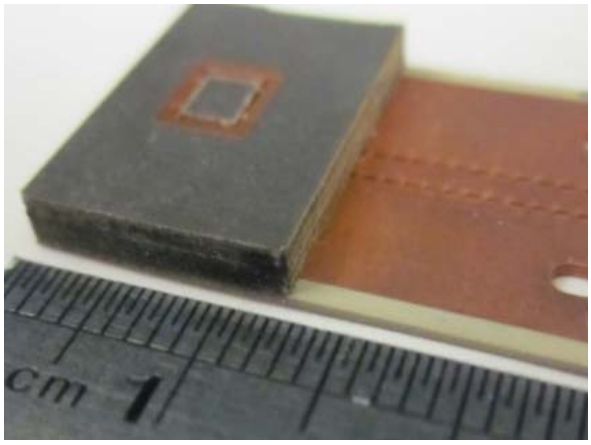

(b)

Figure 4.6. Photograph of the fabricated antenna (a) top view, (b) side view

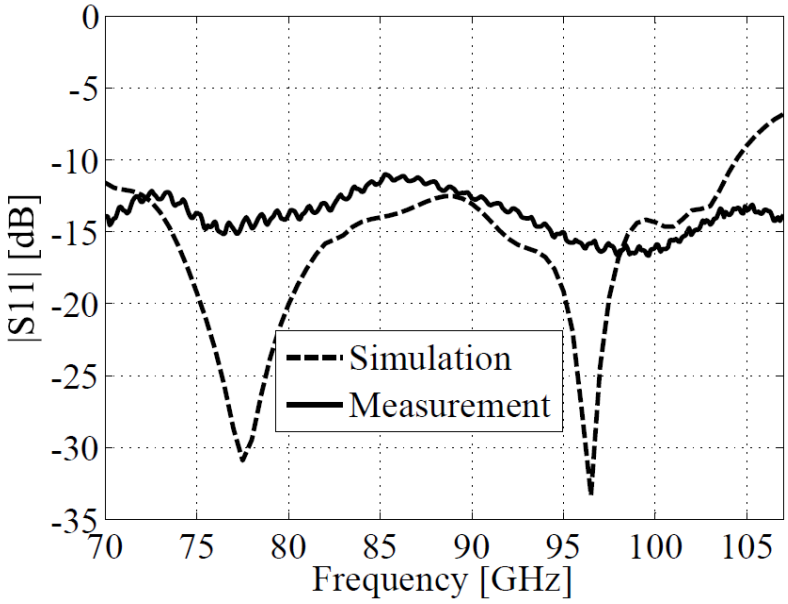

Figure 4.7. Simulated and measured |S11| of the integrated multilayer horn antenna

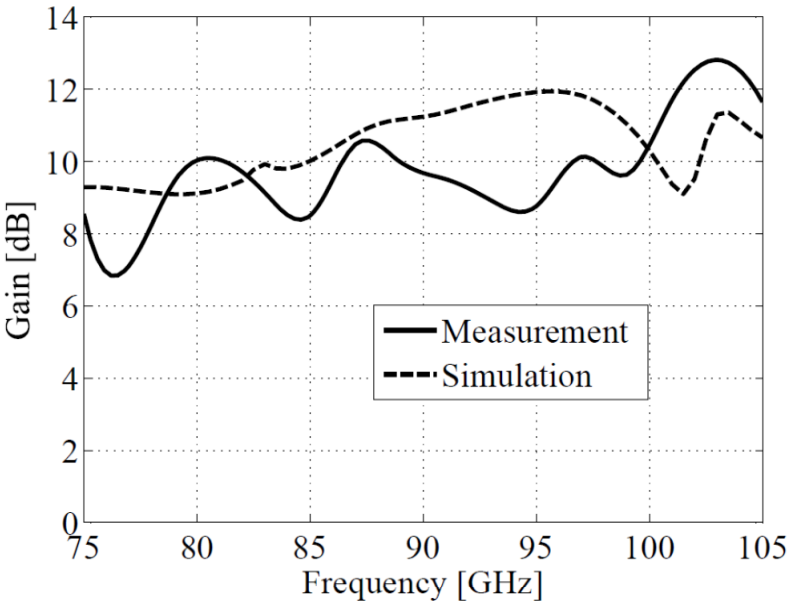

Figure 4.8. Simulated and measured gains of the integrated multilayer horn antenna

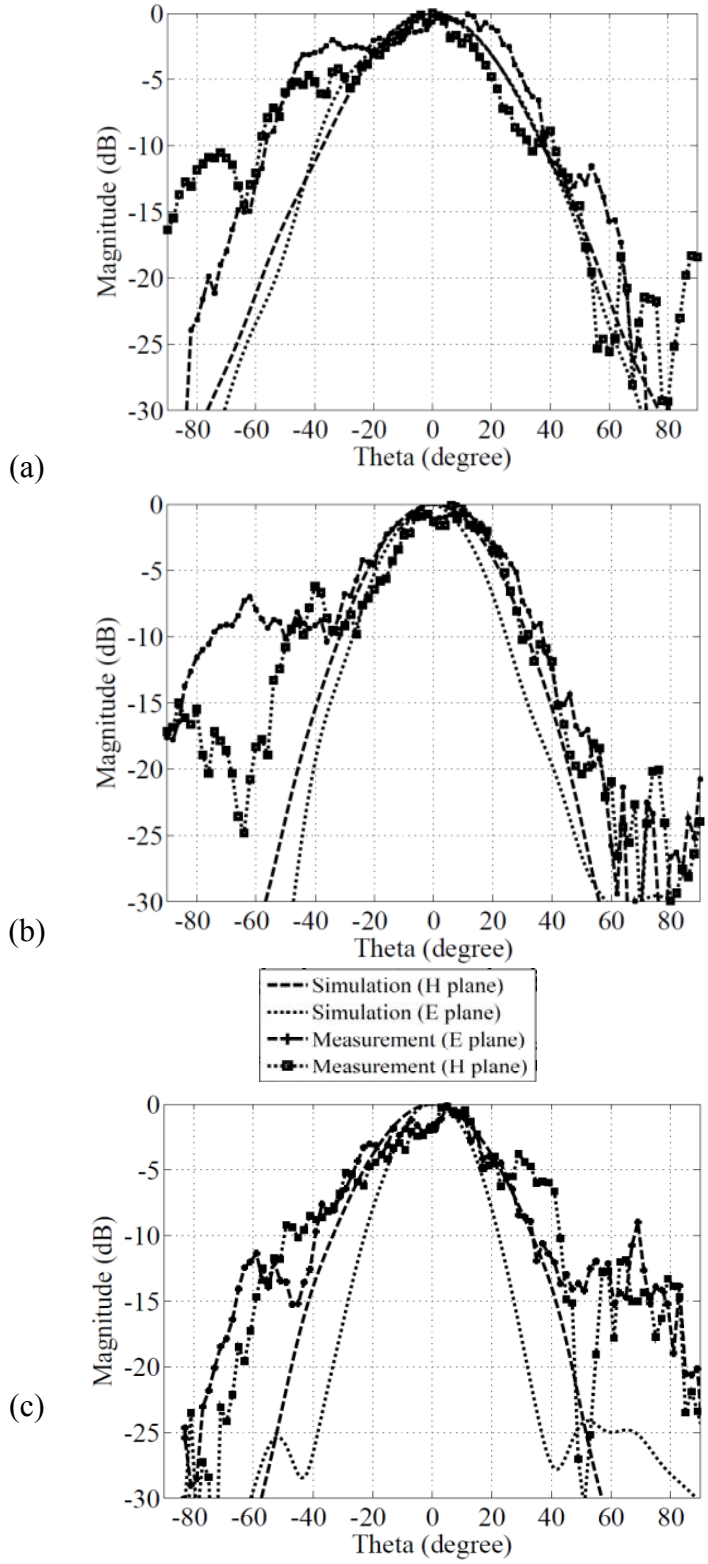

Figure 4.9. Simulated and measured E- and H-plane radiation patterns of the horn antenna at (a) 78 GHz, (b) 88 GHz, and (c) 98 GHz.

4.2 Planar high-gain dielectric-loaded antipodal linearly tapered slot antenna for E/W-band gigabyte point-to-point wireless services

The concept of SIW-fed horn and antipodal linearly tapered slot antenna (ALTSA) are jointly used to design a low-cost, high-gain and efficient planar dielectric-loaded antenna for ultra wideband gigabyte wireless services, which are demonstrated over E/W-band. SIW technique is again used to feed the proposed antenna. To increase the gain of the antenna, a dielectric-loaded slab is used in front of the antenna and works as a dielectric guiding structure. The SIW feed, the proposed antenna, and the loaded dielectric are all integrated in a planar single layer substrate, resulting in low-cost and easy fabrication. Low-cost Printed Circuit Board (PCB) process is utilized to fabricate the antenna structure with rectangular and elliptical shaped loaded dielectrics. Measured bandwidth of the antenna covers both E- and W-bands (70-110 GHz). Measured gain of the single element antenna is 14±0.5 dBi while the measured radiation efficiency of 84.23% is obtained at 80 GHz. Wideband SIW power dividers are used to form a 1×4 array structure. Measured gain of the 1×4 array antenna is 19±1 dBi, while the measured radiation pattern and gain are almost constant within the wide bandwidth of the antenna.

4.2.1 Review and introduction

Several low-cost and highly efficient antenna structures based on SIW technology have recently been presented which exhibit relatively narrow bandwidth, e.g. slot arrays and H-plane horn antennas [80]-[83]. SIW-fed antipodal linearly tapered slot antenna (ALTSA) [85]-[88] and Vivaldi antennas [89] were presented for wideband applications. Using SIW feed can effectively remove the bandwidth–limited balun in conventional ALTSA. Although they have wide bandwidth, they suffer from a relatively low gain when they are not long enough. Recently, it has been shown that by loading a non-planar cylindrically shaped dielectric, the gain of the SIW-fed Vivaldi antenna was increased from 2.3 dBi to 4.76 dBi [89], and a gain of 14.5 dBi was obtained for a 1×8 array structure at X band [89].

In this work, ALTSA and SIW-fed horn antenna are combined so to design a high-gain and highly efficient dielectric loaded ALTSA antenna for ultra-wideband gigabyte point-to-point

wireless services at E- and W-band (70-110 GHz). Dielectric loading is used to increase the gain of the proposed antenna. The antenna and the loaded dielectric are fully integrated in a single layer planar structure, resulting in low cost and easy fabrication. Measured gain of the single element antenna is 14 ± 0.5 dBi within the wide bandwidth of the antenna. Compared to the recently presented dielectric loaded Vivaldi antenna in [89], the proposed antenna exhibits more gain in addition to having planar form and low-cost structure, but it has wider architecture. A wideband planar SIW-based power divider is used to design 1×4 antenna array with 19 dBi gain. Simulated and measured results have good agreement, which have effectively validated the proposed antenna concept.

4.2.2 Dielectric-loaded antipodal linearly tapered slot antenna (single element)

SIW-fed antipodal linearly tapered slot antenna (ALTSA) was presented in [85]-[88] for wideband applications. The use of an SIW feed removes the bandwidth limitation of a balun in conventional ALTSA (Figure 4.10(a)). The cut-off frequency of the SIW feed determines the lowest operating frequency of the antenna. The proposed antenna structure in this work is designed on a Rogers\Duroid6002 substrate with dielectric constant of 2.98 at 10 GHz and the thickness of 0.508 mm. In this demonstration, a relatively thick substrate is used to lower the conductor loss of SIW and also to facilitate the fabrication process. The design procedure of SIW that was presented in [90] is utilized to calculate the spacing between two adjacent vias (S) and the width of SIW (W) [90]. To facilitate the fabrication process of our laser micro-machining, square via holes are utilized in this work although the other shaped via holes may be deployed. In fact, simulation and measurement results show that using square via holes does not change the characteristics of SIW.

To form ALTSA (with reference to Figure 4.10 (a)) the metallization of either side of the substrate is flared in opposite direction to form the tapered slots. To solve a potential mismatch problem, the flaring metals are designed to overlap with each other by defining an appropriate parameter W3 (Figure 4.10 (a)).

(a)

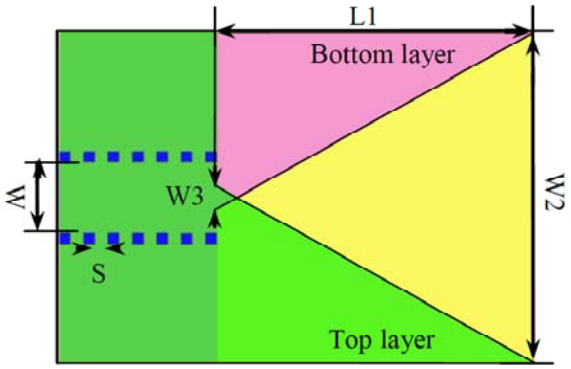

(b)

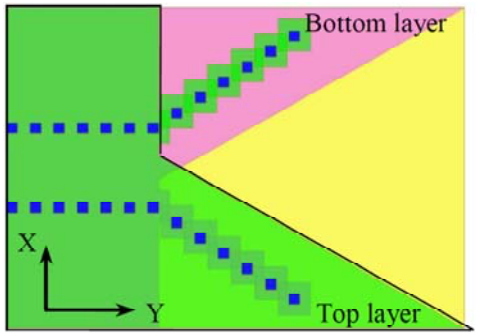

(c)

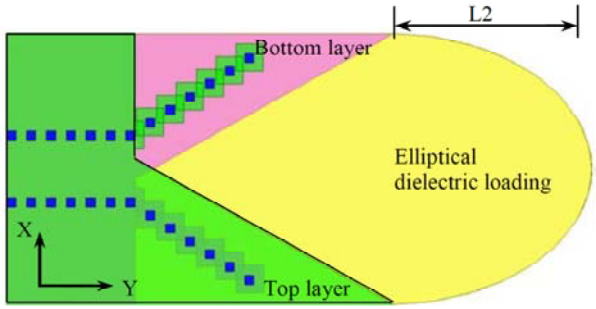

(d)

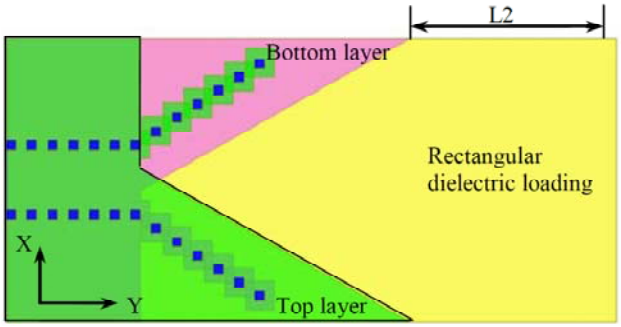

Figure 4.10. Structure of millimeter-wave (a) ALTSA antenna, (b) ALTSA with horn shaped via, (c) elliptical dielectric loaded ALTSA with horn shaped via, and (d) rectangular dielectric loaded ALTSA with horn shaped via.

Width of the ALTSA (W2) should be larger than 2λ. W2 and W3 are optimized to design a wideband ALTSA for E- and W- band applications. All the dimensions of the antenna structure are presented in Table 4.2. Horn shaped via holes (Figure 4.10 (b)) are added to the antenna structure to increase gain of the antenna, especially at high frequencies, and also to reduce the side lobe level. Then, planar elliptical shaped (Figure 4.10 (c)) and rectangular shaped (Figure 4.10 (d)) dielectrics are added in front of the antenna to enhance the gain and also reduce the side lobe level of the antenna. Note that the dielectric slab is designed on the same substrate of the antenna with the same dielectric constant and thickness of the antenna substrate. Thus, the entire structure is easy to fabricate, which also becomes compact. The loaded dielectric slab can be considered as a dielectric guiding structure excited by the ALTSA aperture, resulting in a narrower beamwidth in E-plane. Figure 4.11 shows the top view of simulated electric field distribution at 84 GHz (Ansoft HFSS v.13) of the ALTSA.

Table 4.2: Dimensions of the dielectric loaded ALTSA

Symbol	Value (mm)
W	1.6
W2	7.5
W3	0.24
S	0.3
L1	7.14
L2	3.75

Figure 4.12 and Figure 4.13 illustrate the impact of the horn shaped via and dielectric loading on the gain and radiation pattern of the antenna. Using a horn shaped via holes can effectively reduce the side lobe level of the antenna especially in E-plane while it also increases the gain of the antenna at higher frequency range. Figure 4.12 shows that the rectangular dielectric loading presents a higher gain compared to the elliptical dielectric loading with the same length.

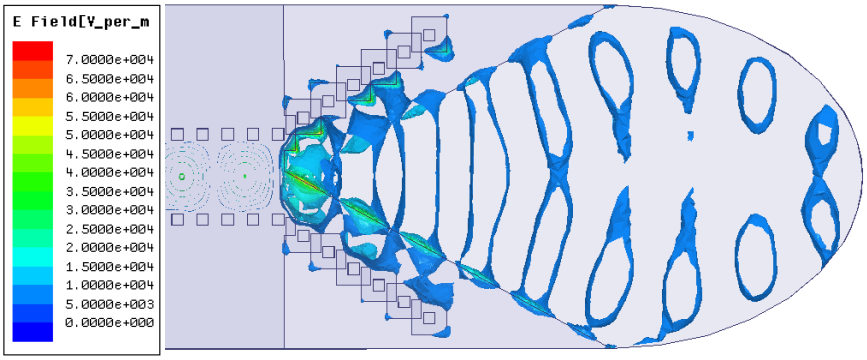

(a)

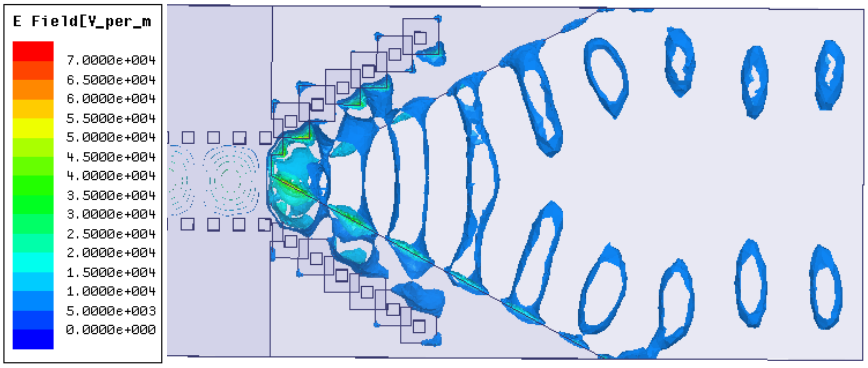

(b)

Figure 4.11. Top view of simulated electric field distribution at 84 GHz (Ansoft HFSS v.13) of the ALTSA antenna with horn shaped via and (a) elliptical, (b) rectangular dielectric loading (L2 = 5.5 mm).

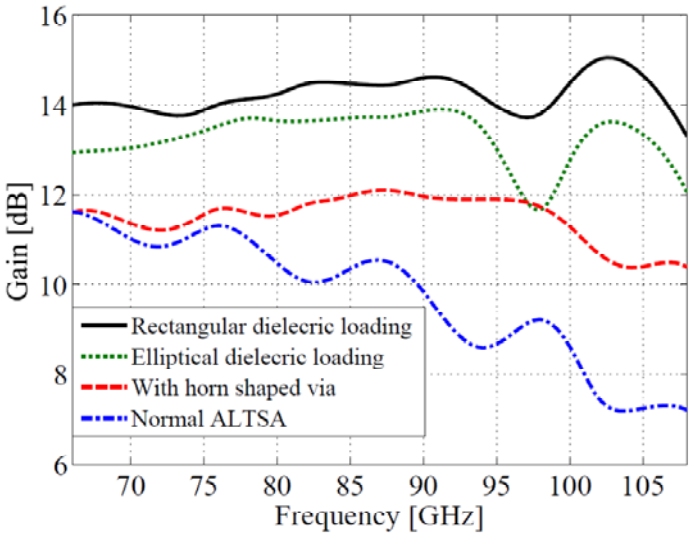

Figure 4.12. Impact of the horn shaped via and dielectric loading on the gain of ALTSA antenna.

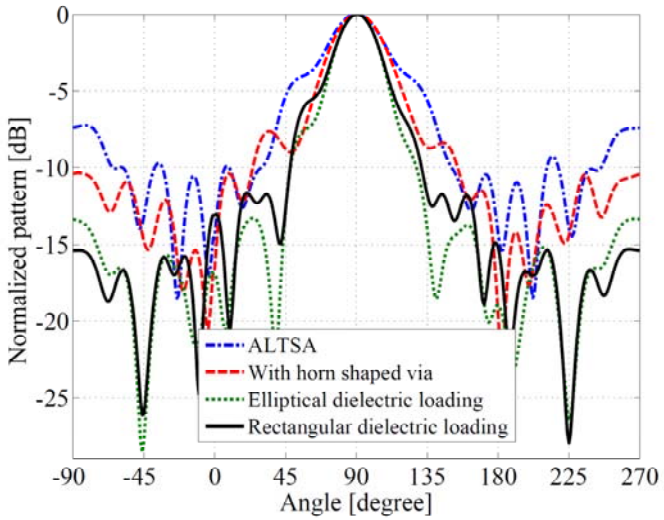

(a)

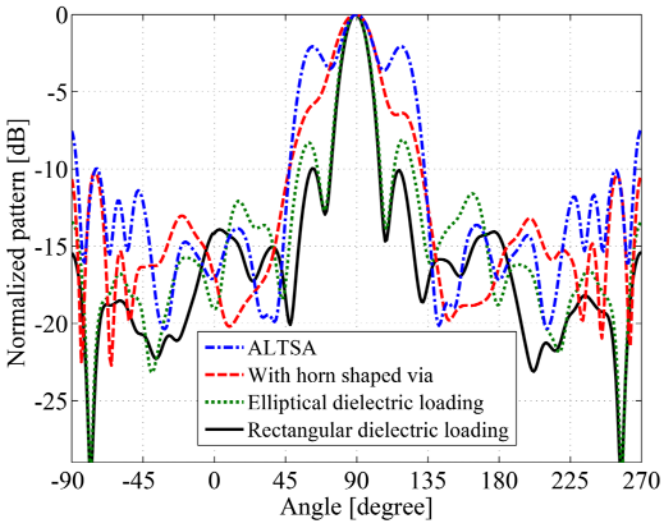

(b)

Figure 4.13. Impact of the horn shaped via and dielectric loading on the radiation pattern of ALTSA antenna at 83.5 GHz (a) YZ (H) plane (b) XY (E) plane.

Although the elliptical dielectric loading yields less side lobe level in H plane (because of the lens shaped structure of the elliptical dielectric), compared to the rectangular dielectric loading, but it has more side lobe level in E plane. The side lobe level in connection with the rectangular dielectric loaded antenna is better than 10 dB in both E- and H-planes, while it has also more gain. Compared to the recently presented dielectric loaded Vivaldi antenna in [89], the proposed antenna exhibits more gain. In addition, it has the advantages of having a planar form and a low

cost structure. The maximum gain of 10.5 dBi was obtained for a single element antenna in [89] with the dimension of 0.5λ×25λ while the proposed structure has the maximum gain of 14.5 dBi with the dimension of 2.35λ×3.5λ. Then the proposed antenna has higher gain and also shorter structure but it has a wider configuration.

Impact of length of the rectangular dielectric loading on the gain of the antenna at 74 GHz, 84 GHz, and 94 GHz is shown in Figure 4.14. As it is described, the maximum gain of 14.25 dBi is obtained for 4 mm length. Figure 4.15 shows the impact of length of the rectangular dielectric loading on the side lobe level of the antenna in both E- and H-planes. Figure 4.16 suggests that the side lobe level is almost minimum when the length is about 4 mm. Then, 4 mm length is chosen for the length of the loaded dielectric.

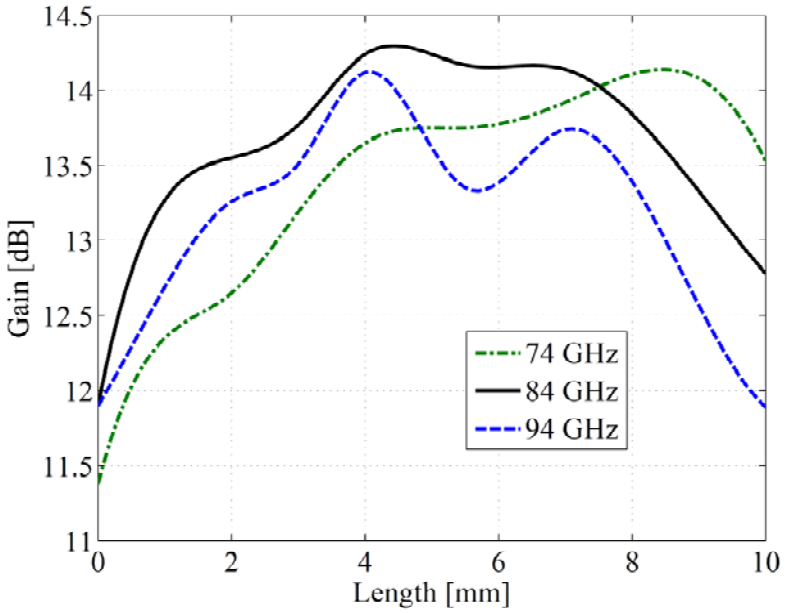

Figure 4.14. Impact of length of the rectangular dielectric loading on the gain of the antenna at 74 GHz, 84 GHz, and 94 GHz.

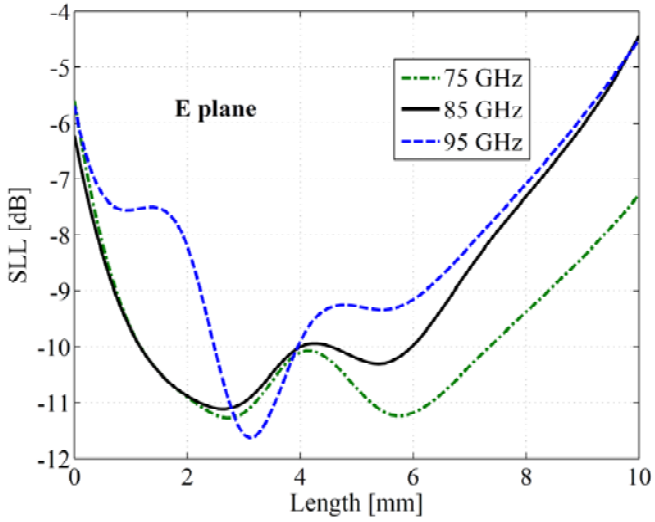

(a)

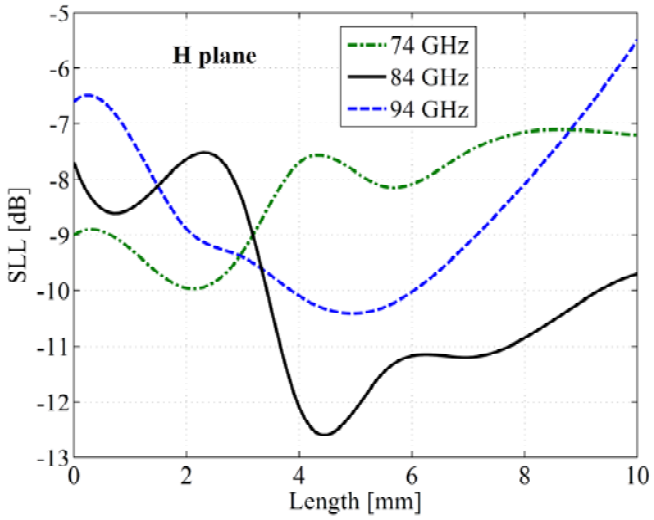

(b)

Figure 4.15. Impact of the length of the loaded dielectric on the side lobe level, (a) E plane, and (b) H plane, at 74 GHz, 84 GHz, and 94 GHz.

Performance of the conventional ALTSA is sensitive to thickness t and dielectric permittivity ε_r of the supporting substrate. Yngvesson [91] defined a factor:

$$f_{substrate} = t(\sqrt{\varepsilon_r} - 1)/\lambda_0 \quad (4.1)$$

when an acceptable range for LTSA operation is $0.005 \leq f_{substrate} \leq 0.03$ while the performance of the LTSA is degraded by substrate modes for substrate thicknesses above the

upper bound [91]. As frequency increases, satisfying this constrain will become more difficult because (a) working and fabricating on very thin substrate are difficult, and (b) fabricating SIW on thin substrate increases the metallic losses and then decreases the efficiency of the antenna.

One of the advantages of the proposed antenna is that we can implement it on thick substrate ($f_{substrate} = 0.1$ in this design). In this new design, an effective combination of SIW-fed horn and dielectric loading is used to design an ALTSA on a thick substrate.

Low-cost Rogers/Duroid 6002 substrate is used to implement the antenna structure. Figure 4.16 shows the photograph of our fabricated elliptical and rectangular shaped dielectric loaded ALTSA. A wideband transition between the rectangular waveguide (WR10) to SIW [60]-[61] is used to measure the antenna parameters at W-band. Return loss of the prototyped antenna is measured by using an Anritsu 3739C vector network analyzer. Figure 4.17 (a) shows the measured return loss of the rectangular dielectric loaded ALTSA. The measured results show that the bandwidth of the antenna covers entire the E/W-band (71-97 GHz). Discrepancy between the simulated and measured |S11| of the antenna is caused by the WR10-to-SIW transition which is used to measure the |S11| of the antenna. Radiation pattern and antenna gain are measured in our anechoic chamber. Figure 4.17 (b) compares simulated and measured gains of the antenna. One of the advantages of the proposed antenna is its relatively stable gain within the wide bandwidth of interest. Note that, due to the measurement limitation, radiation pattern of the antenna is measured from 75 GHz. Figure 4.18 shows simulated and measured radiation patterns of the rectangular dielectric loaded ALTSA antenna at 75 GHz, 85 GHz, and 95 GHz. Good agreement can be observed between simulated and measured patterns. Measured side lobe level is better than 10 dB in both H and E planes over the most of the antenna bandwidth. Simulated and measured cross polarizations of the antenna are better than 10 dB over the most of the antenna bandwidth of interest. For applications in which a more cross polarization reduction is required, decreasing the thickness of the substrate would reduce the cross polarization level, e.g. simulation results showed that decreasing the thickness of the substrate to 0.25, and 0.125 mm would be able to reduce the cross polarization level to 16 dB and 23 dB, respectively. While in this work to reduce the metallic losses of SIW and also facilitate the

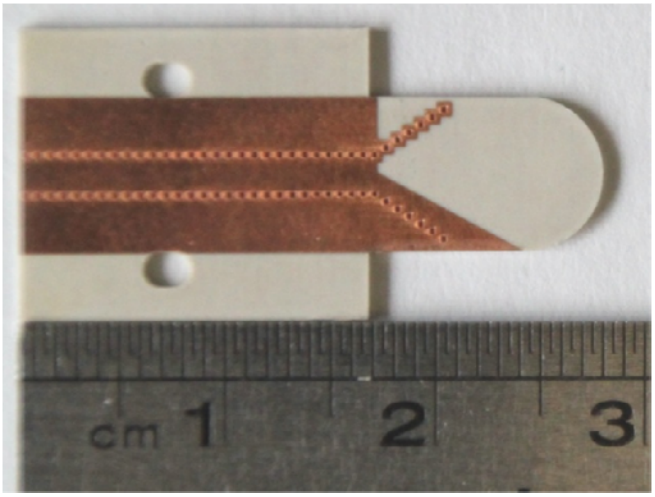

(a)

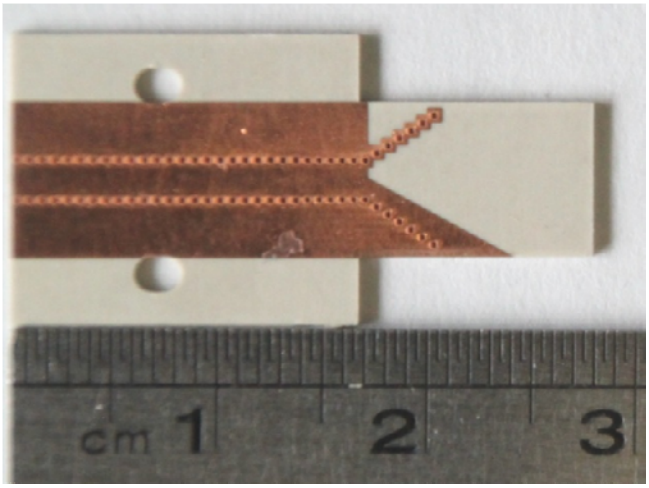

(b)

Figure 4.16. Photograph of the fabricated (a) Elliptical dielectric loaded ALTSA, (b) rectangular dielectric loaded ALTSA.

fabrication and measurement procedure, a relatively thick substrate is chosen. The estimated radiation efficiency from the measured gain and directivity is 84.23% at 80 GHz. $D \cong \frac{32400}{\theta_{1d}\theta_{2d}}$ [92] is used to estimate the directivity from the measured radiation pattern of the antenna. The simulated radiation efficiency is 93.6%. Note that the dielectric and metallic losses have been considered in the simulation results. Over the W-band frequency range, two different lengths of SIW are used to estimate the dielectric loss tangent of the substrate; one to calibrate the vector network analyzer, and the other to measure |S21|. Then, HFSS software is utilized to compare the

simulated |S21| with the measured results so to estimate the dielectric loss tangent at W band. Note that this method was used in [58] to estimate the dielectric loss tangent at 60 GHz. To generate a better estimation, metallic losses and also the roughness of the substrate are considered in the simulation results. Simulation results indicate that, metallic and dielectric losses do not have significant effect on the bandwidth and matching condition of the single element antenna while they decrease the gain of a single element antenna by 0.3 dB.

(a)

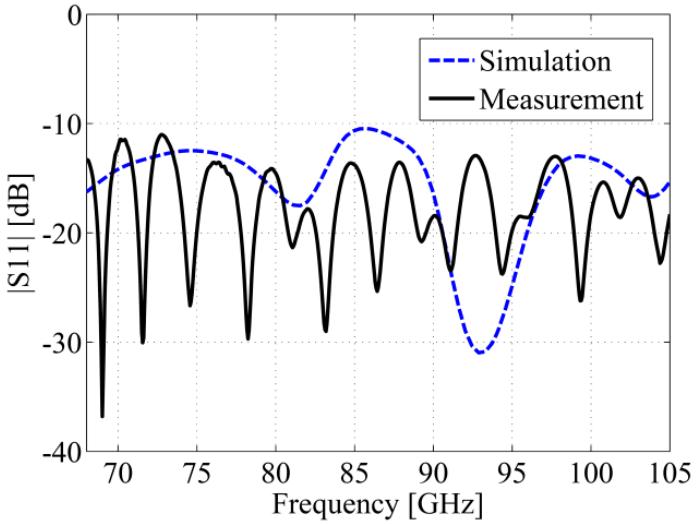

(b)

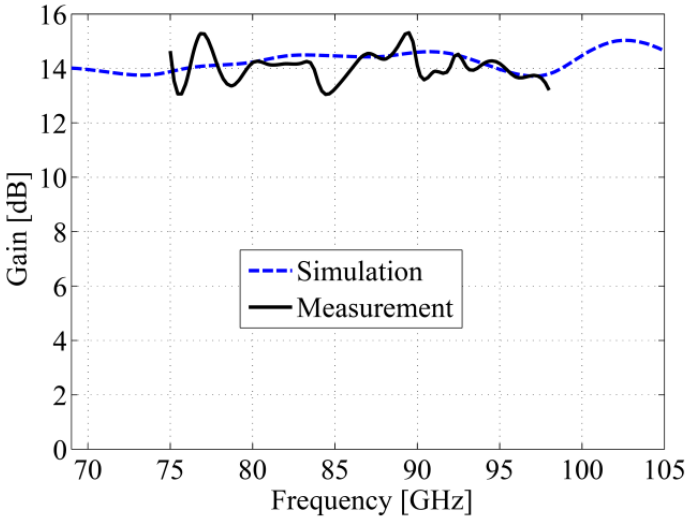

Figure 4.17. Measured and simulated (a) |S11| and (b) Gain of the rectangular dielectric loaded ALTSA.

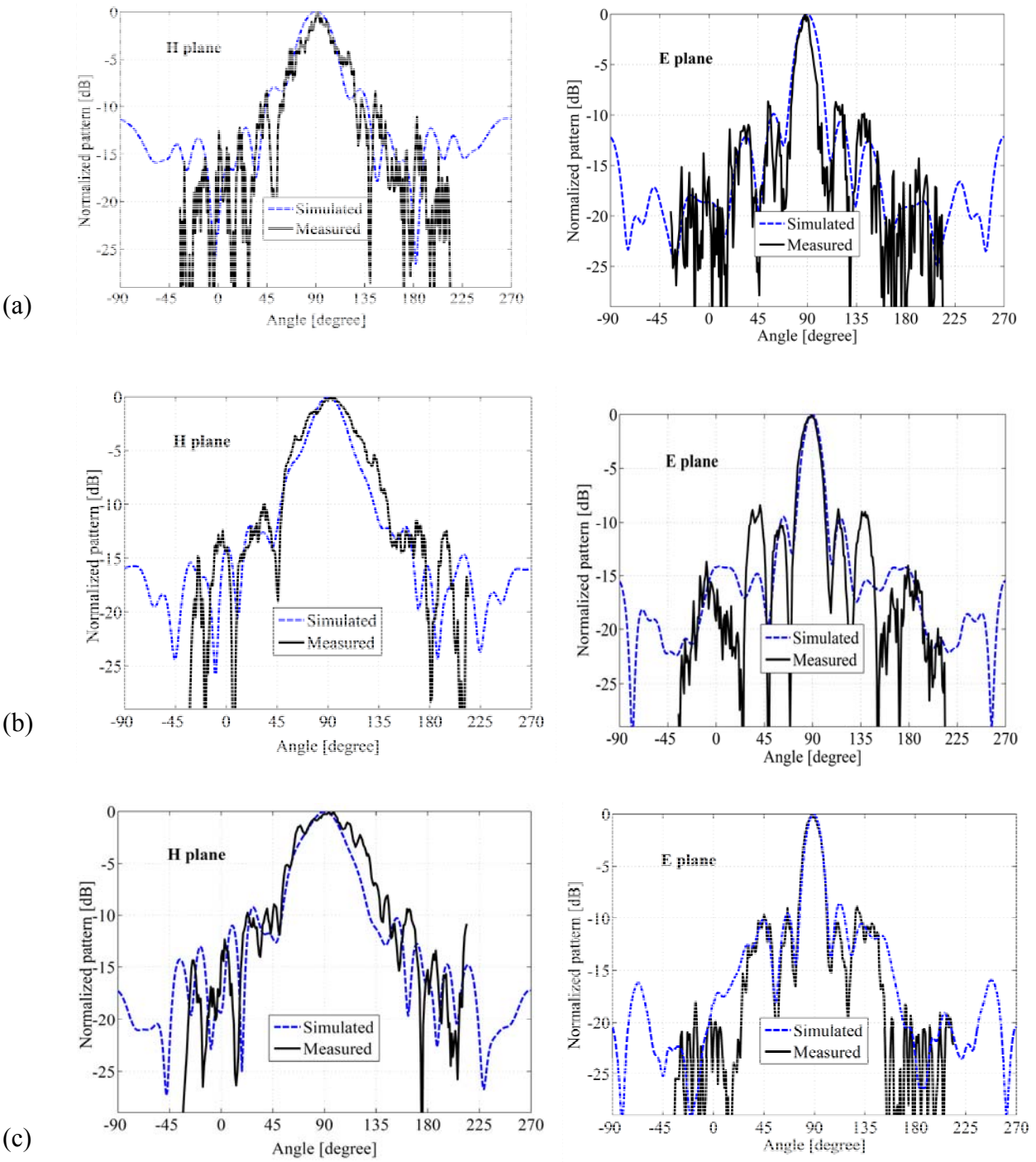

Figure 4.18. Simulated and measured radiation patterns of the rectangular dielectric loaded ALTSA in the E- and H-planes at (a) 75 GHz, (b) 85 GHz, and (c) 95 GHz

4.2.3 1×4 planar array of dielectric loaded ALTSA antenna

Wideband SIW power dividers are used to form a 1×4 array structure. To obtain the maximum gain, the four antenna elements are fed with the same phase and amplitude, and distributions like Dolph-Chebyshev's amplitude, are not used. One T junction and two V junctions are used to form the 1×4 power divider. Simulated |S21| and |S11| plots of the Y- and T-shaped junctions are shown in Figure 4.19.

Due to the narrow beamwidth of the designed single element antenna in E-plane (17 Deg.); increasing the distance between those antenna elements to 2.35 λ, does not increase the side lobe level of the array antenna. E(total) = E(single element at reference point) × [Array Factor], although increasing the distance between elements to 2.35λ creates grating lobes at [array factor]. Because the single element antenna has a very narrow beamwidth, it has very low (less than -15 dB), E (single element at reference point), then E(total) is low and side lobe level of the array antenna is thus low. Simulation results show that the side lobe level of the antenna array is 10 dB in both E and H planes over the most of the desired bandwidth of the antenna. Note that the proposed antenna is designed for E/W-band gigabyte point to point wireless communication, and then the side lobe level is not an issue of concern for this application while in this design, gain, cost and efficiency are the main characteristics. The antenna array structure is fabricated in a single layer structure. Figure 4.20 shows the photograph of the fabricated 1×4 array of the rectangular dielectric loaded ALTSA. The measured and simulated |S11| and gain of the antenna array are shown in Figure 4.21. The bandwidth of the antenna array covers the entire E/W-band of interest (71-97 GHz) while the gain of the antenna is kept almost constant within such a wide bandwidth of the antenna array. The observable discrepancy between the simulation and measured gains might be due to the calibration related tolerance range of the antenna reference in our anechoic chamber. Simulated and measured radiation patterns of the antenna array are shown in Figure 4.22. The measured side lobe level of the antenna array is better than 10 dB over the most of the desired bandwidth of the antenna, which has confirmed our above discussion.

Figure 4.21 (b) compares measured and simulated gains of the antenna array. Simulation results show that metallic and dielectric losses decrease the gain of the antenna array by 1.52 dB while in the single element antenna; losses decrease the gain by 0.3. Simulation results show that much of

the loss is caused by the dielectric loss effect at the feed network. Using low loss material (e.g. glass, or Alumina) can reduce this effect, although it also increases the fabrication cost. The estimated radiation efficiency from the measured gain and estimated directivity is 65.4%at 80 GHz, while the simulated radiation efficiency is 76.5%. Figure 4.23 shows measured |S12| of 28.78 mm long SIW on Rogers 6002 substrate. To measure this |S12|, a TRL calibration kit was used to eliminate the effect of the WR10 to SIW transitions.

(a)

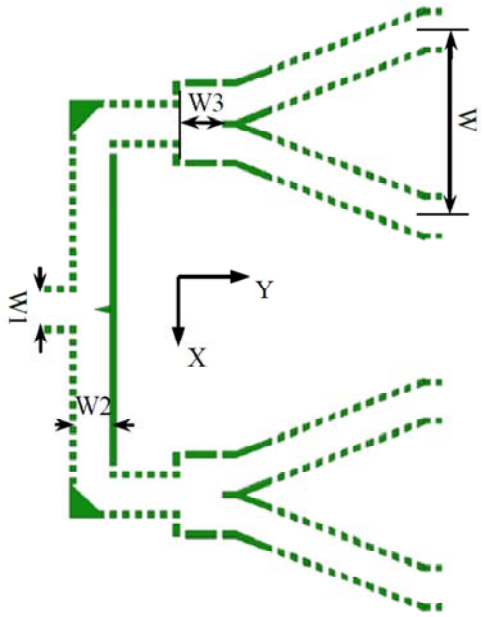

(b)

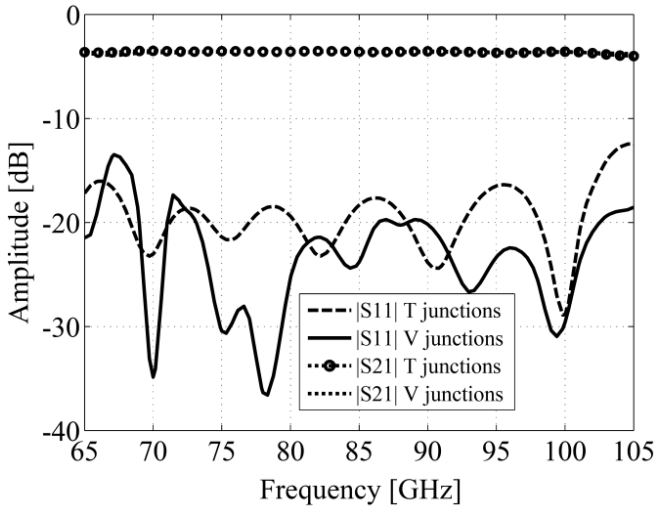

Figure 4.19. (a) Geometry of power divider (b) Simulated |S11| and |S21| of T-shaped and Y-shaped junctions.

Table 4.3: Dimensions of the power divider

Symbol	Value (mm)
W	8.8
W1	1.6
W2	1.6
W3	2.05

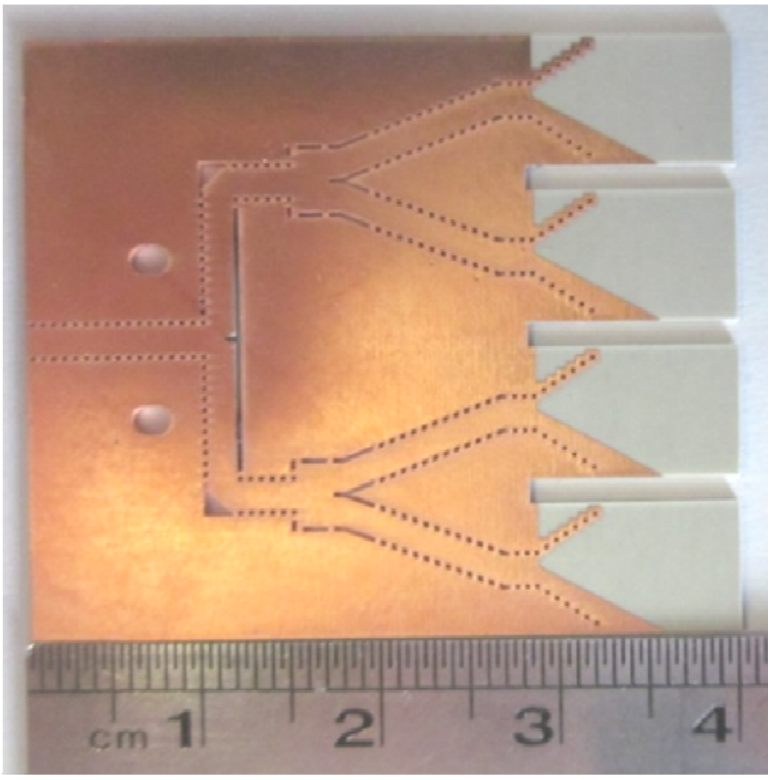

Figure 4.20. Photograph of the fabricated 1×4 array of rectangular dielectric loaded ALTSA.

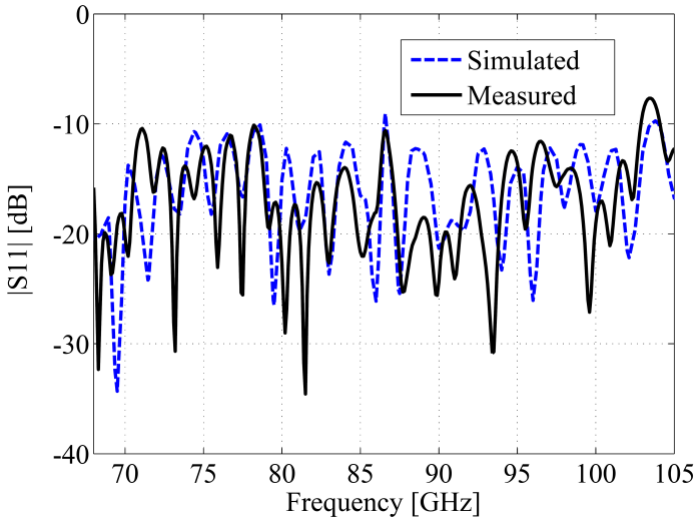

(a)

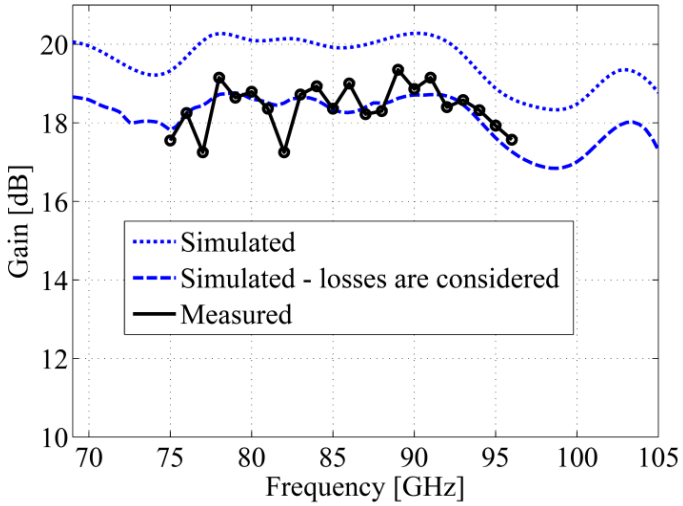

(b)

Figure 4.21. Measured and simulated (a) |S11|, (b) Gain of 1×4 array of rectangular dielectric loaded ALTSA.

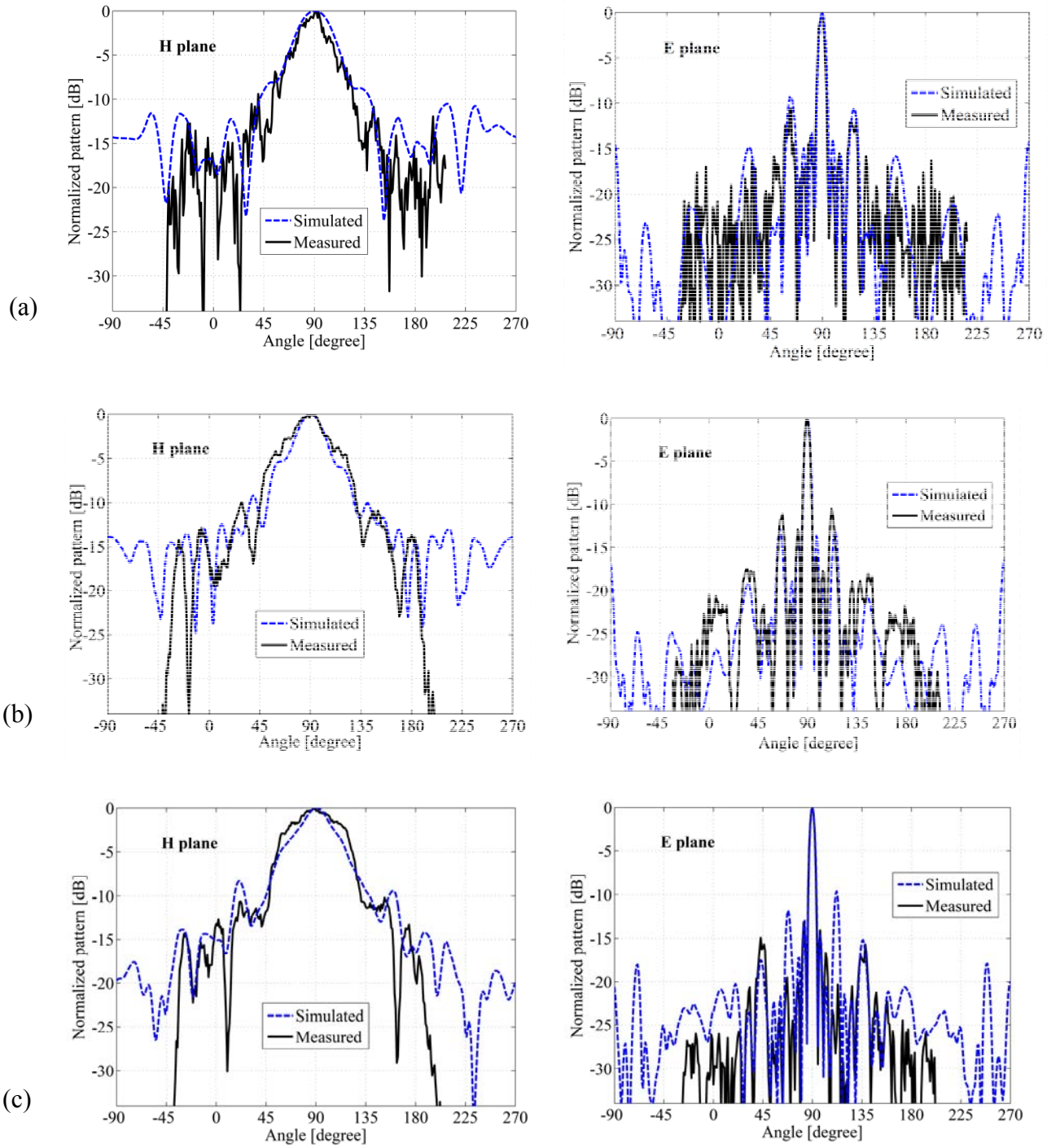

Figure 4.22. Simulated and measured radiation patterns of the rectangular dielectric loaded ALTSA in H and E planes at (a) 75 GHz, (b) 85 GHz, and (c) 95 GHz.

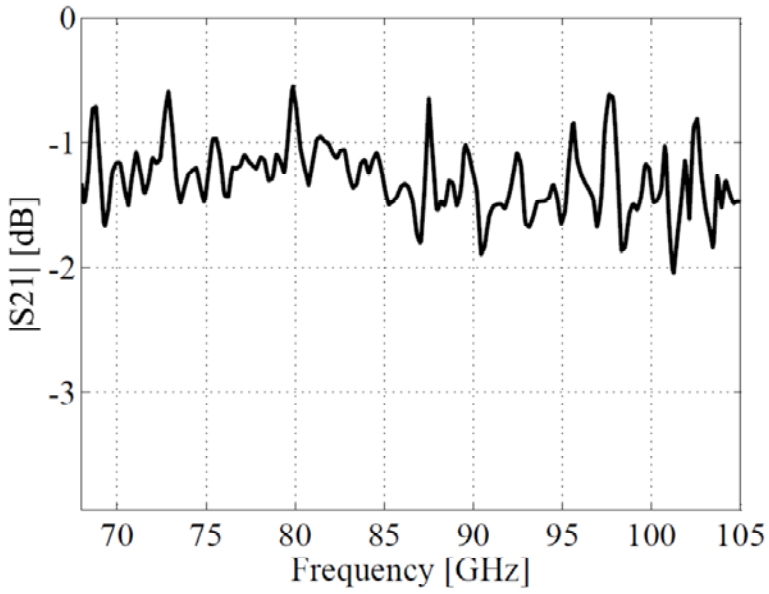

Figure 4.23. Measured |S12| of 28.778 mm long SIW on Rogers 6002 substrate.

4.3 Conclusion

In this chapter, two novel wideband antennas employing the SIW concept are developed for E/W band applications over 71-97 GHz. The two antennas have different characteristics which can use them in different front end structures. The first antenna radiates along the broadside to the substrate while the second antenna radiates into substrate-oriented end-fire. Both antenna structures have the advantages of being wideband, low cost, high gain, and they can be fabricated on low dielectric constant substrate.

The first antenna is a novel integration of the stepped horn antenna and its feeding structure. Featuring a wide bandwidth, a relatively constant gain, and a broadside to substrate radiation, the new structure is well suited for many applications such as gigabyte data transition, millimeter-wave imaging, and on-chip antennas. The proposed horn antenna is fed by SIW, which can easily be connected to coplanar waveguide and active millimeter-wave components. The horn walls are made of metalized via holes through which the opening of the horn is flared from the bottom layer to the top layer. To demonstrate the proposed structure, a multilayer low-cost standard PCB process is utilized to fabricate the horn antenna on Rogers substrates. The calculated and measured results show a good agreement. The measured bandwidth is 40% centered at 87.5 GHz which covers E/W-band. The measured gain of the antenna is relatively constant over the frequency bandwidth of interest and is about 9.5 dBi.

The second antenna is a novel low-cost, high-gain and highly efficient SIW antenna which is presented for the development of wideband gigabyte point-to-point wireless services at E/W-band. The concept of planar SIW-fed horn antenna, and antipodal linearly tapered slot antenna (ALTSA) is jointly used to design a novel broadband high-gain antenna. Then, planar dielectric slab in front of the antenna is used to increase the gain and to decrease the side lobe level. Low-cost PCB process is used to fabricate the antenna structure in single layer structure. Good agreement is obtained between the simulation and measurement results. The effect of dielectric and metallic losses on the performance of the antenna is investigated. The measured bandwidth of the antenna covers the entire E-band. The measured gain of the single element antenna is 14 dBi while 19 dBi gain is obtained for 1×4 antenna array. Measured radiation efficiency of 84.23% is obtained for single element antenna, and 65.4%for the 1×4 array at 80 GHz. This antenna structure can easily be transplanted into higher frequency range including terahertz.

CHAPTER 5 E-BAND BROADBAND TRANSITION OF SIW ON HIGH-TO-LOW DIELECTRIC CONSTANT SUBSTRATES

In emerging millimeter-wave wireless applications at E-bands, active components including LNA and power amplifier are preferred to be fabricated or surface-mounted on materials with a high dielectric constant (like CMOS and MHMIC). On the other hand, antennas should be made on low dielectric constant substrate for the enhancement of gain and bandwidth. Therefore, the development of a wideband transition from high-to-low dielectric constant substrates becomes necessary because the use of wire bonding schemes brings up problems at millimeter-wave frequencies. This chapter presents a novel wideband transition of SIW on high-to-low dielectric constant substrates. The transition has a single layer structure which consists of a tapered high dielectric constant substrate that connects two SIWs. Thanks to the waveguide-based structure of the transition, it has a self-shielded configuration, and its interference is minimum. Simulated and measured results show that the bandwidth of the proposed transition covers almost the entire W and E bands with low insertion loss.

This work is essential in support of the development of the E-band wireless communication demonstration because for E band point to point communication, a high gain antenna with wide bandwidth is needed, and it is much easier to design this antenna on low dielectric constant substrate.

5.1 Introduction

As it has been reported in the literature [93]-[96], active components are preferred to be fabricated and mounted on high dielectric constant substrates such as MHMIC and CMOS carrier substrates for applications over millimeter wave frequency range. On the other hand, antennas or radiating elements are generally designed on low dielectric constant substrate since fabricating antenna on high dielectric constant substrate decreases its gain and bandwidth. As such, the development of a wideband transition of transmission line on high-to-low dielectric constant substrates becomes critical for complete front-end integration. This work is to investigate and demonstrate a wideband low-loss transition of SIW on high-to-low dielectric constant substrates.

As it was shown in [93]-[96], it is not convenient to connect SIW to microstrip line [93] or CPW [95], by utilizing wire bonding techniques, on low-to-high dielectric constant substrates. The insertion loss of such transitions is generally high as anticipated. Of course, there is a large difference in width of microstrip lines between high and low dielectric constant substrates for the same impedance requirement, which also contribute to the limitation of bandwidth. The use of wire bonding schemes brings up problems at millimeter-wave frequencies [97]-[98] such as high interference and limited bandwidth. In applications like passive imaging systems, interference creates serious problems.

The transition to be discussed in this work presents a single layer structure and is designed for applications at E-band (71-97 GHz). The transition consists of a high dielectric constant substrate which is tapered from SIW on high dielectric constant substrate into SIW on low counterpart. Due to the metallic shielded structure of the transition, the effect of the interference is minimum. Simulated and measured results show that the bandwidth of the transition covers almost the entire W- and E-bands with low insertion loss.

5.2 Explanation of the transition

As a showcase, the SIW on high dielectric constant substrate is designed on a substrate with dielectric constant of 10.2, and thickness of 0.5 mm. The top and bottom surfaces of the substrate are covered with copper conductor. In our work, the SIW on low dielectric constant is designed on a substrate with dielectric constant of 2.98 and thickness of 0.5 mm. The two SIWs are designed to work in the same frequency range, and they have different width in this case. As Figure 5.1 shows, the two SIWs are placed on a single layer along each other, and are connected with the high dielectric constant substrate, which is tapered from the SIW on high dielectric constant substrate into its low dielectric constant counterpart. Top view of the simulated electric field distribution (Ansoft HFSS v.13) of the broadband transition of SIW on high-to-low dielectric constant substrates is shown in Figure 5.2. The broadband transition is realized by using a dielectric rod antenna probe inserted into the center of SIW on the low dielectric constant substrate.

WR and LR are the most important parameters that have impact on the input matching of the transition. Figure 5.3 shows |S11| and |S21| of the transition for three different values of WR and LR, which are generated by Ansoft-HFSS package. As Figure 5.3 (a) shows, for WR = 0.4 mm, and LR = 1.4 mm, a better impedance matching is obtained. The bandwidth of the transition covers the entire W band and the insertion loss is less than 0.2 dB. Table 5.1 shows all dimensions of the transition. Simulation results show that the transition does not excite high order propagation modes.

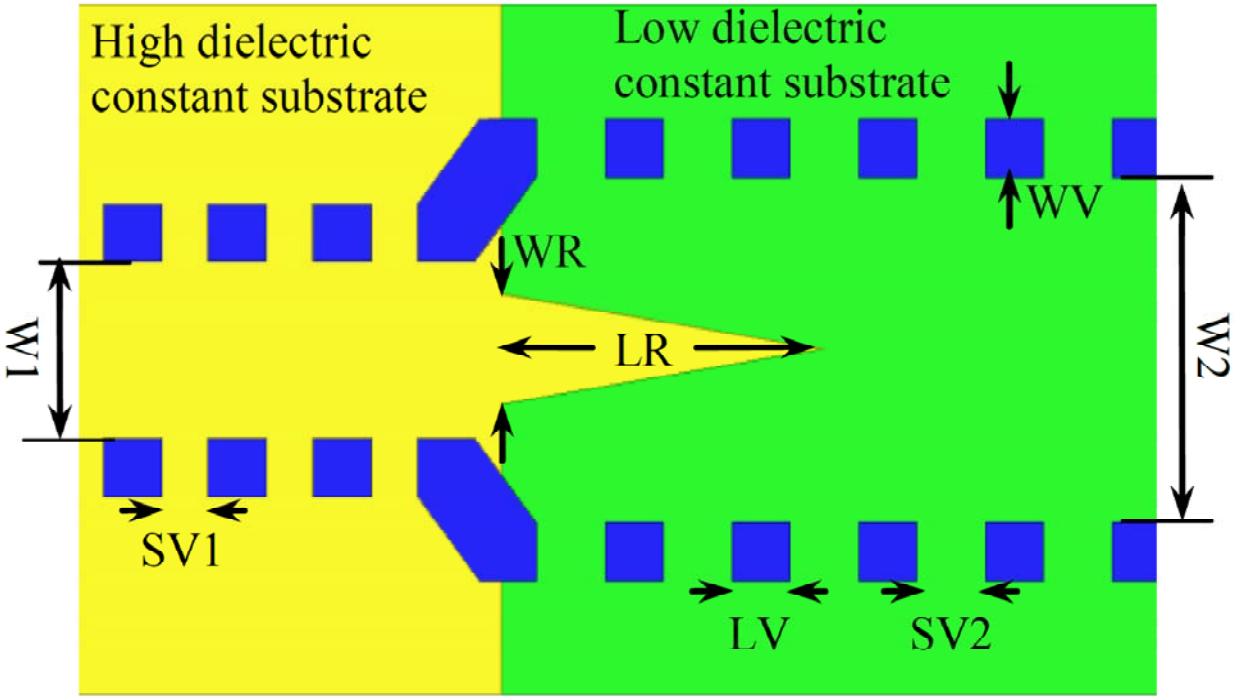

Figure 5.1. Structure of the millimeter-wave broadband transition of SIW on high-to-low dielectric constant substrates with tapered transition.

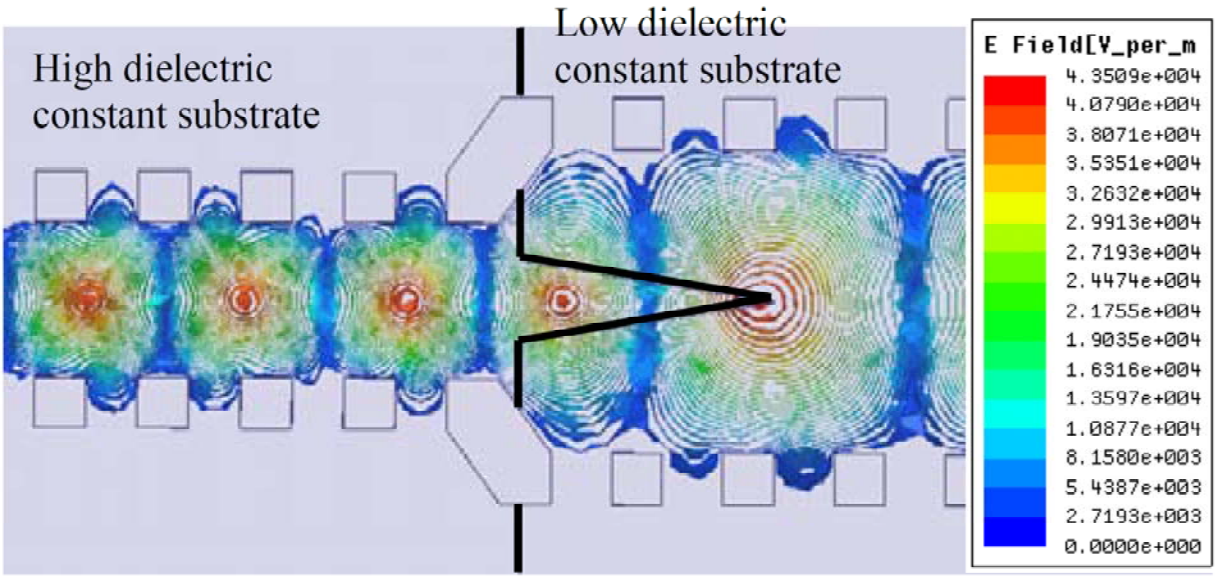

Figure 5.2. Top view of the simulated electric field distribution (Ansoft HFSS v.13) of the broadband transition of SIW on high-to-low dielectric constant substrates.

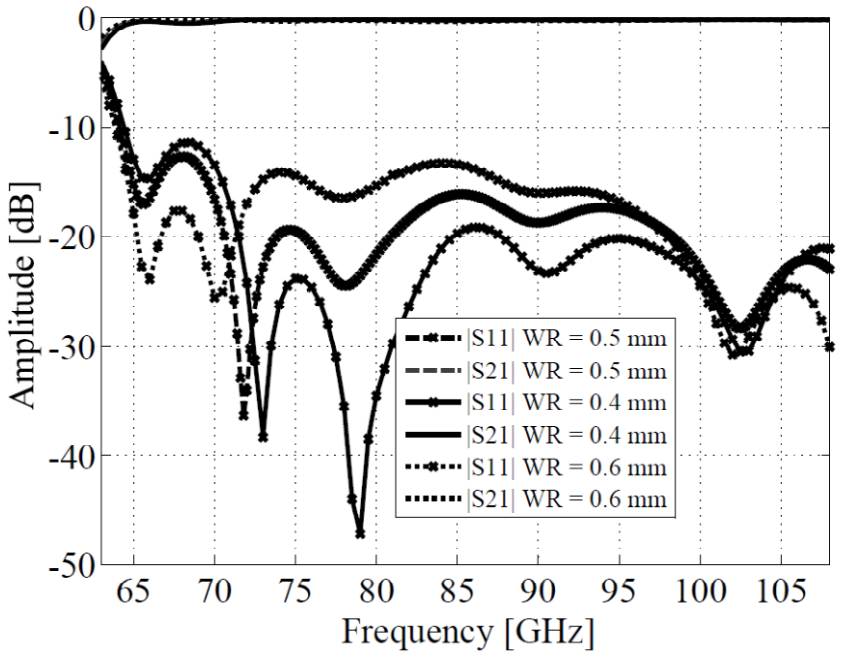

(a)

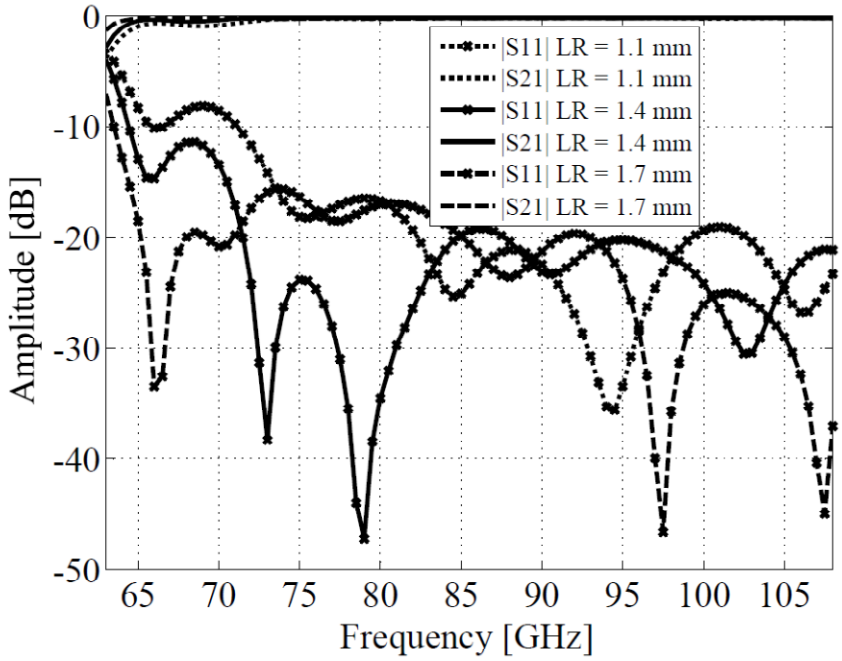

(b)

Figure 5.3. Impact of (a) WR, and (b) LR on |S11| and |S21| of the transition.

Table 5.1: Dimensions of the transition

Symbol	Value (mm)	Symbol	Value (mm)
WV	0.254	WR	0.4
LV	0.254	LR	1.4
SV1	0.2	W1	0.77
SV2	0.3	W2	1.5

Fabrication tolerance is one of the important parameters of a designed component. Figure 5.3 also shows that even significant changes on the dimension of WR and LR do not have serious effect on the bandwidth and insertion loss of the proposed transition. Impact of the gap between the high dielectric constant substrate and the low dielectric constant substrate on the insertion loss of the transition is shown in Figure 5.4. Although utilizing an accurate fabrication process can easily reduce the gap to less than 25µm, but as Figure 5.4 shows even with 100 µm or 200 µm gap, an

acceptable insertion loss is obtained. It means that the gap does not have serious effect on the performance of the transition. Note that in the simulation results of Figure 5.4, the top and bottom layers of the gap are covered with a conductor tape. When considering the gap between the two substrates in Figure 5.4, their top and bottom metal planes are electrically and mechanically connected to each other with the conductor tape. The gap between the two substrates is one between the dielectrics. Note that the conductor tape used to cover the gap should provide a proper DC connection between the two substrates along the gap. If the conductors of the both substrates are made of copper, soldering them can also be used to cover the gap.

Matching the two substrates in the vertical direction is usually easy and accurate. If the two substrates are deposited on a flat surface, they should get matched in the vertical direction. The roughness of Rogers substrates used in our case studies are usually less than 0.5 μm, becomes negligible against the thickness of substrates (0.5 mm). Obviously, this does not have a significant effect on the performance of the transition.

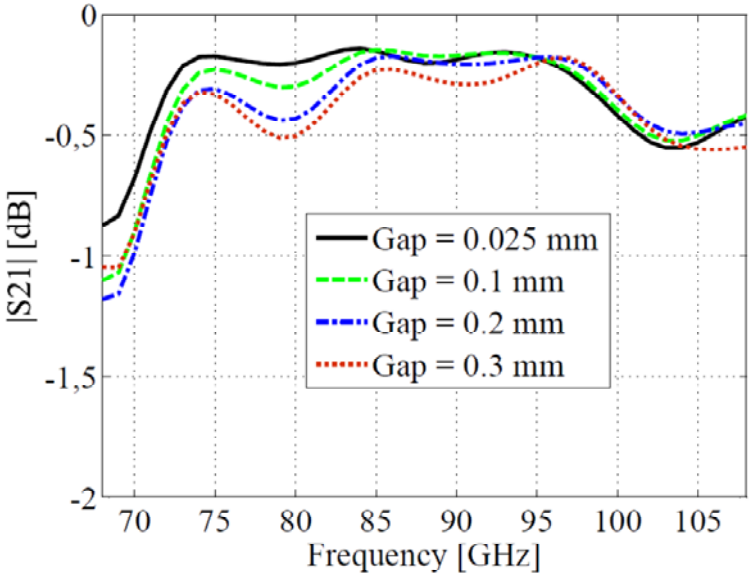

Figure 5.4. Impact of the gap between the high dielectric constant substrate and the low dielectric constant substrate.

Dimensions of the transitions on different high to low dielectric constant materials for different materials are given in Table 5.2. The transitions are designed to cover all the E and W frequency

bands (71-110 GHz) with less than 0.2 dB insertion losses. Empirically, the dimension of the transition can be approximated from the following formulation:

$$\mathrm{LR} \approx \left(1 - \frac{\sqrt{\varepsilon_{r_l}}}{\sqrt{\varepsilon_{r_h}}}\right) \times \frac{\lambda_0}{2} \qquad (5.1)$$

$$\mathrm{WR} \approx \frac{\lambda_0}{4} \times \left(\frac{1}{\sqrt{\varepsilon_{r_l}}} - \frac{1}{\sqrt{\varepsilon_{r_h}}}\right) \qquad (5.2)$$

in which λ_0 is the wavelength of the cut-off frequency of SIW, ε_{r_h} is the higher dielectric constant, and ε_{r_l} is the lower dielectric constant. The other dimension of the transition such as the width of SIW and the dimensions of via holes can be calculated with the design procedure of SIW which was detailed in [84]. Although (5.1) and (5.2) give a proper approximation of length and width of the tapered high dielectric constant substrate, an optimization procedure can reduce the insertion loss. The optimized dimensions of transitions on various high-to-low dielectric constant materials are described in Table 5.2.

Note that simulation results show that thickness of the substrate have negligible effect on the performance of the transition. In this work, for easiness of fabrication and measurement, a 20 mils thickness substrate has been used. As Table 5.2 shows the proposed transition can be used to connect antenna to a silicon chip.

Dielectric and metallic losses are considered in the simulation results. To facilitate the comparison between those results, dielectric loss tangent of the low dielectric constant substrate is assumed to be 0.0012, and dielectric loss tangent of the high dielectric constant substrate is assumed to be 0.0001. Although the thickness of substrate yields a negligible effect on the performance of the transition, reducing the thickness of substrate would increase the metallic losses of SIW. To make the results comparable in all the simulations, the thickness of substrate is chosen to be 0.5 mm, and then the metallic losses would be minimum at E-band.

Table 5.2: Dimensions of the transition for different materials (unit: mm)

	Alumina $\varepsilon_r = 9.8$	Silicon $\varepsilon_r = 11.9$
$\varepsilon_r = 2.2$	W1 = 1.75 W2 = 0.77 WR = 0.5 LR = 1.5	W1 = 1.75 W2 = 0.7 WR = 0.36 LR = 1.5
$\varepsilon_r = 2.98$	W1 = 1.5 W2 = 0.77 WR = 0.4 LR = 1.4	W1 = 1.5 W2 = 0.7 WR = 0.36 LR = 1.5
$\varepsilon_r = 3.55$	W1 = 1.5 W2 = 0.77 WR = 0.36 LR = 1.3	W1 = 1.5 W2 = 0.7 WR = 0.36 LR = 1.3

5.3 Fabrication and Measurement Results

To measure the characteristics of the proposed transition, a back-to-back arrangement is designed (Figure 5.5) and fabricated. Rogers RT/duroid 6002 with the dielectric constant of 2.98 is used as the low dielectric constant substrate, and Rogers RT/duroid 6010 with the dielectric constant of 10.2 is used as the high dielectric constant substrate. The center of the low dielectric constant substrate is cut by a laser micromachining and then the high dielectric constant substrate is inserted inside it. To effectively integrate the two substrates, a conductor tape is added to the top and bottom sides of the transition. Note that copper of two substrates should have proper connections to form the top and bottom metal of the SIW without any leak. Figure 5.5 shows the micro-photograph of the fabricated back-to-back transition (before adding the conductor tape). An Anritsu 3739C vector network analyzer is used to measure characteristics of the fabricated transition. Since the output of this network analyzer at W-band is waveguide (WR10), a wideband waveguide (WR10)-to-SIW transition [60] is used to measure the characteristics of the proposed transition at W-band frequency range. Different configurations for rectangular waveguide-to-SIW transitions were presented and explained in detail [100]-[103]. Figure 5.6 shows the measurement setup of the transition. |S11| and |S21| of the transition are measured by using an Anritsu 3739C vector network analyzer. Figure 5.7 shows the measured and simulated |S11| and |S21| of the back-to-back transition. It can be seen that the bandwidth of the transition covers almost the entire W-and E-bands. To eliminate the effects of the WR10-to-SIW transition, a TRL kit is designed, fabricated and deployed in the measurements. The reference plane is shown in Figure 5.5.

Note that dielectric and metallic losses are considered in the simulation results of Figure 5.7. To estimate the dielectric loss tangent of the substrate at W-band, two different lengths of SIW are again used as usual; one to calibrate the vector analyzer, and the other to estimate the total loss. Then, HFSS software is used to compare the simulated |S21| with the measured results.

Simulation results show that 1.65 dB of the measured insertion loss of the back-to-back transition is caused by the high loss tangent of the high dielectric constant substrate. Eliminating the effect of dielectric loss reduces the measured insertion loss to 0.52 dB. Using a low loss material like Alumina can help reduce the insertion loss.

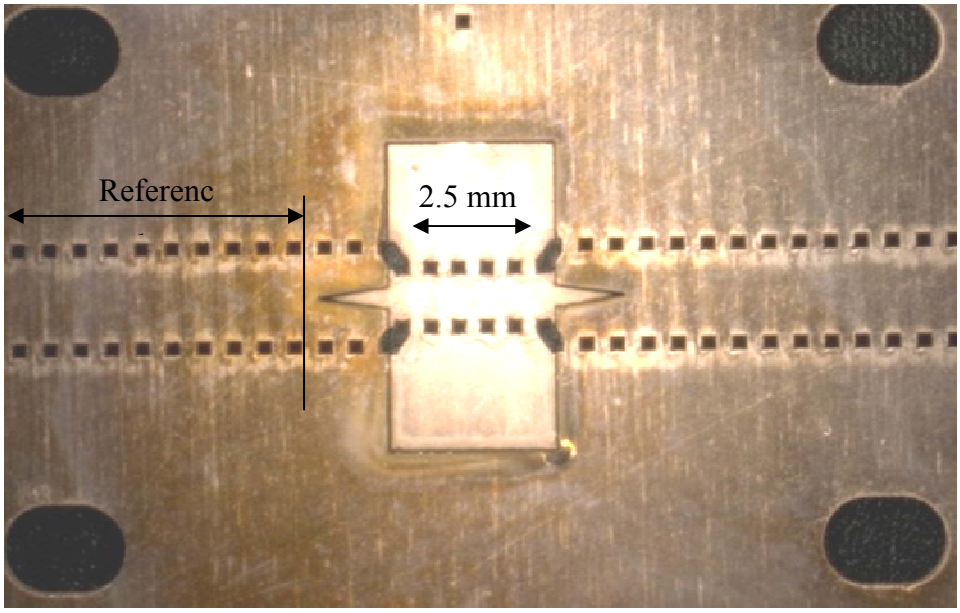

Figure 5.5. Micro-photograph of the fabricated back-to-back transition (before adding the conductor tape).

Figure 5.6. Measurement setup of the transition

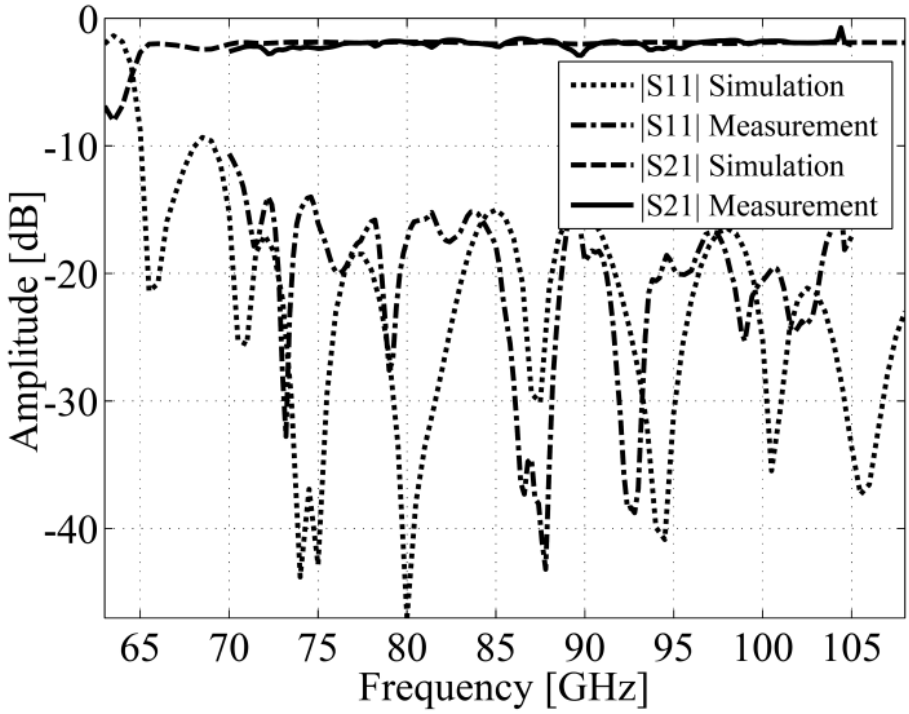

Figure 5.7. Measured and simulated |S11| and |S21| of the back-to-back transition.

5.4 Conclusion

A novel wideband transition of SIW on high-to-low dielectric constant substrates is presented in this chapter. The transition is designed for applications at E- and W-bands and it has a single layer structure. The transition consists of a triangle shaped high dielectric constant substrate which is tapered from SIW on high dielectric constant substrate into its low dielectric constant counterpart. Thanks to the waveguide-based structure of the transition, it has a self-shielded configuration, and its interference is minimum. The proposed transition can be used to connect high gain and broadband antennas to chips at E and W band. Simulated and measured results show that the useful bandwidth of the transition covers almost the entire W- and E-bands with a low insertion loss.

CHAPTER 6 LOW COST, E-BAND (81-86 GHZ) RECEIVER FRONT-END, FOR GIGABYTE POINT-TO-POINT WIRELESS COMMUNICATIONS

This chapter presents an attractive low-cost E-band (81-86 GHz) receiver front-end solution based on the SIW technology. The proposed broadband (up to 5 GHz) subsystem is designed and developed for gigabyte point-to-point wireless communication systems. Active components are surface-mounted on alumina substrate utilizing the MHMIC technology. To ensure the quality of via on alumina substrate, a technique is used to fabricate grounded CPW (GCPW) on alumina substrate using the MHMIC process. To increase gain and bandwidth of the antenna, and also to reduce fabrication cost, antenna and passive components are designed and fabricated on a Rogers 6002 substrate with low dielectric constant. To fabricate passive components, a low-cost PCB process is used as in the previous investigations. Then, the two substrates are integrated together by a simple wire bonding process. With this design and implementation technique, our E-band front-end receiver subsystem demonstrates attractive advantages and features such as broad bandwidth, low cost, compact size, light weight, and repeatable performance. The minimum detectable power density is 0.41 $\mu W/cm^2$ $\frac{mW}{cm^2}$.

6.1 Introduction

Figure 6.1 illustrates the block diagram and the photograph of the demonstrated E-band (81-86 GHz) receiver front-end. The receiver front-end is designed based on traditional heterodyne architecture. In this work, SIW is effectively combined with microstrip and CPW to integrate active and passive components. The active components (commercial MMICs chips) are recommended to be surface-mounted on alumina substrate with high dielectric constant. To increase its gain and bandwidth, the antenna array should be designed and fabricated on low dielectric constant substrate. The two substrates are then connected together utilizing a wire bonding technique.

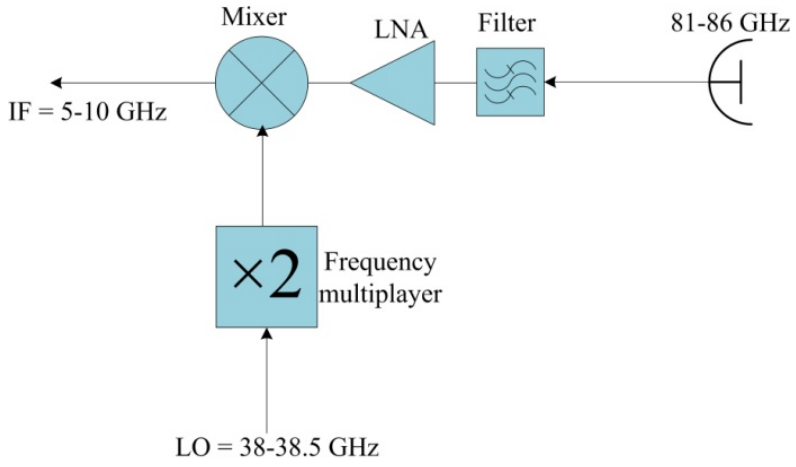

(a)

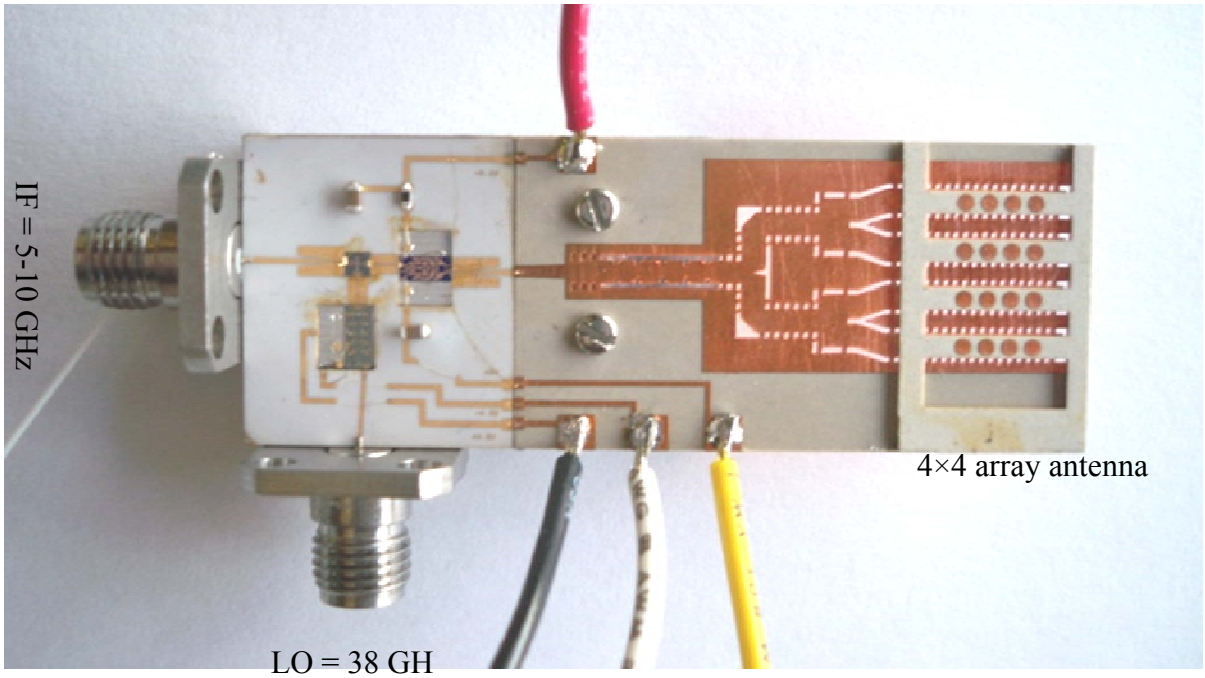

(b)

Figure 6.1. (a) Block diagram, and (b) photograph, of the demonstrated E band (81-86 GHz) receiver front-end

6.2 High-efficient patch antenna array for E-Band (81-86 GHz) Gigabyte Point-to-Point Wireless Services

This section presents a low-cost, high-gain, and high-efficiency 4×4 circular patch array antenna which is used for developing the receiver front end structure. The antenna structure consists of two layers. The feed network is placed at the bottom layer while the circular patches are on the top layer. To increase the efficiency of the antenna array, SIW is used to feed the circular patches through longitudinal slots etched on the top metallic surface. Simulated and measured bandwidths of the antenna array are 7.2% which covers the desired frequency range of 81 - 86 GHz. Measured gain of the 4×4 antenna array is 18.5 dBi which is almost constant within the antenna bandwidth. Measured radiation efficiency of 90.3% is obtained.

6.2.1 Design of the patch antenna array

The schematic of the 4×4 array antenna is shown in Figure 6.2. The antenna structure consists of two layers. The bottom layer is used to support the design of the SIW feeding network and power dividers which are made of a 20 mil Rogers/Duroid 6002 substrate. The top layer involves circular patches which are fed through longitudinal slots etched on the SIW top surface. The slots are placed half a wavelength apart to feed the patches in phase. To align the slots at peaks of the standing wave along the SIW structure, SIWs are terminated by short circuits that are three quarter wavelengths away from the center of the last slot. The slots are placed half a guided wavelength apart, at the center frequency, in order to be allocated at the standing wave peaks, and also get excited with the same phase. The design procedure of the slots is similar to that of the SIW slot array which was presented in [55]. One T-type and two V-type power dividers are used to feed the 1×4 array antennas in phase. Simulated |S21| and |S11| of the Y- and T-shaped junctions are presented in Figure 6.3. It is noted that the T junction leads to a higher reflection coefficient than the Y junction due to the existence of 90° degree bends in this structure while T junction has smaller footprint and also it is shorter, especially at the first stage. Note that dielectric and metallic losses have been considered in the simulation results of the power dividers.

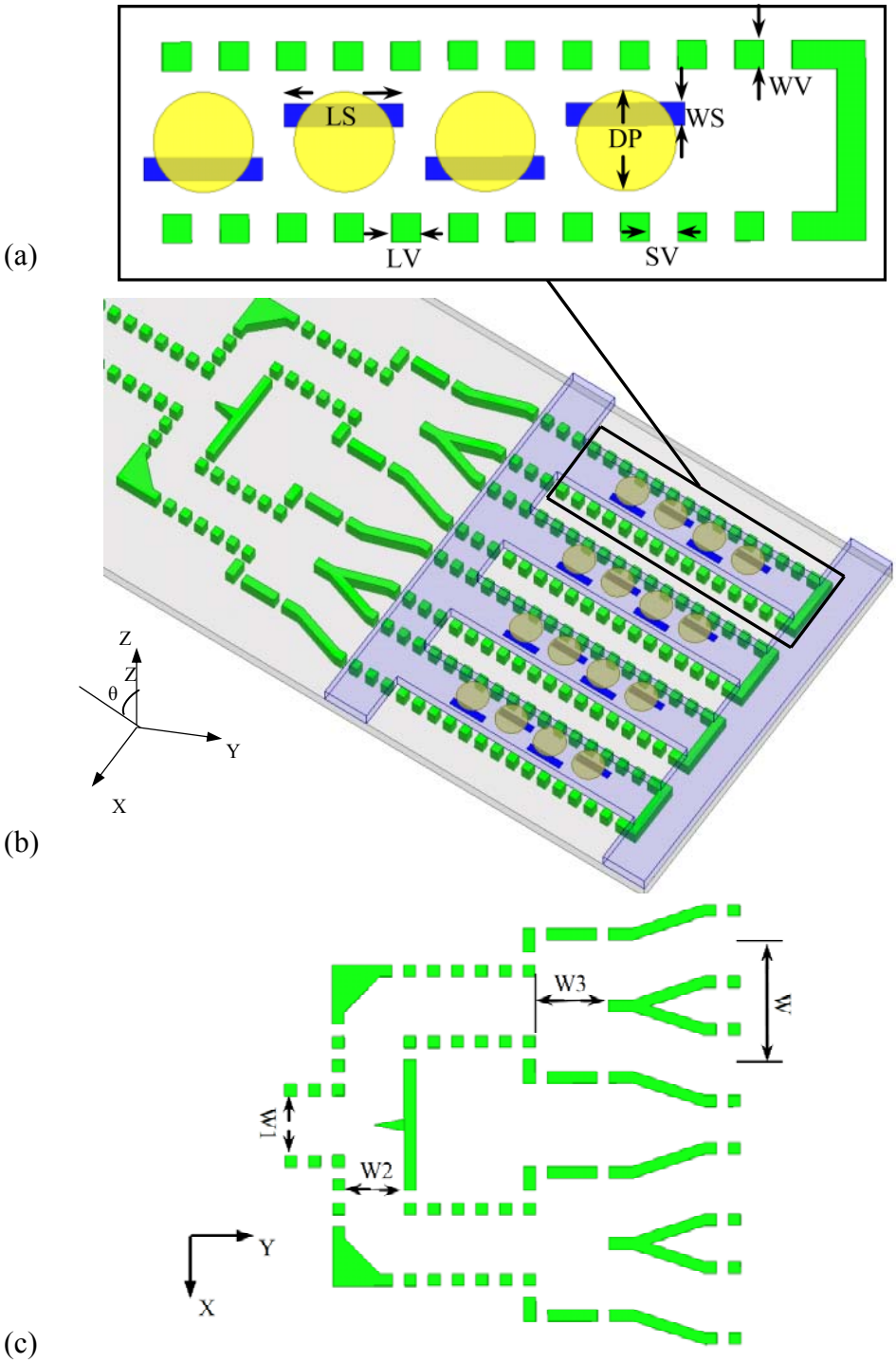

Figure 6.2. Geometry and 3-D view of the (a) 1×4 antenna array, (b) 4×4 antenna array, and (c) power divider.

The circular patches are designed on Rogers/Duroid 5880LZ substrate. To reduce mutual coupling between the 1×4 antenna arrays, the substrate between them (on the second layer) is removed and the separation between them is increased to 0.83λ. Simulation results show that removing the substrate between 1×4 arrays can increase the gain of the 4×4 antenna array by 1.6 dB and also decrease the side lobe level by 1 dB. Due to the narrow beamwidth of the 1×4 antenna arrays at E plane, increasing the distance between the 1×4 antenna arrays does not increase the side lobe level. The resonant frequency of a circular patch depends on its diameter and also the dielectric constant of its bottom layer. Table 6.1 illustrates the dimension of the antenna array.

Table 6.1: Dimensions of the 4×4 array of patch antennas

Symbol	Value (mm)	Symbol	Value (mm)
LS	1.24	WV	0.3
LV	0.3	SV	0.3
DP	1.05	W	3
WS	0.24	W1=W2	1.5
WV	0.24	W3	1.85

As shown in [57], increasing the thickness of substrate under the patches would increase the gain of the aperture-coupled patch antennas. Figure 6.4 shows the influence of increasing the thickness of the top layer on the gain of a 1×4 array of patch antennas that are fed through the longitudinal slots on the top metallic surface of SIW at 83 GHz (Figure 6.2a). As Figure 6.4 suggests, increasing the thickness of the substrate from 0.1 mm to 0.5 mm (0.15 λg) improves the gain of a 1×4 antenna array by 2 dB. Then, the total thickness of the antenna is one millimeter, i.e. the thickness of the bottom layer (feed network) is 0.5 mm and the thickness of the top layer is also 0.5 mm. Compared to the previously presented SIW-based antennas in chapter 3, the fabrication process of the proposed antenna is much easier and it is thinner, while it has almost the same gain, bandwidth and radiation efficiency. Compared to the Yagi-like antenna [53], the number of layers is reduced from six layers to two layers in this work and the thickness of the antenna is

also reduced from 0.53λ to 0.28λ. Feed network of the proposed antenna is chosen to be similar to the feed network of [53], to facilitate the comparison between the two antennas.

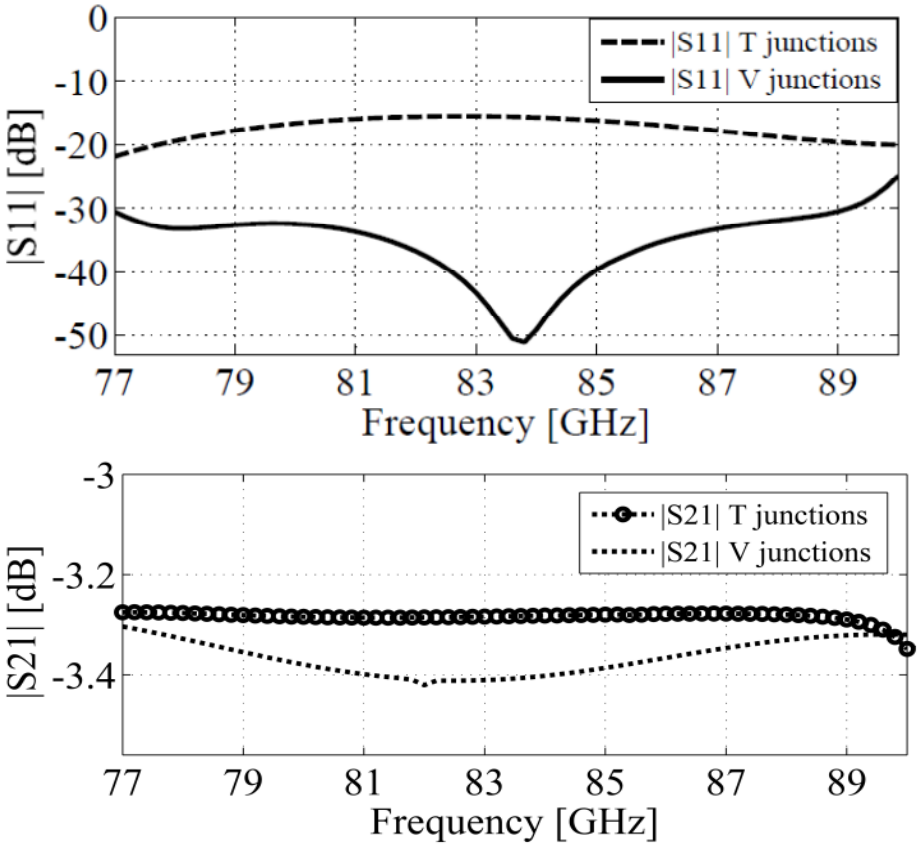

Figure 6.3. Simulated |S11| and |S21| of the T-shaped and Y-shaped junctions.

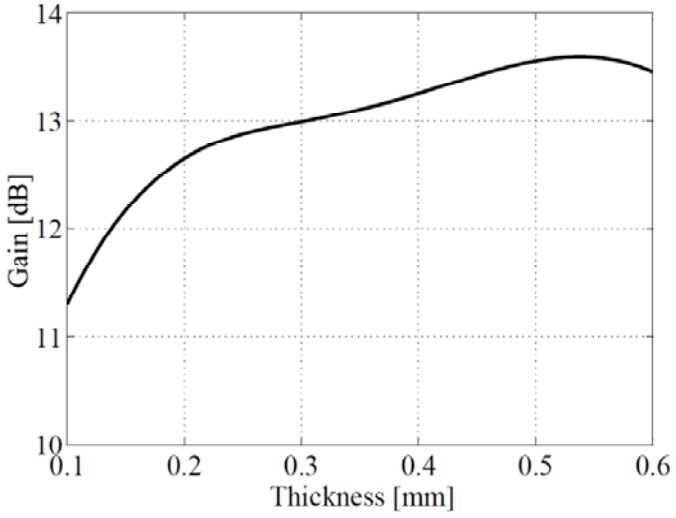

Figure 6.4. Influence of the thickness of the top dielectric layer on the gain of a 1×4 antenna array at 83 GHz.

6.2.2 Fabrication and measurement results of 4×4 array of patch antennas

Low-cost PCB process is used to fabricate the antenna prototype in two layers. The SIW feeding network (bottom layer) is fabricated on a 20 mils Rogers/Duroid 6002 substrate with dimension of 34 mm×14 mm. The patches (top layer) are etched on a 20 mils Rogers/Duroid 5880LZ substrate with dimension of 12 mm×14 mm. The two substrates are glued together using an epoxy with dielectric constant of 3.5 and thickness of 5 μm. Effect of the adhesive is considered in the simulation results. Figure 6.5 shows the photograph of the fabricated 4×4 array of patch antennas.

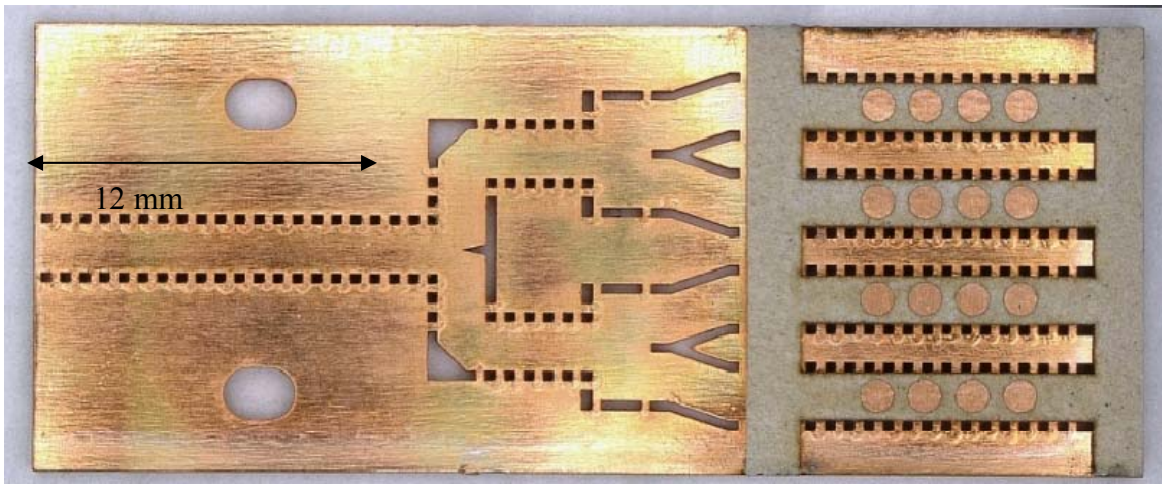

Figure 6.5. Photograph of the fabricated 4×4 antenna array of patch antennas.

To measure the parameters of the array antenna, a wideband waveguide (WR10) to SIW transition is used [60]. Due to the large size of the WR10 to SIW transition, it has some effect on the measured radiation pattern of the antenna. The input line of 12 mm is used to increase the distance between antenna and the transition. Note that the effect of the WR10 to SIW transition and the 12 mm input line is concealed from the measurement results by using a TRL kit. Figure 6.6 shows the simulated and measured |S11| of the antenna array. The measured bandwidth of the antenna array covers the desired frequency range (81-85 GHz). The 7.2% simulated bandwidth (|S11| ≤ -10 dB) of the proposed antenna array represents a considerable improvement regarding the bandwidth of slot array (2.7% in [54], and 4.1% in [55]) which was previously reported. The bandwidth of the antenna is increased because coupling between slots and patches are better than the coupling between slots and air.

Figure 6.7 shows the effect of dielectric and metallic losses on the gain of 4×4 array of patch antennas. Simulation results show that metallic loss decreases the gain of the antenna array by 0.117 dB while dielectric loss decreases the gain by 0.83 dB. To estimate the dielectric loss tangent of the substrate at 83.5 GHz, SIW structures with two different lengths are used. The estimated dielectric loss tangent of Rogers/Duroid 6002 at 83 GHz is 0.002. Measurement result shows that the insertion loss of 28.78 mm long SIW on Rogers 6002 substrate is about 1.15 dB at 83.5 GHz. Note that in the simulation results of Figure 6.4, dielectric and metallic losses are not considered. Figure 6.7 also compares the simulated and measured gains of the antenna array. Figure 6.7 shows that one of the advantages of the proposed structure is that the gain of the antenna is almost constant within the desired bandwidth of the antenna. This is an important parameter in the development of wideband point-to-point communication systems. Compared to the SIW-based slot arrays, the proposed antenna has more gain and bandwidth. It has also more stable radiation pattern within the bandwidth of the array.

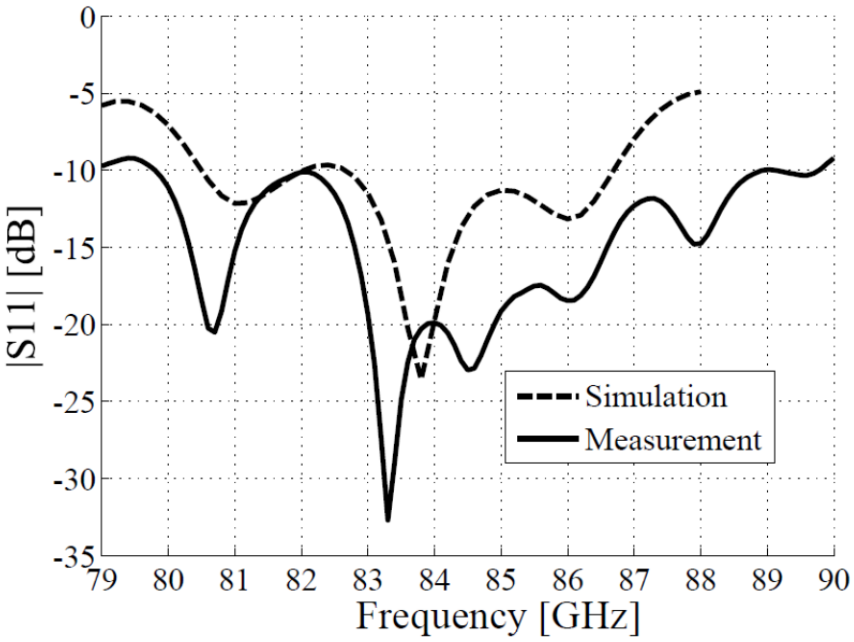

Figure 6.6. Measured and simulated impedances of the 4×4 array of patch antennas.

Figure 6.9 compares simulated and measured radiation patterns and gains of the antenna array. Good agreement is obtained between the simulated and measured radiation patterns. Note that effect of dielectric and metallic losses, roughness and thickness of the metallic layer and also

effect of the adhesive between the layers have been considered in the simulation of the antenna. Discrepancy between the simulated and measured H-plane radiation patterns at -90 to -50 degree is caused by the effect of the WR10-to-SIW transition which is used to measure the antenna in our anechoic chamber. The simulated and measured side lobe levels of the 4×4 antenna array are less than 13 dB in both E- and H-planes at 82.5 GHz. The E- and H-plane measured cross polarizations of the antenna array are less than 20 dB in both planes (Figure 6.9). Note that the discrepancy between the simulated and measured cross polarizations of the antenna could be caused by misalignment of the antenna in our anechoic chamber during the measurement. The estimated aperture efficiency of 85.76% is obtained at 84.5 GHz from the measured gain and estimated directivity of the antenna. Figure 6.8 compares the simulated and estimated radiation efficiencies which are obtained from the measured gain and estimated directivity of the antenna.

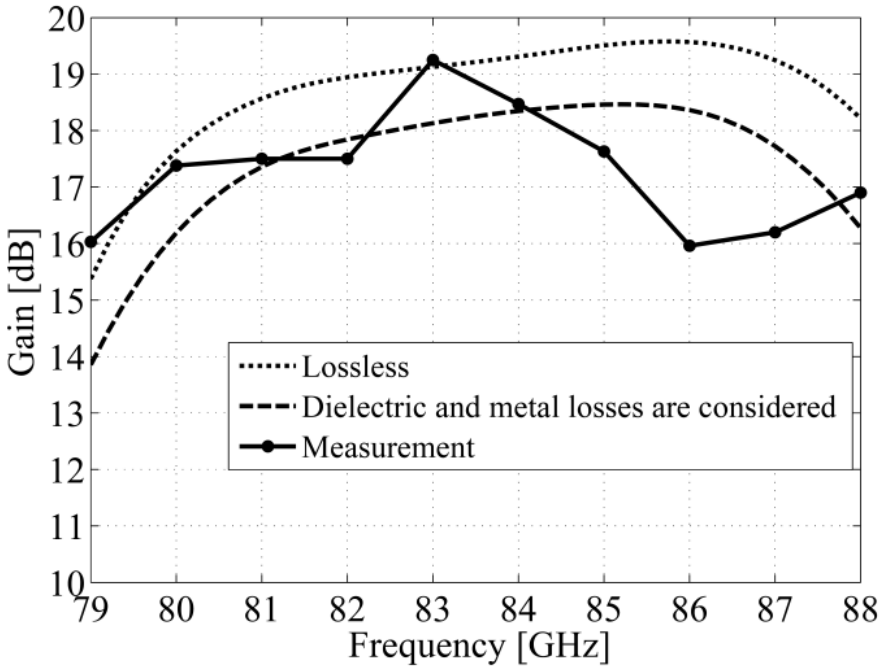

Figure 6.7. Simulated and measured gains of the 4x4 antenna array considering the effect of the dielectric and metallic losses.

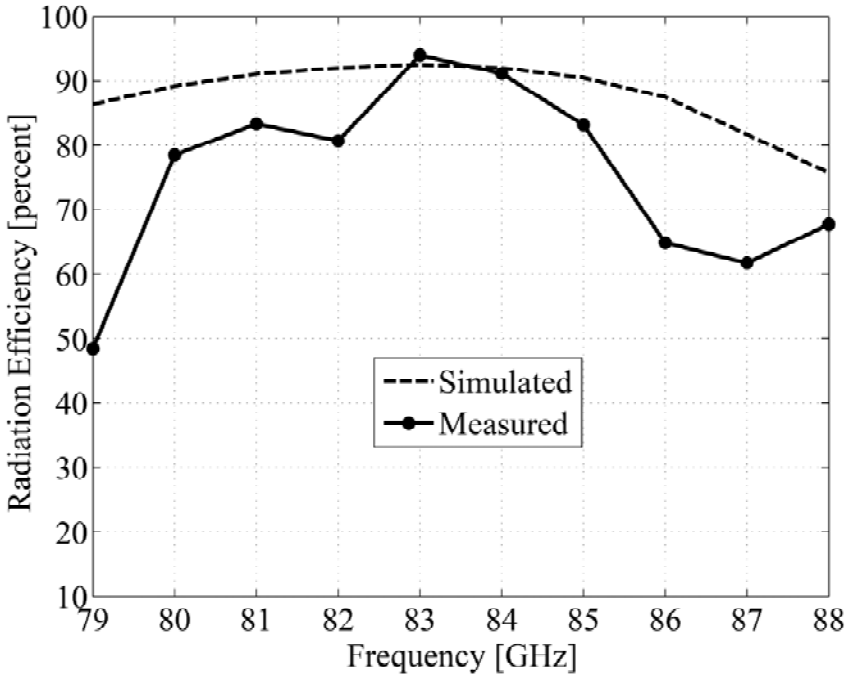

Figure 6.8. Measured and simulated radiation efficiencies of the 4×4 array of patch antennas.

(a)

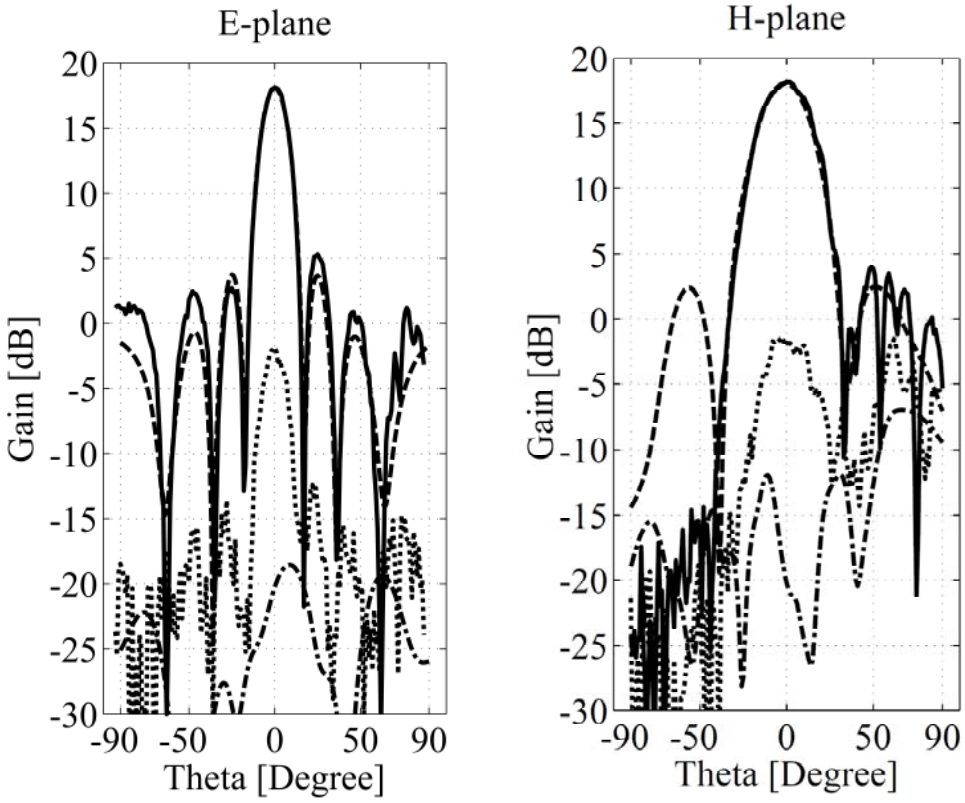

(b)

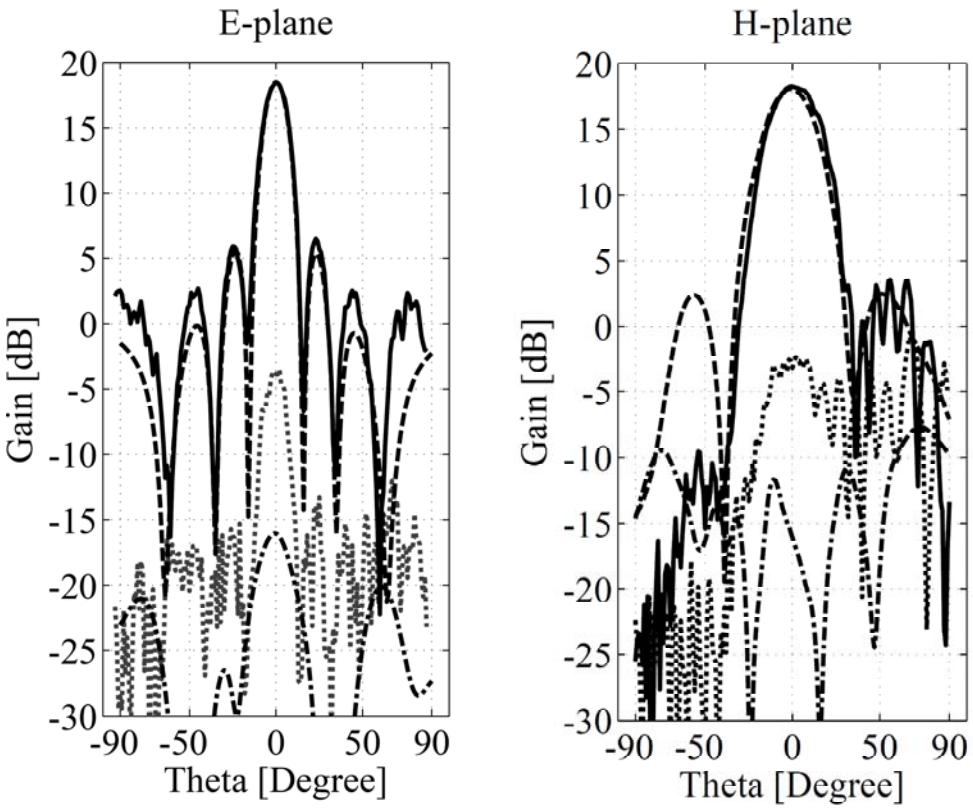

Figure 6.9. Simulated radiation pattern in XZ plane, (E plane), and YZ plane (H plane), (c.f. Figure 6.2) of the 4×4 antenna array at (a) 82.5 GHz, and (b) 84.5 GHz. Solid: measured, dashed: simulated, dotted: measured cross-polarization, and dotted-dashed: simulated cross-polarization.

6.3 4 order Chebyshev SIW cavity filter

Figure 6.10 shows the structure of the proposed 4th order Chebyshev SIW cavity filter that is used in the receiver architecture. The resonant frequency of each cavity filter is calculated by utilizing:

$$\mathbf{f_{r(TE_{m0q})}} = \frac{\mathbf{c_0}}{2.\sqrt{\mu_r \varepsilon_r}} \sqrt{(\frac{\mathbf{m}}{\mathbf{W}})^2 + (\frac{\mathbf{q}}{\mathbf{L}})^2} \tag{6.1}$$

where m and q are the indices of mode, W and L are width and length of the cavity, εr and μr are the permeability and the permittivity of substrate, and C0 is the velocity of light in free space.

B, C and D stand for the width of the coupling gaps, and E and F for the length of the cavities. Table 6.2 gives dimensions of the designed filter. The thickness of the coupling gaps is equal to that of via holes and is 0.254 mm. Note that this is the minimum size of a via hole that we can fabricate in our laboratory utilizing our low cost PCB process. Figure 6.11 shows the photograph of the fabricated filter on Rogers\Duroid 6002 substrate, and Figure 6.12 compares the simulated and measured |S11| and |S12| of the filter. Simulated and measured results show that the proposed low-cost SIW filter has a good performance for E-band applications.

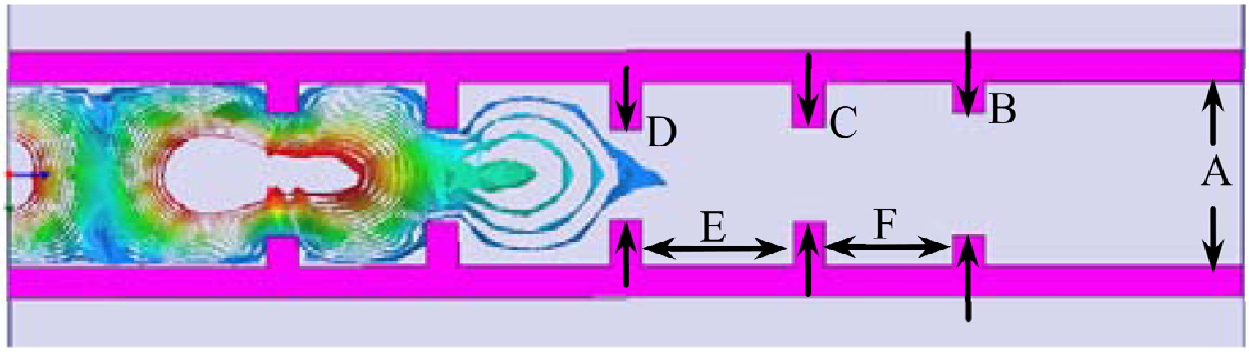

(a)

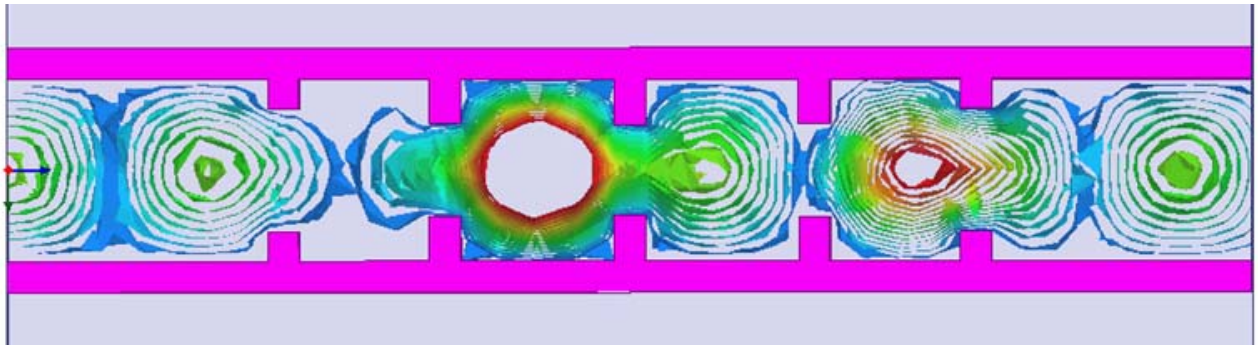

(b)

Figure 6.10. Structure of the filter and simulated electric field distribution at (a) 76 GHz, and (b) 84 GHz.

Table 6.2: Dimensions of the filter

Symbol	Value (mm)
A	1.5
B	1.01
C	0.76
D	0.73
E	1.24
F	1.05

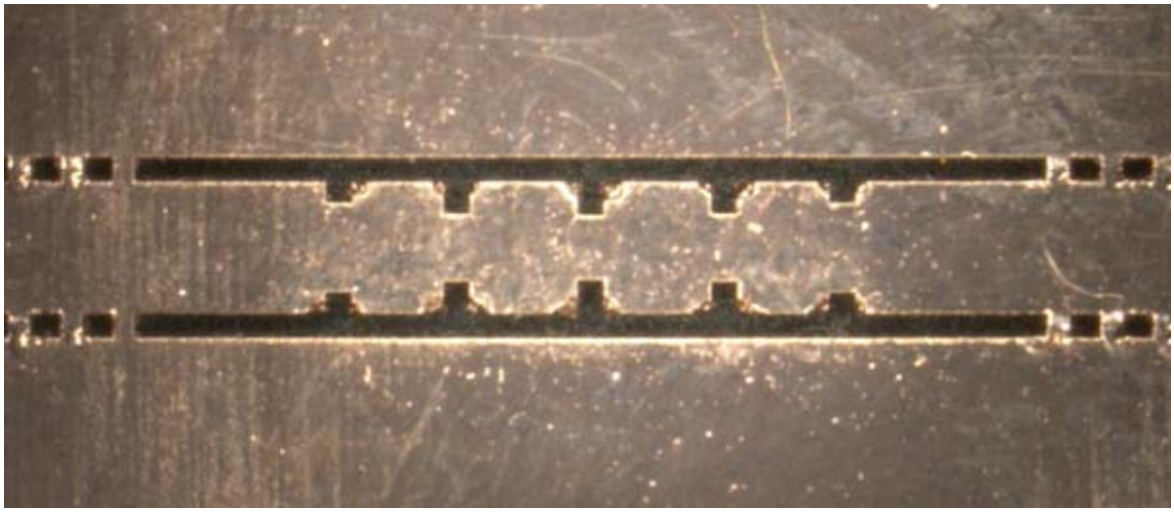

Figure 6.11. Photograph of the fabricated filter.

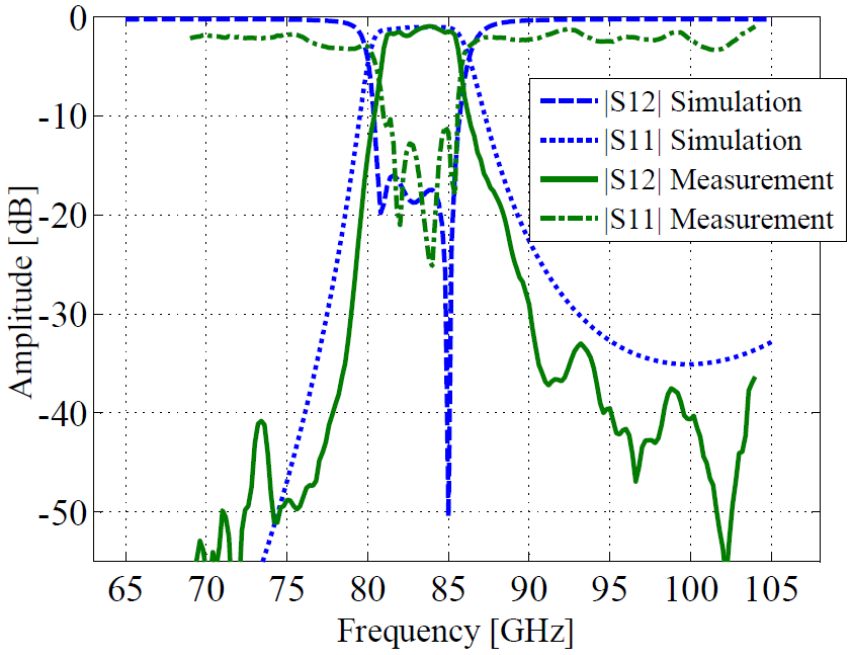

Figure 6.12. Simulated and measured |S11| and |S12| of the filter.

6.4 Wire-bondings, transitions and GCPW transition lines

To connect the LNA chip and other components, GCPW line is used. The reason of utilizing GCPW rather than microstrip is that a narrow strip is required to connect the chip's pad which has a size of 2×2 mil and also radiation loss of GCPW is generally less than microstrip. In this way, a narrower middle strip than microstrip can be designed on the same substrate. To prevent the excitation of higher order modes of the GCPW, two rows of via holes are implemented to connect the ground planes to each other. To enhance the quality of via on alumina substrate, a technique is used to fabricate GCPW on alumina substrate using MHMIC fabrication process named via-filled MHMICs, which has been not common for this type of processing technique. A laser micro-machining is used to cut via holes on alumina substrate. A thin layer of cupper is deposited on vias on one side only (Figure 6.13). This thin layer of copper enables a good electrical contact to the entire surface under need, and makes it possible to use electroplating to fill those via holes. A special electroplating technique named pulse reverse electroplating is used to fill completely those via holes. Figure 6.13 shows those post-processing geometries. Note that the copper has overflowed the surface of substrate in this case. Subsequently, a fine diamond

polishing is used to planarize the surface of alumina and to reduce the roughness (Figure 6.14). The substrate used for this application is the fired type. The roughness of fired substrate is more than 2 micron. The conductor loss would increase significantly at high frequencies if not polished. This process would enable the use of a standard high resolution photoresist lithography technique. With the photoresist process rather than the photosensitive tape, the accuracy of the fabrication can be increased significantly, making it usable for high frequency applications.

(a)

(b)

Figure 6.13. Micro-photograph of via after (a) drill by laser, and (b) sputter copper coated.

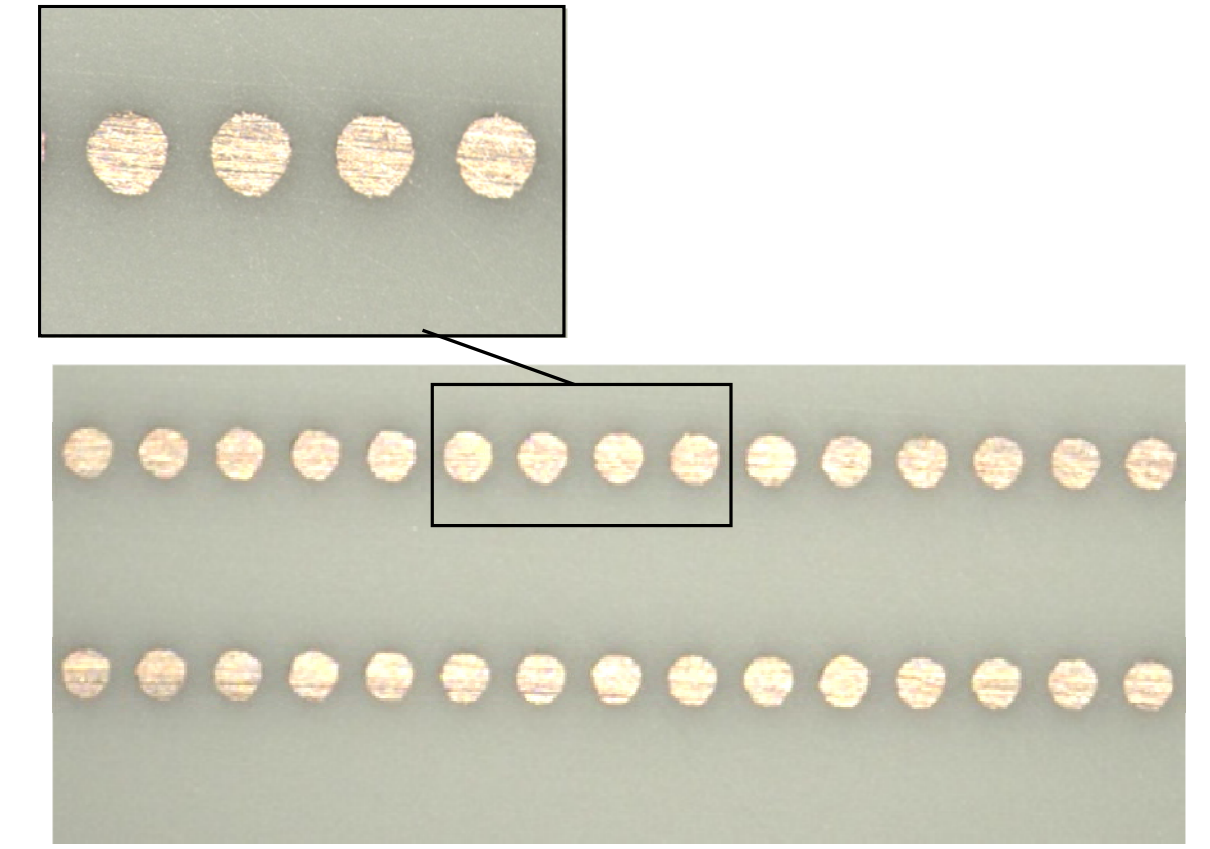

(a)

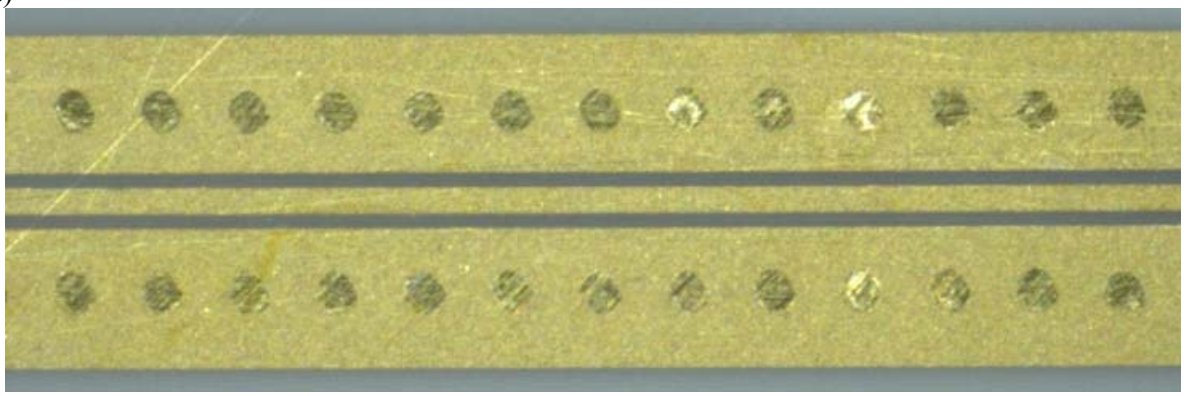

(b)

Figure 6.14. Micro-photograph of the fabricated GCPW on Alumina substrate (a) after filling via holes and polishing the surface, (b) after gold sputtering and photolithography.

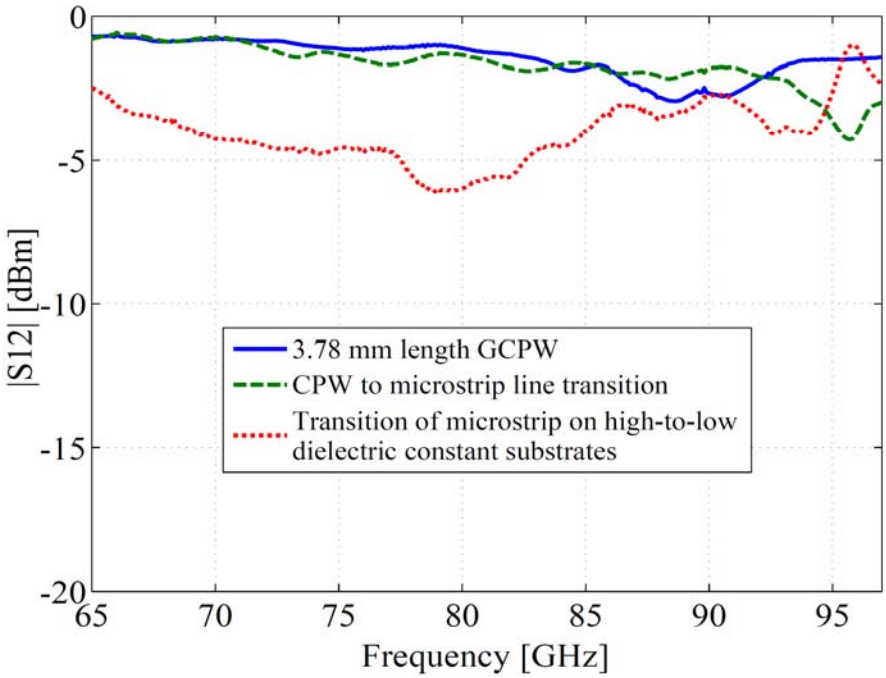

Figure 6.15. Measured |S12| of 3.78 mm length GCPW fabricated on Alumina substrate (solid), and CPW to microstrip line transition (dashed), and transition of microstrip line on high-to-low dielectric constant substrate (dotted).

Connection between the microstrip lines on high dielectric constant substrate (alumina) and low dielectric constant substrate (Rogers/Duroid 6002) is made by wire bonding (Figure 6.16). Note that the simulation results showed that, transition of microstrip line-on-high to low dielectric constant substrates is much better than that of GCPW line on high-to-low dielectric constant substrate. Therefore, a wideband SIW to microstrip transition is designed on the low dielectric constant substrate (Figure 6.16), and a wideband CPW to microstrip transition is designed on alumina substrate (Figure 6.16). To measure the insertion loss of each transition, a back-to-back transition is fabricated and measured. Figure 6.15 shows the |S12| of the CPW to microstrip line transition, and also transition of microstrip line on high-to-low dielectric constant substrate.

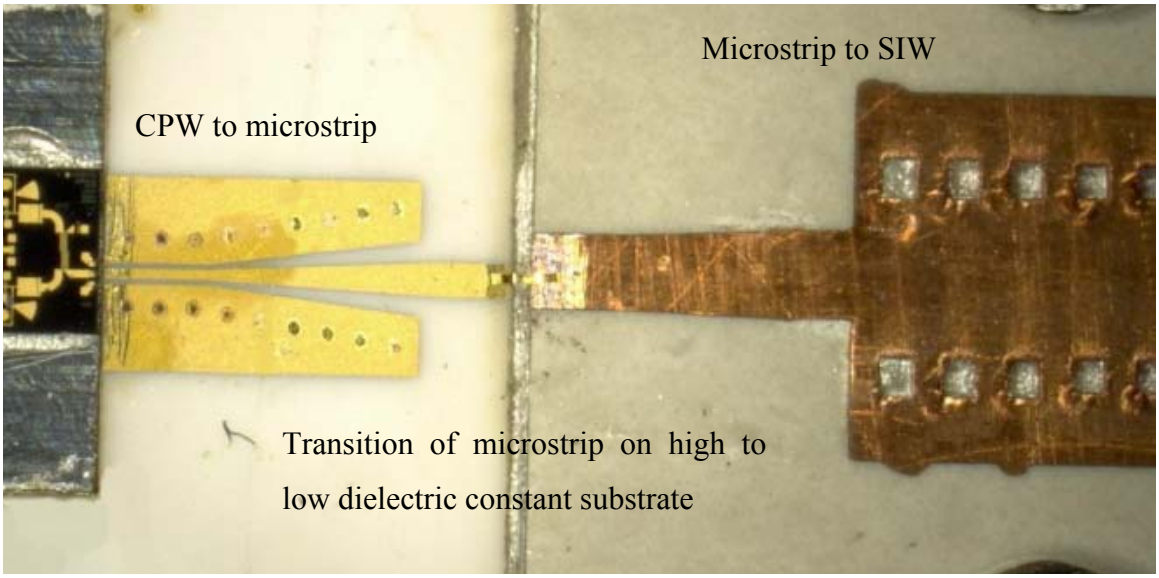

Figure 6.16. Transition from SIW to microstrip, microstrip on high to low dielectric constant substrate, and microstrip to CPW transition

6.5 Active components

Hittite HMC-ALH509, three stages GaAs HEMT MMIC low noise amplifier (LNA) operating between 71 and 86 GHz, is used to amplify the received RF signal. This die chip LNA features 12-14 dB gain, 5 dB of noise figure and an output power of +12 dBm with a +2 V supply voltage. According to Hittite, it is recommended to use MHMIC process for the HMC-ALH509 LNA chip on alumina substrate with 10 mil thickness and dielectric constant of 9.8 (Figure 6.17).

Hittite HMC-MDB277, a passive double-balanced MMIC mixer that utilizes GaAs hetero-junction bipolar transistor (HBT) Shottky diode technology, is used as down-converter. This mixer operates between 70-90 GHz in LO and RF, with conversion loss of 12 dB. This die chip MMIC mixer requires a minimum driving power of 14 dBm. Therefore, a CHU3277 multiplier/MPA from United Monolithic Semiconductor (UMS) is used to obtain enough driving power (18 dBm). CHU3277 is a GaAs monolithic microwave IC which integrates an input buffer/power divider and two chains in parallel combined at the output. Each one includes a frequency multiplier and a four stage medium power amplifier. The frequency multipliers are based on active transistors and allow for operation at low input level with required power consumption. The input frequency of this multiplier is 38- 38.5 GHz and then the operating

output frequency is 76- 77 GHz. One of the advantages of utilizing this multiplier is that 38 GHz oscillator and connectors present lower cost than E-band oscillator and connectors.

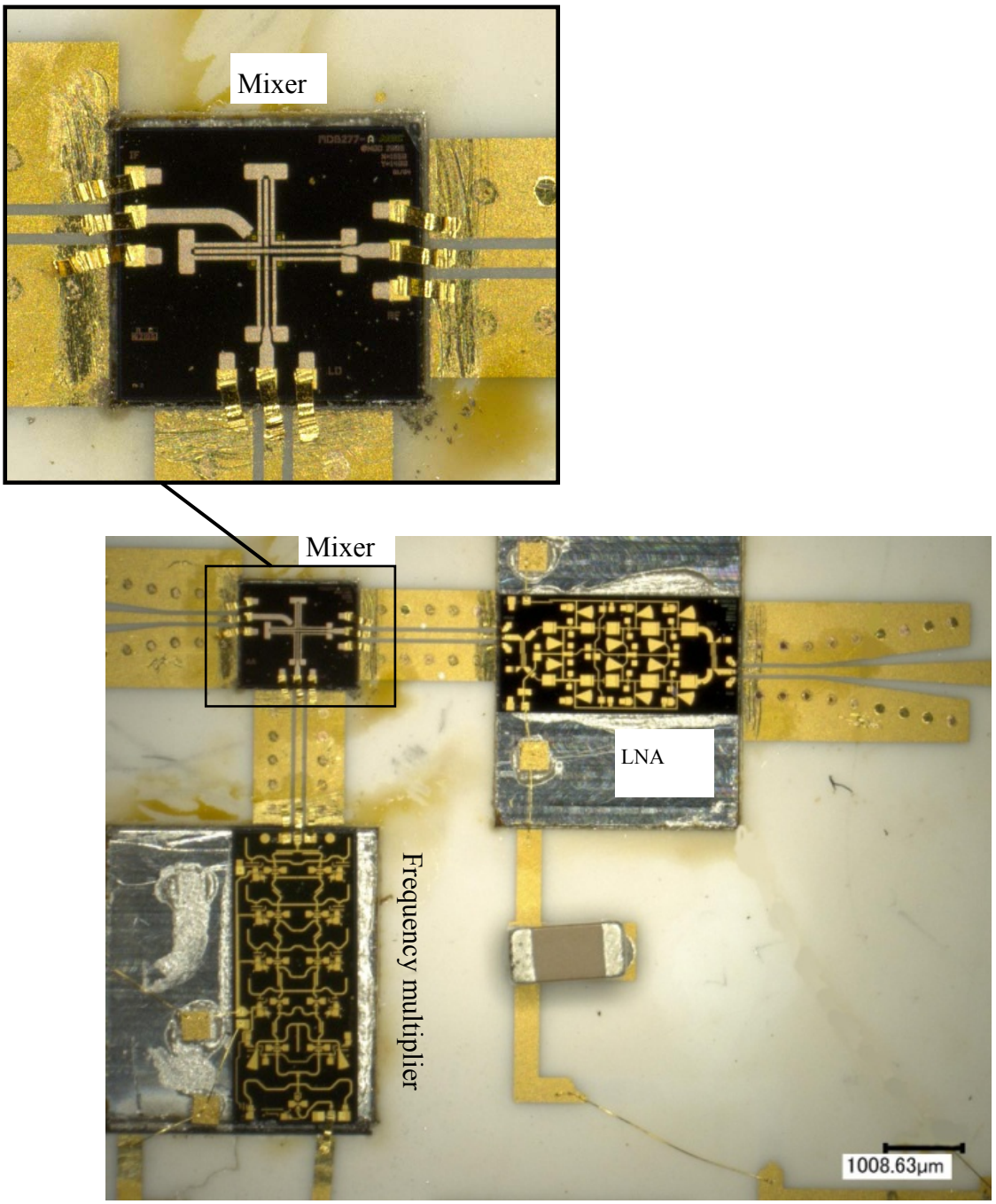

Figure 6.17. Active components on Alumina substrate

Wire bonding technique is used to connect the active components to Alumina substrate. The effect of wire bonding, loss, and mismatch, at millimeter wave is investigated in detain in [104]-[107].

6.6 Test setup and measurements of receiver front-end

To measure the characteristics of the proposed front-end receiver, 81-86 GHz system measurement is carried out with a distance of 33 cm between the transmitter and the receiver, which determines a path loss (L_p) of about 61.3 dB which can be calculated by:

$$L_P(dB) = 20\log\left(\frac{4\pi d}{\lambda}\right) \tag{6.2}$$

Figure 6.18 shows the photograph of the E-band system test setup. At the transmitter side, Anritsu 68177C generates 13.5-14.33 GHz signal. Then, Anritsu 54000-5WR10 millimeter wave multiplier is used to multiplier the frequency by six and generates 81-86 GHz transmitted signal. A scalar horn antenna from Quinstar is used to transmit the signal. The measured transmitted power is $P_{TX} = 2$ dBm . At the receiver side, Anritsu MG 3694A signal generator is used to drive the 38 GHz LO input of the demonstrated receiver front-end. Agilent PXA N9030A signal analyzer is used to record signal spectrum that is shown in Figure 6.19.

The received IF signal $(P)_r$ at the output of the mixer can be expressed by

$$P_r = P_t + G_t - L_p + G_r + L_f + L_{wt} + G_{lna} + L_m \tag{6.3}$$

where P_t is the transmitted power, G_t is the gain of the transmitter antenna, L_p is the path loss, G_r is the gain of the receiver antenna, L_f is the insertion loss of the filter, L_{wt} is the total loss of the wire bonding, transitions and GCPW transition lines, $G_{lna}$is the gain of the LNA, and L_m is the conversion loss of the mixer. The measured received signal over 5 GHz bandwidth of the demonstrated receiver front-end is shown in Figure 6.20. The measured received power at 83.5 GHz is about -41 dBm. Compared to previously presented 60 GHz sub systems [95] and [99], the proposed structure has almost twice more bandwidth and less minimum detectable power density at the receiver point.

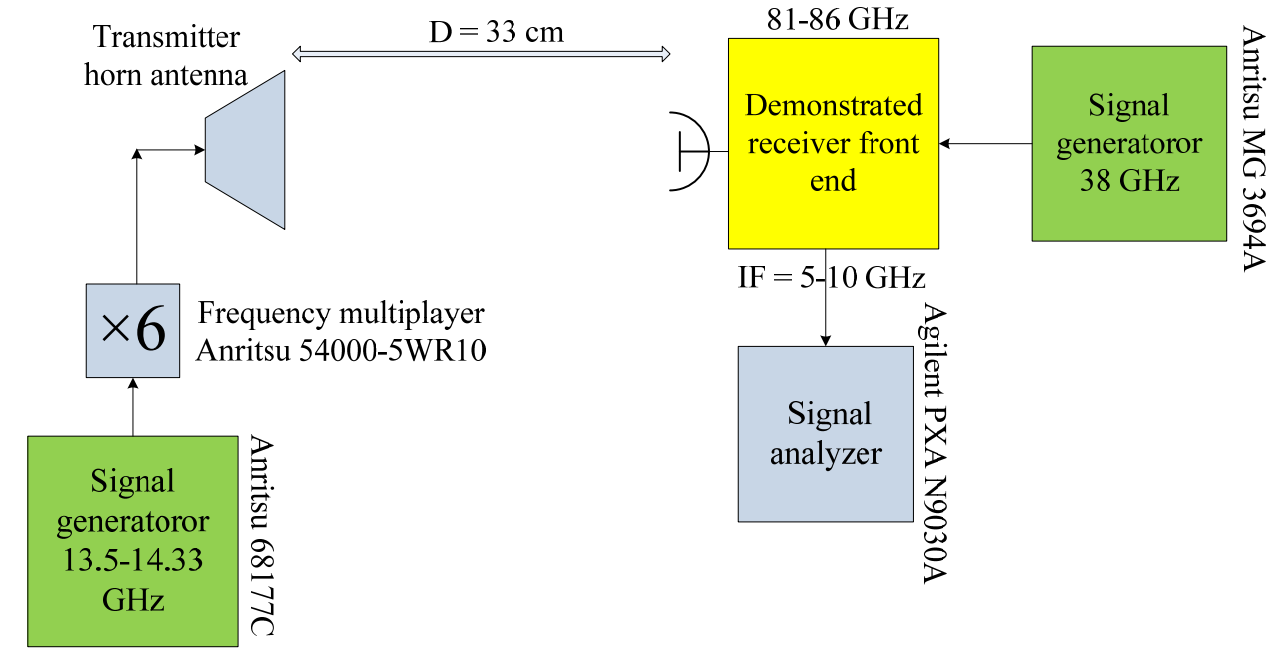

(a)

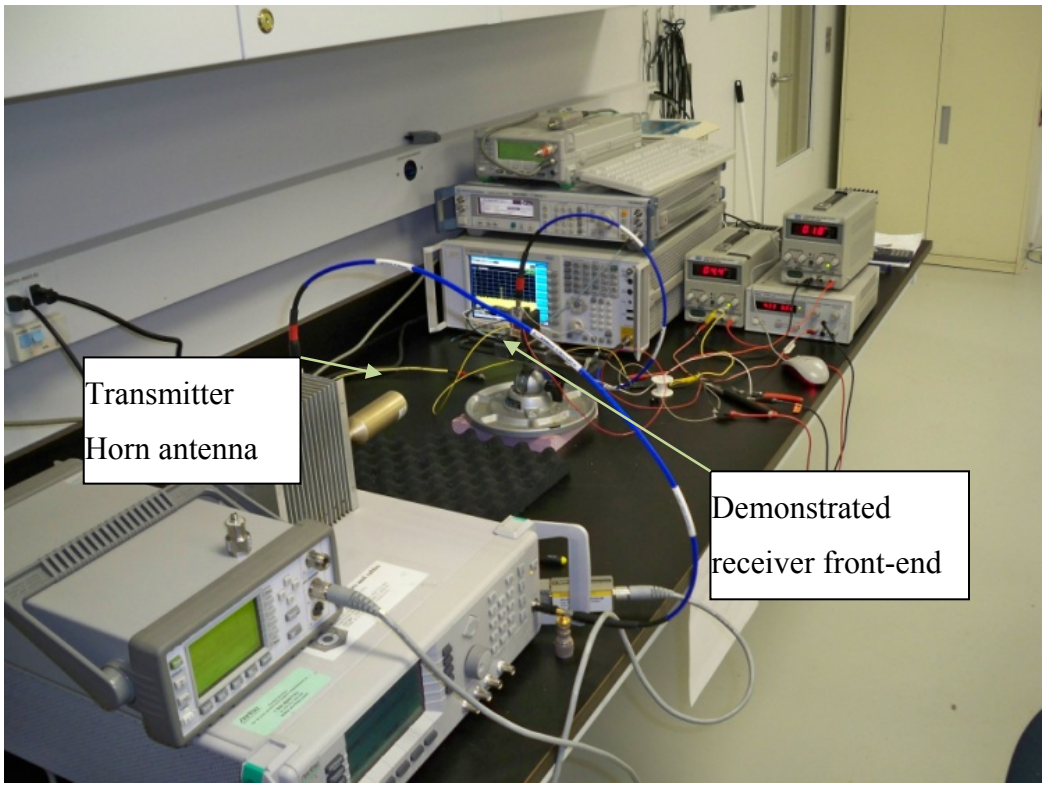

(b)

Figure 6.18. (a) Experimental setup diagram of E-band (81-86 GHz) receiver sub system, (b) photograph of the measurement setup.

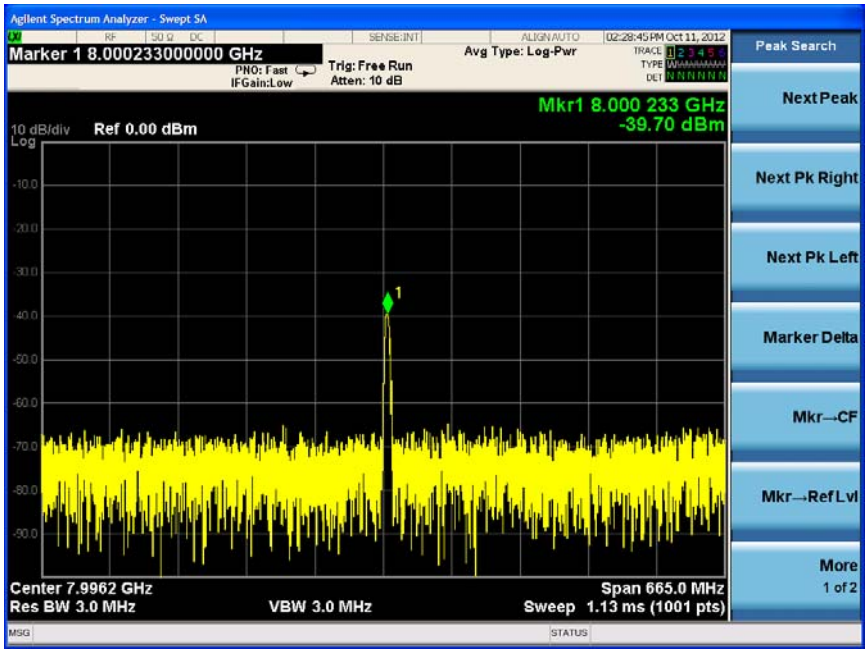

Figure 6.19. Spectra of the received IF signal

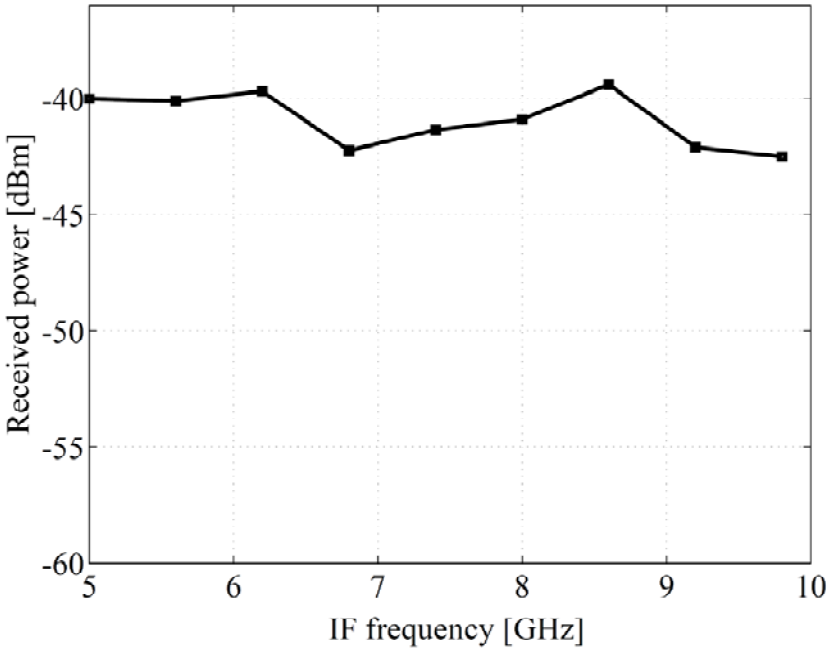

Figure 6.20. Measured received IF signal at the output of the mixer.

6.7 Conclusion

A low-cost and wideband SIW receiver front-end for gigabyte point-to-point applications at E-band (81-86 GHz) is presented in this chapter. A high gain 4×4 antenna array, and a 4th order Chebyshev SIW cavity filter, are used in the receiver architecture and are fabricated by utilizing a low-cost PCB process. To enhance its gain and bandwidth, the antenna array is designed on low dielectric constant substrate. To improve the efficiency of the active components, LNA, mixer, and frequency multiplier are surface-mounted on high dielectric constant substrate (Alumina) using our MHMIC technology. Subsequently, the two substrates of different type are connected together by using a wire bonding technique. The effect of the wire bonding and the CPW-to-microstrip transition on the performance of the receiver is investigated experimentally. To ensure the quality of via on alumina substrate, a technique is developed to fabricate GCPW on alumina substrate using the MHMIC fabrication process. The measured bandwidth of the proposed receiver front end covers the desired bandwidth (81-86 GHz), and the measured dynamic range of the receiver is 72 dB.

CHAPTER 7 CONCLUSIONS AND FUTURE WORK

7.1 Conclusions

In order to explore a less-crowded part of the electromagnetic spectrum and to provide a wider bandwidth in support of exploding data transmission, operating frequency of wireless communication systems has constantly been increasing now to millimeter-wave range and even terahertz band in a not-so-distant future. The atmospheric absorption decreases to less than 1dB/km for free-space signal propagation over the E/W-band frequency range. Frequency bands of 71-76 GHz, 81-86 GHz, and 94.1-97 GHz over E/W-Band have been allocated by the US Federal Communication Commission (FCC) for use as gigabyte wireless spectrum. Wide available bandwidth and low atmospheric absorption provide the capability of a long-range gigabyte point-to-point wireless data transmission. This presents numerous applications such as local area networks or broadband metropolitan links or even back-haul interconnections and transmissions among next generation base-stations over E/W-band.

As frequency increases to the higher-end millimeter-wave band (especially at E/W-band), the efficiency of planar microstrip line suffers from serious losses particularly at bends and transmissions. Although classical waveguide technology is popular in the design of high-performance millimeter-wave systems, it is not suitable for low-cost and mass productions because of its generally expensive and bulky structures without the possibility of integration. The non-planar nature of the waveguide presents a great difficulty of connecting itself to planar active components. Substrate integrated waveguide (SIW) was proposed to overcome the mentioned hurdles. SIW enjoys not only the advantages of rectangular waveguide features, but also other benefits, namely, low-cost, compact size, light-weight, easy-to-fabricate using PCB and other planar processing technologies, and also being easily connected to coplanar waveguide and utilizing a wideband and uniplanar transition.

The scope of this Ph.D. dissertation focuses on the SICs based antenna techniques and related receiver front end integration with antennas for E/W-band gigabyte point-to-point applications. The major contribution from this work can be concluded as the followings:

- Fabrication cost of the proposed antenna and receiver front-end at E/W band by utilising SIC technology can be reduced significantly with conventional PCB and MHMIC processing techniques.
- Highly original, low cost, and high efficient antennas are presented based on SIC technology, which can be exploited for E/W-band system applications with broadband, constant gain, and small footprint.
- A novel 4×4 antenna array is proposed and demonstrated using substrate-integrated waveguide (SIW) technology for the design of its feed network. Dielectric cubes of low-permittivity material are placed on top of each 1×4 antenna array to increase the gain of the circular patch antenna elements. Measured impedance bandwidths of the two 4×4 antenna arrays are about 7.5 GHz (94.2–101.8 GHz) at 19 dB gain level.
- A planar dielectric rod antenna which is fed by Substrate Integrated Non-Radiative Dielectric (SINRD) waveguide. This antenna presents numerous features such as broad bandwidth (94-104 GHz), relatively high and stable gain, use of high dielectric constant substrate, and substrate-oriented end-fire radiation.
- A novel compact, uniplanar, circularly polarized, coplanar waveguide (CPW) spiral antenna for wideband applications. The antenna is directly fed by a 50 Ω CPW from the outside edge of the spiral, thus a balun for matching is not required. This feed provides the capability to have an entire uniplanar array of spirals. This spiral antenna is desirable due to its uniplanar structure which offers easy fabrication at millimeter-wave frequencies.
- A novel W band integrated pyramidal horn antenna which is made of low cost multilayer printed circuit board (PCB) process, which has broad bandwidth that covers 71-76 GHz, 81-86 GHz, and 94.1-97 GHz.
- Original design of a dielectric loaded antipodal linearly tapered slot antenna (ALTSA) which the concept of SIW-fed horn and ALTSA are jointly used to design a low-cost, high-gain and efficient planar dielectric-loaded antenna for ultra wideband gigabyte wireless services at E band (71-97 GHz).
- A novel broadband transition of substrate integrated waveguide on high-to-low dielectric constant substrates which it's bandwidth covers the entire E band.

- A 81-86 GHz substrate integrated receiver system with a broadband up to 5.5 GHz is presented for the first time. The proposed sub system integrates the active and passive components within a single package.

7.2 Future works

Subsequent to the projects and studies described in this doctoral dissertation, a number of technical issues should be addressed in future investigations:

- Other fabrication processing techniques such as LTCC, MEMS and even CMOS, should be explored and exploited to design and develop high-performance and compact-sized millimetre-wave SICs-based antenna and front-end subsystems for wideband applications at E/W-band and beyond.
- Using advanced semiconductor processes will extend the development range with reference to frequency from E/W-band to several-hundred GHz or THz. Indeed, SICs and MMICs can fully be integrated into a single portfolio.
- Utilizing SIW and SINRD and their mixed topologies for wideband applications at 140 GHz, 220 GHz, 340 GHz, and 410 GHz (frequency windows) could trigger many investigations and applications.
- The work presented in this thesis only scratches the surface of utilising SICs technology as the first step for E/W-band applications. Much more efforts are required to accomplish a well-developed and optimized wireless system for E/W-band gigabyte point-to-point wireless system.

REFERENCES

[1] D. M. Pozar, Microwave Engineering, 2nd ed. New York:Wiley, 1998, pp. 424–427, 162.

[2] E. E. Altshuler and R. A. Marr, "A comparison of experimental and theoretical values of atmospheric absorption at the longer millimeter wavelengths," IEEE Trans. Antennas Propag., vol. AP-36, no. 10, pp. 1471–1480, Oct. 1988.

[3] FCC 03-248, "Allocation and service rules for the 71-76GHz, 81-86GHz, and 92-95GHz bands," Federal Communication Commission, Nov. 2003.

[4] SPP 2006-11, "Planning of the 71-76 GHz and 81-86 GHz bands for millimeter wave high capacity fixed link technology," Australian communication and media authority, Dec. 2006.

[5] Y. Lee, X. Lu, Y. Hao, S. Yang, J.R.G. Evans, and C.G. Parini, "Narrow-beam azimuthally omni-directional millimetre-wave antenna using freeformed cylindrical woodpile cavity," IET Microwaves, Antennas & Propagation, vol. 4, no.10, pp. 1491-1499, Oct. 2010.

[6] B.D. Nguyen, J. Lanteri, J.-Y. Dauvignac, C. Pichot, and C. Migliaccio, "94 GHz folded Fresnel reflector using C-patch elements," IEEE Trans. Antennas Propag., vol. 55, pp. 3373–3381, Nov. 2008.

[7] C. C. Ling and G. M. Rebeiz, "A 94 GHz planar monopulse tracking receiver," IEEE Trans. Microwave Theory Tech., vol. 42, no. 10, pp. 1863–1871, Oct. 1994.

[8] Hodges, R.J. Badley, and Tarsier, "A millimeter wave radar for airport runway debris detection," in Proc. European Radar Conf., Amsterdam, 2004.

[9] L. Yujiri, M. Shoucri, and P. Moffa, "Passive millimeter wave imaging," IEEE Microwave Magazine, vol. 4, pp. 39-50, 2003.

[10] E. Moldovan, S.O. Tatu, T. Gaman, K. Wu, and R.G. Bosisio, "A new 94-GHz six-port collision avoidance radar sensor," IEEE Trans. Microwave Theory Tech., vol. 52, no. 3, pp. 751–759, Mar. 2004.

[11] http://web.mst.edu/~mobildat/E-band%20Frequencies/index.html

[12] K. Wu. D. Deslandes, and Y. Cassivi, “The substrate integrated circuits - A new concept for high-frequency electronics and optoeletronics,” Telecommunications in Modern Satellite, Cable and Broadcasting Service, 2003. TELSIKS 2003. 6th International Conference, vol. 1, Oct., 2003. Pages: P-III – P-X.

[13] K. Wu, “Integration and interconnect techniques of planar and non-planar structures for microwave and millimeter-wave circuits - current status and future trend,” in Proc. Asia-Pacific Microwave Conference, vol. 2, Taipei, Taiwan, Dec. 2001, pp. 411–416.

[14] K. Wu, “Substrate integrated circuits (SICs) for low-cost high-density integration of millimeter-wave wireless systems,” in Proc. RWS2008, Jan. 2008, pp.683-686.

[15] D. Deslandes and K. Wu, “Integrated microstrip and rectangular waveguide in planar form,” IEEE Microwave and Wireless Components Letters, vol. 11, no. 2, pp. 68–70, Feb. 2001. 175

[16] L. Yan, and W. Hong, “Investigations on the propagation characteristics of the Substrate Integrated Waveguide based on the Method of Lines,” IEE Proc.-H: Microwaves Antennas Propag.，vol.152, no.1, pp.35-42, 2005.

[17] Y. Cassivi and K. Wu, “Substrate integrated non-radiative dielectric waveguide,” IEEE Microwave and Wireless Components Letters, vol. 14, no. 3, pp. 89–91, Mar. 2004.

[18] Y. Cassivi and K. Wu, “Substrate integrated NRD (SINRD) guide on high dielectric constant substrate for millimeter wave circuits and systems”, IEEE Int. Microwave Symp. Dig., pp. 1639-1642, Fort Worth, 2004.

[19] F. Xu, K. Wu, and W. Hong, “Substrate integrated nonradiative dielectric waveguide structures directly fabricated on printed circuit boards and metallized dielectric layers,” IEEE Trans. Microw. Theory Tech., vol. 59, no. 12, pp. 3076–3086, Dec. 2011.

[20] Y. Cassivi, “Étude et développement de la technologie hybride circuit planaire/guide NRD dans le contexte d'un émetteur/récepteur onde millimétrique,” PHD dissertation, École Polytechnique de Montréal, Montreal, Canada, 2004.

[21] A. Patrovsky and K. Wu, “Substrate integrated image guide (SIIG)—a planar dielectric waveguide technology for millimeter-wave applications,” IEEE Transactions on Microwave Theory and Techniques, vol. 54, no. 6, pp. 2872–2879, Jun. 2006.

[22] W. Hong, et al (Invited Talk) “Half Mode Substrate Integrated Waveguide: A New Guided Wave Structure for Microwave and Millimeter Wave Application,” Joint 31st Int. Conf. on Infrared and Millimeter Waves and 14th Int. Conf. on Terahertz Electronics, Shanghai, Sept. 18-22, 2006.

[23] B. Liu, W. Hong, Y. Q. Wang, Q. H. Lai and K. Wu, “Half mode substrate integrated waveguide (HMSIW) 3dB coupler,” IEEE Microwave Compon. Lett., vol.17, no.1, pp.22-24, 2007.

[24] B. Liu, W. Hong, Y. Zhang, H. J. Tang, X. X. Yin, and Ke Wu, “Half Mode Substrate Integrated Waveguide 180 3-dB Directional Couplers,” IEEE Trans. Microwave Theory Tech., vol.55, no.12, pp.2586-2592, 2007.

[25] Y. J. Cheng, W. Hong, and K. Wu, “Half Mode Substrate Integrated Waveguide (HMSIW) Directional Filter,” IEEE Microwave Compon. Lett., vol.17, no.7, pp.504-506, 2007.

[26] Y. Q. Wang, W. Hong, Y. D. Dong, B. Liu, H. J. Tang, J. X. Chen, X. X. Yin, and K. Wu, “Half Mode Substrate Integrated Waveguide (HMSIW) Bandpass Filter,” IEEE Microwave Compon. Lett., vol.17, no.4, pp.265-267, 2007.

[27] J. F. Xu, W. Hong, H. J. Tang, Z. Q. Kuai, and K. Wu, “Half-mode substrate integrated waveguide (HMSIW) leaky-wave antenna for millimeter-wave applications,” IEEE Antennas Wirel. Propag. Lett., vol.7, pp.85-88, 2008.

[28] Y. D. Dong, W. Hong, Z. Q. Kuai, C. Yu, Y. Zhang, J. Y. Zhou, and J. X. Chen, “Development of ultrawideband antenna with multiple band-notched characteristics using half mode substrate integrated waveguide cavity technology,” IEEE Trans. Antennas Propag., vol.56, no.9, pp. 2894-2902, 2008.

[29] G. H. Zhai, W. Hong, and K. Wu et al, “Folded half mode substrate integrated waveguide 3 dB coupler,” IEEE Microwave Compon. Lett., vol.18, no.8, pp.512-514, 2008.

[30] N. Grigoropoulos, B. S. Izquierdo, and P. R. Young, “Substrate integrated folded waveguides (SIFW) and filters,” IEEE Microwave Wireless Compon. Lett. Vol.15, pp.829-831, 2005.

[31] W. Che, L. Geng, K. Deng, and Y. L. Chow, “Analysis and experiments of compact folded substrate-integrated waveguide,” IEEE Trans. MTT, vol.56, pp.88-93, 2008.

[32] Yan Ding, and Ke Wu, “A 4x4 Ridge Substrate Integrated Waveguide (RSIW) Slot Array Antenna,” IEEE antenna and wireless propag. Lett., vol. 8, pp.561-564, 2009.

[33] F. He, “Innovative Microwave and Millimeter wave Components and Subsystems Based on Substrate Integrated Waveguide,” PHD dissertation, École Polytechnique de Montréal, Montreal, Canada, 2011.

[34] Patrovsky and K. Wu, “Substrate integrated circuits (SICs)—providing a low-cost and low-loss approach for millimeter-wave circuit and system integration (invited paper),” in Proceedings 8th MINT Millimeter-Wave Int. Symp. and 9th Topical Symp. on Millimeter Waves, Seoul, Korea, February 26-27, 2007, Seoul, South Korea, Feb. 2007, pp. 9–14.

[35] Y. Cassivi, L. Perregrini, P. Arcioni, M. Bressan, K. Wu, and G. Conciauro, “Dispersion characteristics of substrate integrated rectangular waveguide,” in IEEE Microwave Wireless Compon. Lett., vol. 12, Sep. 2002, pp. 333–335

[36] D. Deslande and K. Wu, “Single-substrate integration technique of planar circuits and waveguide filters,” IEEE Trans. Microw. Theory Tech., vol. 51, no. 2, pp. 593–596, Feb. 2003.

[37] X. Feng and W. Ke, “Guided-wave and leakage characteristics of substrate integrated waveguide,” IEEE Trans. Microw. Theory Tech., vol. 53, pp. 66–73, 2005.

[38] T. Djerafi, K. Wu, D. Deslandes, "A temperature compensation technique for substrate integrated waveguide cavities and filters," IEEE Trans. On Microwave Theory and Technique, Vol. 60, pp. 2448-2455, Aug. 2012.

[39] T. Djerafi, K. Wu, D. Deslandes, “Temperature drift compensation technique for substrate integrated waveguide oscillator” IEEE Microwave and Wireless Components Letters, Vol. 22, pp. 489-491, 2012.

[40] J. Kaiser, “The Archimedean two-wire spiral antenna,” IRE Transactions on Antennas and Propagation, vol. 8, no. 3, pp. 312–323, 1960.

[41] C. Wang and D. Hsu, "Studies of the novel CPW-fed spiral slot antenna," IEEE Antennas and Wireless Propagation Letters, vol. 3, pp. 186–188, 2005.

[42] S. Park, N. Kim, S. Rhee, and S. Lee, "Spiral slot antenna fed by coplanar waveguide using magnetic phase difference," Microwave and Optical Technology Letters, vol. 52, no. 1, pp. 28–30, 2010.

[43] C. Wang, "A CPW-fed wideband spiral slot antenna with circular polarization," Microwave and Optical Technology Letters, vol. 52, pp. 1204-1208, 2010.

[44] D. Muller and K. Sarabandi, "Design and analysis of a 3-arm spiral antenna," IEEE Transactions on Antennas and Propagation, vol. 55, no. 2, pp. 258–266, 2007.

[45] D. Rutledge, D. Neikirk, and D. Kasilingam, "Integrated-circuit antennas," Infrared and Millimeter Waves. New York: Academic, 1983, pp. 1–90.

[46] A. Babakhani, X. Guan, A. Komijani, A. Natarajan, and A. Hajimiri, "A 77-GHz phased-array transceiver with on-chip antennas in silicon: Receiver and antennas," IEEE Journal of Solid-State Circuits, vol. 41, no. 12, pp. 2795–2806, 2006.

[47] W.L. Stutzman and G.A. Thiele, Antenna Theory and Design, New York: John Wiley & Sons, 1981.

[48] Y. Qian, W. Deal, N. Kaneda, and T. Itoh, "Microstrip-fed quasi-Yagi antenna with broadband characteristics," Electron. Lett., vol. 34, pp. 2194–2196, Nov. 1998.

[49] G. Zheng, A.A. Kishk, A.B. Yakovlev, and A.W. Glisson, "Simplified feed for a modified printed Yagi antenna," Electron. Lett., vol. 40, no. 8, pp. 464–465, Apr. 2004.

[50] A. Hoorfar, "Analysis of a 'Yagi-like' printed stacked dipole array for high gain applications," Microwave Opt. Technol. Lett., pp. 317-321, April 1998.

[51] A. Hoorfar, "Evolutionary programming in electromagnetic optimization: a review," IEEE Trans. Antennas Propagat., vol. 55, pp. 523-537, Mar. 2007.

[52] O. Kramer, T. Djerafi, and K. Wu, "Vertically multilayer-stacked Yagi antenna with single and dual polarizations," IEEE Trans. Antennas Propagat., vol.58, pp.1022-1030, Apr. 2010.

[53] O. Kramer, T. Djerafi, and K. Wu, "Very small footprint 60 GHz stacked Yagi antenna array," submitted to IEEE Trans. Antennas Propagat.

[54] Z. Li and K. Wu, "24-GHz frequency-modulation continuous-wave radar front-end system-on-substrate," IEEE Trans. Microwave Theory Tech., vol. 56, pp. 278–285, Feb. 2008.

[55] X.-P. Chen, K. Wu, L. Han, and F. He, "Low-cost high gain planar antenna array for 60-GHz band applications," IEEE Trans. Antennas Propagat., vol. 58, pp. 2126–2129, June. 2010.

[56] D. Stephens, P.R. Young, and I.D. Robertson, "W-band substrate integrated waveguide slot antenna," Electron. Lett., vol. 41, no. 4, pp. 165–167, Feb. 2005.

[57] J.R. James and P.S. Hall, Handbook of Microstrip Antennas. London, U.K.: Peregrinus, 1989.

[58] D. Liu, B. Gaucher, U. Pfeiffer, and J. Grzyb, Hoboken, "Advanced Millimeter-wave Technologies,"NJ: Wiley, 2009, pp. 167–170.

[59] H. Vettikalladi, O. Lafond, and M. Himdi, "High-efficient and high-gain superstrate antenna for 60-GHz indoor communication," IEEE Antennas Wireless Propag. Lett., vol. 8, pp. 1422–1425, 2009.

[60] T. Djerafi, "Étude et Réalisation de Matrices à Commutation de Faisceaux en Technologie Guide d'Onde Intégrée aux Substrats," PHD dissertation, École Polytechnique de Montréal, Montreal, Canada, 2011.

[61] E. Moldovan, R. G. Bosisio, and K.Wu, "W-band multiport substrate integrated waveguide circuits," IEEE Trans. Microw. Theory Tech., vol. 54, no. 2, pp. 625–632, Feb. 2006.

[62] T. Yoneyama and S. Nishida, "Non-radiative dielectric waveguide for millimeter-wave integrated circuits," IEEE Trans. Microw. Theory Tech., vol. MTT-29, no. 11, pp. 1188–1192, Nov. 1981.

[63] Y. Cassivi and K. Wu, "Substrate integrated non-radiative dielectric waveguide," IEEE Microw. Wireless Compon. Lett., vol. 14, no. 3, pp. 89–91, Mar. 2004.

[64] Y. Cassivi and K. Wu, “Substrate integrated NRD (SINRD) guide on high dielectric constant substrate for millimeter wave circuits and systems”, IEEE Int. Microwave Symp. Dig., pp. 1639-1642, Fort Worth, 2004.

[65] F. Xu, K. Wu, and W. Hong, “Substrate integrated nonradiative dielectric waveguide structures directly fabricated on printed circuit boards and metallized dielectric layers,” IEEE Trans. Microw. Theory Tech., vol. 59, no. 12, pp. 3076–3086, Dec. 2011.

[66] Y. Cassivi, “Étude et développement de la technologie hybride circuit planaire/guide NRD dans le contexte d'un émetteur/récepteur onde millimétrique,” PHD dissertation, École Polytechnique de Montréal, Montreal, Canada, 2004.

[67] G. E. Mueller andW. A. Tyrrell, “Polyrod antennas,” Bell. Syst. Tech. J., vol. 26, pp. 851–837, Oct. 1947.

[68] J. P. Pousi, D. V. Lioubtchenko, S. N. Dudorov, and A. V. Raisanen, “High permittivity dielectric rod waveguide as an antenna array element for millimeter waves,” IEEE Trans. Antennas Propag., vol. 58, no. 3, pp. 714–719, Mar. 2010.

[69] J. Richter and L.-P. Schmidt, “Dielectric rod antennas as optimized feed elements for focal plane arrays,” in Proc. IEEE AP-S Int. Symp., Washington, DC, Jul. 3–8, 2005, vol. 3A, pp. 667–670.

[70] D. Lioubtchenko, S. Dudorov, J. Mallat, and A. V. Räisänen, “Dielectric rod waveguide antenna for W band with good input match,” IEEE Microw. Wireless Compon. Lett., vol. 15, no. 1, pp. 4–6, Jan. 2005.

[71] Patrovsky, A., and Wu, K.: ‘94-GHz planar dielectric rod antenna with substrate integrated image guide (SIIG) feeding’, IEEE Antennas Wirel. Propag. Lett., 2006, 5, (1), pp. 435–437

[72] M. N. Afsar, “Dielectric measurements of millimeter-wave materials,” IEEE Trans. Microwave Theory Tech., vol. MTT-32, pp. 1598–1608, Dec. 1984.

[73] F. J. Zucker and R. C. Johnson, “Surface-wave antennas,” in Antenna Engineering Handbook, 3rd ed. New York: McGraw-Hill, 1992, pp. 12.1–12.29.

[74] R. Douville, M. Cuhaci, and S. Meszaros, “MHMIC: Technology for the integration of microwave sub-assemblies,” in engineering Inst. of canada, canadian conference on electrical and computer engineering, 1991.

[75] G. M. Rebeiz, “Millimeter-wave and terahertz integrated circuit antennas,” Proc. IEEE, vol. 80, pp. 1748–1770, Nov. 1992.

[76] J. A. Encinar and J. M. Rebollar, “A hybrid technique for analyzing corrugated and noncorrugated horns,” IEEE Trans. Antennas Propagat., vol. AP-34, pp. 961–968, Aug. 1986.

[77] T. Wriedt, K.-H. Wolff, F. Arndt, and U. Tucholke, “Rigorous hybrid field theoretic design of rectangular waveguide mode converters including the horn transitions into half-space,” IEEE Trans. Antennas Propagat., vol. 37, pp. 780–789, June 1989.

[78] C. A. Mentzer and JR. Leon Peters, “Pattern analysis of corrugated horn antennas,” IEEE Trans. Antennas Propagat., vol. AP-24, pp. 304–309, May 1976.

[79] P. Focardi, A. Freni, S. Maci, and G. Vecchi, “Efficient analysis of arrays of rectangular corrugated horns: The synthetic aperture function approach,” IEEE Trans. Antennas Propag., vol. AP-53, no. 2, pp. 601–607, Feb. 2005.

[80] Z. L. Li and K. Wu, “A new approach to integrated horn antenna,” in Proc. Int. Symp. on Antenna Technology and Applied Electromagnetics, Jul. 2004, pp. 535–538.

[81] Hao Wang, Da-Gang Fang, Bing Zhang, Wen-Quan Che, “Dielectric Loaded Substrate Integrated Waveguide (SIW) H-Plane Horn Antennas,” IEEE Trans. Antennas and Propagation, , vol.58, no.3, pp.640-647, March 2010.

[82] B.Pan, Y. Li, G. E. Ponchak, J.Papapolymerou, andM.M.Tentzeris, “A 60-GHz CPW-fed high-gain and broadband integrated horn antenna,” IEEE Trans. Antenna Propag., vol. 57, no. 4, pp. 1050–1056, Apr. 2009.

[83] W. Che, B. Fu, P. Yao, Y. L. Chow, “Substrate integrated waveguide horn antenna with dielectric lens,” Microwave and optical technology letters, vol. 49, No. 1, pp168-170, January 2007.

[84] S. Yang, "Antennas and arrays for mobile platforms - Direct broadcast satellite and wireless communication," PHD dissertation, University of Tennessee, Knoxville, USA, 2008.

[85] Z. C. Hao, W. Hong, J. X. Chen, X. P. Chen, and K. Wu, "A novel feeding technique for antipodal linearly tapered Slot Antenna Array," IEEE IMS 2005, Long Beach, California, pp.1641-1644, June 12-17, 2005.

[86] Y.J. Chen, W. Hong and K. Wu, " Design of a Monopulse Antenna Using a Dual V-Type Linearly Tapered Slot Antenna," IEEE trans. On Ant. and Prop. vol. 56, no. 9, p. 2903-2909 Sept 2008.

[87] Yu Jian Cheng, Yong Fan, "Millimeter-wave miniaturized substrate integrated multibeam antenna," IEEE Transactions on Antennas and Propagation, vol. 59, no. 12, pp. 4840-4844, Dec. 2011.

[88] Y. J. Cheng, W. Hong, and K. Wu, "Millimetre-wave monopulse antenna incorporating substrate integrated waveguide phase shifter," IET Microw. Antennas Propag., vol. 2, no. 1, pp. 48–52, Jan. 2008.

[89] R. Kazemi, E. Fathy, and R. Sadeghzadeh, "Dielectric Rod Antenna Array With Substrate Integrated Waveguide Planar Feed Network for Wideband Applications" IEEE Trans. Antennas Propagat., vol. 60, No. 3, March. 2012.

[90] W. Che, K. Deng, D. Wang, and Y. L. Chow, "Analytical equivalence between substrate-integrated waveguide and rectangular waveguide," IET Microw. Antennas Propag., vol. 2, no. 1, pp. 35–41, 2008.

[91] K. S. Yngvesson, T. L. Korzeniowski, Y. S. Kim, E.L. Kollberg and J. F. Johansson, "The Tapered Slot Antema - A New Integrated Element for MM Wave Applications", IEEE Trans. Microwave Theory and Tech., Vol.37, No.2 pp.365-374, Feb. 1989.

[92] R. S. Elliott, "Beamwidth and Directivity of Large Scanning Arrays," Last of Two Parts, The Microwave Journal, pp. 74–82, January 1964.

[93] Z. Zhang, Y. R. Wei, and K. Wu, "60 GHz Transceiver Architectures Deploying Substrate Integrated Circuits (SICs) Technique," in Proc. European Microwave Conference, Sep. 2010, Paris, France, pp.33-36.

[94] Z. Zhang, “Substrate Integrated Waveguide Devices and Receiver Systems for Millimeter Wave Applications,” PHD dissertation, École Polytechnique de Montréal, Montreal, Canada, 2011.

[95] Fanfan He, Ke Wu, Wei Hong and Xiao-Ping Chen “Realization of a Low Cost 60 GHz Smart Antenna Receiver Sub-System Based on Substrate Integrated Waveguide Technology” IEEE Transactions on Microwave Theory and Techniques. vol. 60, No. 4, 2012.

[96] F. He, “Innovative Microwave and Millimeter wave Components and Subsystems Based on Substrate Integrated Waveguide,” PHD dissertation, École Polytechnique de Montréal, Montreal, Canada, 2011.

[97] D. Jung, K. Eun, and C. Park, “High-Q Circular LTCC Resonator Using Zigzagged Via Posts and a λ/4 Short Stub for Millimeter-Wave System-on-Package Applications ,” Advanced Packaging, IEEE Transactions on, vol. 32, pp. 216-222, 2009.

[98] D. Choudhury, P. H. Lawyer, J. A. Foschaar, M. D. Wetzel, and D. B. Rensch, “A Solder-Free Interconnect Approach for Integrating Millimeter Wave High-Power Devices With Planar Circuitry,” Advanced Packaging, IEEE Transactions on, vol. 26, pp. 417-424, 2003.

[99] Z. Zhang, Y. R. Wei, and K. Wu, “60 GHz Transceiver Architectures Deploying Substrate Integrated Circuits (SICs) Technique,” in Proc. European Microwave Conference, Sep. 2010, Paris, France, pp.33-36.

[100] H. Jin, W. Chen, and G. Wen, “Broadband transition between waveguide and substrate integrated waveguide based on quasi-Yagi antenna,” Electron. Lett., vol 48, pp. 355–356, 2012.

[101] J. Li, G. Wen, and F. Xiao, “Broadband transition between rectangular waveguide and substrate integrated waveguide”, Electron. Lett., vol 46, pp. 223–224, 2010.

[102] C.L. Zhong, J. Xu, and Z.Y. Zhi, “Broadband substrate integrated waveguide to rectangular waveguide transition with fin-line”, Electron. Lett., vol 45, pp. 205–207, 2009.

[103] L. Xia, R. Xu, B. Yan, J. Li, Y, Guo, and J. Wang, “Broadband transition between air-filled waveguide and substrate integrated waveguide,” Electron. Lett., Vol. 42, pp. 1403–1405, Nov. 2006.

[104] S. Beer, B. Ripka, S. Diebold, H. Gulan, C. Rusch, P. Pahl, and T. Zwick, “Design and measurement of matched wire bond and flip chip interconnects for d-band system-in-package applications,” in IEEE MTT-S Microw. Symp. Dig., Jun. 2011, pp. 1–4.

[105] S. Beer, H. Gulan, M. Pauli, C. Rusch, G. Kunkel, and T. Zwick,“122-GHz chip-to-antenna wire bond interconnect with high repeatability,”in Proc. IEEE MTT-S Int. Microwave Symp. Dig., Jun. 2012,pp. 1–3.

[106] Beer, S., Gulan, H., Ripka, B., Pahl, P., & Zwick, T. (2011, September). Packaging and interconnect solutions for a low cost surface-mountable millimeter-wave radar sensor. In Semiconductor Conference Dresden (SCD), 2011 (pp. 1-4). IEEE.

[107] Beer, Stefan, Christian Rusch, Heiko Gulan, B. Goettel, M. Girma, J. Hasch, W. Winkler, W. Debski, and T. Zwick. "An Integrated 122-GHz Antenna Array With Wire Bond Compensation for SMT Radar Sensors." IEEE Transactions on Antennas and Propagation, Vol. 61, No. 12, Dec. 2013.